ANALYSES OF INTERACTION BETWEEN A LUG OF LUGGED WHEEL AND WET COHESIVE SOIL(Dissertation_全文)

AUTHOR(S):

Nakashima, Hiroshi

ANALYSES OF INTERACTION BETWEEN A LUG OF LUGGED WHEEL AND WET COHESIVE SOIL

HIROSHI NAKASHIMA

ANALYSES OF INTERACTION BETWEEN A LUG OF LUGGED WHEEL AND WET COHESIVE SOIL

1989

HIROSHI NAKASHIMA

Acknowledgments

The author is fully indebted to Professor Takashi Tanaka, Department of Agricultural Engineering, Kyoto University, for his continuous instruction throughout this study which was begun in 1981 as his research advisor on wet cohesive soil terramechanics and the author also sincerely thanks to other members of his Dissertation Committee, Professor Kiyoshi Namikawa and Professor Ritsuya Yamashita, for their constructive suggestions and keen discussions in reviewing the manuscript.

In design and manufacture of experimental facilities, positive advise made by Associate Professor Minoru Yamazaki and former Instructor Dr. Akira Oida (currently Associate Professor of Niigata University) is gratefully acknowledged.

For theoretical analysis, the author wishes to express his gratitude to Associate Professor Takeshi Tamura, Department of Civil Engineering, Kyoto University, for his instructive seminar and encouraging advise on Rigid Plastic Finite Element Method for soil structures.

This study was partly supported by Grant-in-Aid for Science Research from the Ministry of Education (No.61760208) for the development of computer program on numerical simulation and its result visualization.

The author got kind cooperation with Messrs. Shoji Nakae, Mitsuya Nakano, Hikaru Suzuki, Akihiko Kishida, Hiroyuki Riichi in several experiments and Takaaki Nagi, Shigeo Kawashima for computer programming.

Finally, the author has to express his heartiest thanks to his wife, Hiroko, for her understanding and encouragement and to his son, Yusuke, for his patience during manuscript writing stage, without which this dissertation could be accomplished.

Table of Contents

Notations

d	ξ-component of distance between A and acting point of soil reaction
d_{rmax}	d value at R_{max}
e	ξ-component of distance of O^* and A
$\bar{\dot{e}}$	equivalent stain velocity
e_L	length of lug plate
h	η-component of distance of O^* and A
i_w	wheel slippage
ℓ_{24}	length of common boundary between elements I and II
l_1	direction cosine
l_2	direction cosine
m_1	direction cosine
m_2	direction cosine
n	wheel revolution
n_L	total lug number in model lugged wheel
r_{min}	minimum coefficient of loading
$\mathbf{s}$	deviatric stress vector
t	time
$\dot{\mathbf{u}}$	nodal velocity vector
$\dot{u}_n$	x-component of nodal velocity vector
$\dot{u}_i$	velocity vector
$\dot{\mathbf{u}}_i$	nodal velocity vector of i-th step
u_I	x-component of displacement on centroid of element I
u_{II}	x-component of displacement on centroid of element II
$\dot{v}_n$	y-component of nodal velocity vector
v_I	y-component of displacement on centroid of element I
v_{II}	y-component of displacement on centroid of element II
w_L	width of lug plate
x	x-coordinate
x_{g*}	x-coordinate of centroid on element *
$\mathbf{x}_i$	nodal coordinate vector of i-th step
y	y-coordinate
y_{g*}	y-coordinate of centroid on element *
A_1	constant in regression analysis

A_2	constant in regression analysis
A_3	constant in regression analysis
A	lug outer tip
B	differential operator matrix
B	lug inner tip
B_n	B-matrix component
B_r	B-matrix for RBSM
C	cohesion
C_u	undrained shear strength of wet cohesive soil
D	D-matrix in stress-strain relation
D_p	Plastic D-matrix
D_1	component of D-matrix
D_2	component of D-matrix
D(*)	internal plastic energy dissipation
E	Young's modulus
F_n	normal component of soil reaction on a lug
F_t	tangential component of soil reaction on a lug
G	transformation matrix
H	ξ-component of distance between two neighboring centroids
H_I	ξ-component of distance from centroid of an element I to common bounds of neighboring elements I and II
H_{II}	ξ-component of distance from centroid of an element II to common bounds of neighboring elements I and II
J	transformation matrix
K	penalty number
K_n	normal spring constant
K_r	stiffness matrix for RBSM
K_s	tangential spring constant
K_1	constant
K_2	constant
L	lift of lug
L_{ave}	average lift of lug
L_{max}	maximum lift of lug
L_n	component of L_v vector
L_v	differential operator vector
LL	liquid limit
M	reaction moment on O^*
M_c	calculated moment on lug centroid

M_{cI}	rotational moment at centroid of element I
M_{cII}	rotational moment at centroid of element II
N_n	shape function component
O_w	center of lugged wheel
O^*	center of moment cell
P	pull of lug
P	force vector for RBSM
P_a	average of P_w
P_{ave}	average pull of lug
P_{max}	maximum pull of lug
P_w	estimated wheel gross traction
P_{xI}	x-component of reaction at centroid of element I
P_{xII}	x-component of reaction at centroid of element II
P_{yI}	y-component of reaction at centroid of element I
P_{yII}	y-component of reaction at centroid of element II
PL	plastic limit
Q	matrix for coefficient change
R	soil reaction on a lug
R	surface traction vector at S_f
R_0	radius of wheel, or the distance from O_w to A
R_i	surface traction at S_f
R_{max}	maximum soil reaction on a lug
R_p	distance between O_w and an point P on a lug
R^2	coefficient of determination
S_f	stress boundary
S_m	additional matrix for D_p
S_{11}	component of S_m
S_{12}	component of S_m
S_{21}	component of S_m
S_{22}	component of S_m
T	estimated wheel torque
T_a	average of T
T_l	lug torque
T^*	measured wheel torque
U	displacement vector of an point P in an element
$\bar{\mathbf{U}}$	displacement vector of an point P in ξ-η system
$\mathbf{U}_i$	displacement vector of centroids in adjacent elements
$\tilde{U}_i$	ξ-component of $\bar{\mathbf{U}}$ for element I

$\bar{U}_{II}$	ξ-component of $\bar{U}$ for element II
V	volume of soil
V_c	velocity of soil bin carrier
V^P	lug velocity at an point P on a lug
V_{rmax}	velocity of lug at R_{max}
V_w	circumferential velocity of lugged wheel
$V_w{}^P$	wheel circumferential velocity at an point P on a lug
V_x	x-component of lug velocity vector
V_y	y-component of lug velocity vector
V_z	sinkage variation velocity
$\bar{V}_I$	η-component of $\bar{U}$ for element I
$\bar{V}_{II}$	η-component of $\bar{U}$ for element II
W	body force vector
W_i	body force
WL	wheel load
Z	sinkage of wheel
Z_0	magnitude of sinkage variation
Z_a	average sinkage of wheel
α	lug angle
$\boldsymbol{\alpha}$	prescribed lug velocity
β	adjustment coefficient in Newton-Raphson method
γ	specific weight of soil
$\boldsymbol{\delta}$	relative displacement vector
δ_n	ξ-component of relative displacement vector
δ_s	η-component of relative displacement vector
δ_R	absolute angle of R_{max} to wheel travel direction
δ_V	absolute angle of V_{rmax} to wheel travel direction
$\boldsymbol{\epsilon}$	strain vector
ϵ_n	ξ-component of strain vector
ϵ_s	η-component of strain vector
$\dot{\boldsymbol{\epsilon}}$	strain velocity vector
$\dot{\epsilon}_{ij}$	strain velocity tensor
$\dot{\epsilon}_{kk}$	volumetric strain velocity tensor
$\dot{\epsilon}_v$	volumetric strain velocity
ζ	angle of soil reaction R to η-axis on a lug
ζ'	angle of soil reaction R to ξ-axis on a lug
η	axis of local coordinates

η_t	traction efficiency
θ	rotational angle of lugged wheel
θ_e	rotational angle at initial contact of lug to soil
θ_{lmax}	rotational angle at L_{max}
θ_{pmax}	rotational angle at P_{max}
θ_{rmax}	rotational angle at R_{max}
θ_I	rotational component of displacement on centroid of element I
θ_{II}	rotational component of displacement on centroid of element II
λ	additional angle of an point P on a lug
ν	Poisson's ratio
ξ	axis of local coordinates
σ	stress vector
σ_{ij}	stress tensor
σ_n	ξ-component of stress vector
σ_0	von Mises yield stress
τ_s	η-component of stress vector
ϕ	internal friction angle
ϕ'	clock for A/D conversion
ϕ_{rmax}	angle between R_{max} and horizon measured from travel direction
ϕ_0	phase shift at initial contact of lug to soil
ω	angular velocity of wheel
Δt	time increment
$\Delta \delta$	angle difference
Φ	strain energy stored at contact boundary area of elements
Ψ_p	functional of Penalty formulation
Ω	angular velocity which depends on n_L

Chapter 1 INTRODUCTION

1.1 Objectives and Significance

Rice production calendar generally includes the period of soil puddling and transplanting of rice seedling processes in which rice field soils are in flooded or slurry-like condition. At this period, wheeled farm vehicles have to struggle with severe loss of their mobility even in the field with appropriate hardpan. Thus several types of traction and/or flotation devices, such as open-lugged wheel and strakes--hereafter they are simply referred to as lugged wheel--, have been developed and widely used with conventional tires or instead of tires in many rice producing countries in Asia.

However, the mechanism of pull and lift generation of a lug of lugged wheel is not sufficiently studied and the design of such wheels is mainly based on engineers' trial-and-error experiences without well developed theories which can predict the performance of lugged wheel even now.

One of the reasons of no established formulae comes from the fact that the behavior of soil under lug and the action of lug to soil are very complicated that we cannot directly apply the civil engineering disciplines such as passive earth pressure theory to soil-lug system problems.

It is clear that the action of lug to soil is composed of rotation as well as translation. The motion of translation is very easy to deal with by passive soil resistance theory or by slip line method, especially for single lug condition. But the combined motion of translation and rotation of lug which is encountered in the real situation

is very difficult to analyze since the effect of rotation is not permitted in conventional theories. At the same time, the deformation of soil with preceding lug trench must be considered when the multiple lugs of lugged wheel act on soil so that the practical action of them can be analyzed and the working reaction on lugs can be predicted.

The main purposes of this study are to analyze the soil reaction on a lug and soil behavior under a lug of lugged wheel by laboratory experiments and by numerical methods which take both translational and rotational action of lug into consideration with the influence of wheel sinkage variation, and to clarify the possibility of lugged wheel performance prediction whose foundation is the numerical estimation of basic soil reaction on a lug of lugged wheel.

The present thesis is considered as the first basic step for the rational design of lugged wheel by CAD system, since even now there are not other practical methods of performance prediction by numerical analysis where professional experience and intuition for calculation are not required.

1.2 Organization

This thesis begins with the state-of-art survey of previous literatures on lugged wheels and soil-lug interactions in Chapter 2. Then, basic standpoint and approach of this research are stated.

In Chapter 3, results of soil reaction measurement using the laboratory experimental facility are presented and discussed in terms of the effect of lug angle, total number of lug and wheel slippage on wheel traction generation. Sinkage variation of wheel is also discussed and the velocity equation of lug using the trigonometric function

is proposed.

Chapter 4 states some soil behaviors under a lug of lugged wheel which are concurrently observed during laboratory experiments for soil reaction measurements. Relation of soil behavior and soil reaction is discussed. Preliminary data on sand behavior under a lug are also shown to emphasize the difference of wet cohesive soil behavior under a lug.

In Chapter 5, Rigid Body Spring Model (RBSM) which is one of the upper bound methods is applied to analyze the lug reaction as the first level simple and quick simulation and its applicability is discussed.

As for analysis on both soil behavior and soil reaction, Finite Element Method with rigid-plastic constitutive relation which is known as Rigid Plastic Finite Element Method (RPFEM) is applied in Chapter 6 and the validity of this method as the second level more precise simulation for soil-lug system is discussed.

In Chapter 7, procedures and example of computer simulation of soil-lug interaction are demonstrated with the current requirements and limitations such as data preparation, capacity of computers etc.

In this thesis, the following several studies by the author which were published or are to appear in the Journal of the Japanese Society of Agricultural Machinery are summarized; Tanaka and Nakashima(1986a), Nakashima and Tanaka(1988a) for soil reaction experiments in Chapter 3, Nakashima and Tanaka(1988b) for soil behavior in Chapter 4, and Nakashima and Tanaka(1988c) for numerical analysis by RPFEM.

Chapter 2 STATE OF THE ART ON SOIL-LUG INTERACTION ANALYSIS

2.1 Introduction

In order to clarify the state of art on researches of soil-lug interaction problems, many papers in academic journals and reports were reviewed in terms of experimental and theoretical methods. The approach in this thesis is then stated. In this thesis, moisture content data are all expressed in dry basis unless stated otherwise.

2.2 Experimental Methods

The experimental researches on soil-lug interactions can be classified into three approaches as follows; (a) Field experiments, (b) Soil reaction measurement and (c) Soil deformation observation. As the moisture content of soil is considered as an important state parameter for cohesive soil, the auxiliary classification of (i) Below Liquid Limit (LL) condition and (ii) Equal or Over Liquid Limit condition will be used in order to clarify the current tendency of studies on soil-lug system. If the term "flooded" is appeared in the paper, it is considered to be in the group of (ii).

2.2.1 Field Experiments

In order to get the information on traction generated by lugged wheel, some field experiments were done as a basic approach for this discipline. Generally the soil reaction at soil-lug interface is indirectly evaluated in terms of drawbar pull which is caused by lugs in contact of soil instead of the direct measurement of reaction force

which is created by the action of each lug of lugged wheel.

Below Liquid Limit Condition

Tsunematsu and Matsui(1954) made the experiments on power tiller with some lugged wheels of different lug shape in clay loam soil. The moisture content varied from 7.3% to 44.7%, although there was no indication of LL data. They found that the drawbar pull was increased in proportion to the increase of lug height. They also observed that the decrease of lug angle brought the increase of drawbar pull. Subsequently, in 1956 they reported that the effect of lug angle on rolling resistance of wheel could not be seen for soft soil condition using the same test facilities.

Later, Dickson *et al.*(1981) investigated the tractive performance and soil compaction by open flat-lugged wheels and found that the degree of soil compaction by lugged wheel was low although the tractive performance was rather poor compared with the conventional tires. Their experiments were done with clay and clay loam with relatively low moisture content (below Plastic Limit).

Dickson *et al.*(1983) mainly observed soil compaction in succession under same lugged wheel and confirmed that the zero lug angle wheel produced little compaction and that compaction increased in proportion with lug angle.

Equal or Over Liquid Limit Condition

Tanaka *et al.*(1965) investigated the mobility of tractor with various running devices in wet clay field without hardpan and in clay loam field with hardpan with various moisture conditions. They found that the drawbar pull became small in case of submerged field in all devices tested but the strake type wheel showed better performance of

19% reduction only in drawbar pull compared with that of half tracks which showed 44% reduction.

Masuda *et al.*(1966) investigated the performance of float-lug wheel as a reference for performance evaluation of crawler tractors and they found that the wheel with float-lug produced maximum drawbar pull at 63% slippage. Their paper did not include the details of soil moisture condition except for the term "muddy."

Okabe(1972) observed the effect of lug width on lugged wheel torque for rice transplanters and he could find no remarkable effect of lug width. Lug angles of the used wheel were 22, 30 and 35 deg. Soil texture was clay and the field was flooded with no LL data.

Gee-Clough *et al.*(1981) measured the effect of lug angle and spacing on tractive performance in a flooded, puddled Bangkok clay soil and found that optimum spacing was 30 deg which meant 12-lug in a wheel and highest drawbar power was transmitted at 30 deg lug angle. LL value of the soil was 47.8%.

Through these investigations, it could qualitatively be predicted that the lug with smaller lug angle might produce effective gross traction even at the very soft soil condition. At the same time, it is evident that the difficulty of controlling soil conditions during experiments remains unchanged as long as the field experiments are concerned.

2.2.2 Soil Reaction Measurement

Soil reaction, or lug force, characteristics are systematically examined by laboratory experiments using single lug tester or model lugged wheel and soil bin.

Below Liquid Limit condition

Tanaka(1961) measured the horizontal resistance of lug plate with fixed lug experiments with air-dried soil. He found that the specific resistances of soil which was defined by the ratio of horizontal resistance to vertically projected area of lug under contact of soil were independent of lug angle.

Tsuchiya and Honami(1962) firstly measured the normal component of soil reaction on a lug of motor driven model lugged wheel on sand. They used the wheel carrier system to allow the wheel to sink with the increase of its slippage which was decided by giving the proper traction load, which simulated the real working condition of lugged wheel. They found that the maximum drawbar horse power was obtained between 20% and 30% wheel slippage and that the value of horse power became large when the width of lug and lug angle were small and when the wheel load and lug height were large.

Yamanaka(1962) also measured soil reaction as a normal pressure on a lug with constant wheel sinkage. Although his investigation lacked the tangential component of soil reaction on a lug in his measurements, he concluded that the lug angle of 30 deg was suitable for generation of traction. Used soil was sand, clay and sand-clay mixture for single lug experiments with various moisture content and sand-clay mixture with from 15.5% to 18.0% moisture content for wheel type experiments although LL value was not indicated.

Some discussions on soil reaction and rolling resistance were done by Tsuchiya and Honami(1965) and they concluded that the normal component of soil reaction on a lug varied with lug height and total number of lug. They also pointed out that the negative part of normal component became decreased as pull load and wheel load increased.

Recently, Hashiguchi *et al.*(1988) measured both wheel lug and rim reaction from soil by using small two-wheeled tractor. The soil was sandy clay loam and the moisture content was 17.7-20.5% with 34.7% LL value. They found that the effect of wheel rim reached about 60% of wheel lug reaction and the traction efficiency became maximum at about 15% of slippage and 60 deg lug angle. And they concluded that the best performance might be realized at 40 deg lug angle in the soft soils with a high void ratio.

Wang *et al.*(1988) measured the slippage variation with the experimental apparatus which was the same as in Tsuchiya and Honami(1962) in the function of wheel drive system. They used silt loam soil with 19.4% moisture condition whose PL and LL values were 23.3% and 47.7%. Although they did not show the definition of wheel slippage in their report, clear relation of sinkage variation was obtained, where the increase in drawbar load caused the decrease in the magnitude of sinkage fluctuation. The behavior of normal component of reaction force with respect to drawbar load was similar to the behavior in the paper of Tsuchiya and Honami(1965).

Equal or Over Liquid Limit Condition

Gee-Clough and Chancellor(1976) firstly measured the wet soil reaction on a single lug by small 2-axial force transducer under fixed sinkage condition, although they used the manual rotation mechanism of the shaft for single lug tester. The soil was Maahas clay loam with flooded condition of 39.9% moisture content. Among their practical observations, it was noted that the effect of lug width on the soil reaction was linear.

Zhang and Shao(1984) measured the soil reaction of wet paddy

field soil by single lug tester with constant sinkage condition. The soil texture was loam by USDA classification and the soil seemed in flooded condition. They observed that when the slippage was kept constant, the maximum lift force increased according as the lug angle increased, but the maximum traction force remained in nearly the same level.

Lu and Shao(1987) measured the soil reaction for both single lug and multiple lug conditions and they obtained two dimensionless coefficients K_1 for lug pull force and K_2 for lug lift force. It was shown that K_1 remained constant value of about 0.77-0.78 with the increase of lug angle from 15 to 35 deg.

Through the review of soil reaction, it is understood that there were few previous studies which measured the soil reaction on a lug of lugged wheel on wet cohesive soil. It is also noted from the survey that the soil-lug interaction may be treated as two-dimensional problem as long as the flat lug plate is used and that pull force by a lug becomes large as the lug angle decreases in wet cohesive soil condition, and the reason of this phenomenon might be connected with the sinkage of wheel. In terms of experimental methods, there seems to be two categories in reaction measurements; (i) by using single lug tester and (ii) by using model wheel. It is easy to correct single lug reaction by multiplying some factors in order to predict lugged wheel performance as Lu *et al.*(1987). But there might be the limit of such approach, since the single lug experiments are, at any rate, necessary and that the mechanism of interaction in wheel is considered different from the single lug condition.

2.2.3 Soil Deformation Observation

As a fundamental but important data, soil behavior under a lug is observed by some researchers.

Below Liquid Limit Condition

Tanaka(1958) firstly observed the deformation of air-dried clay powder under the model wheel with 100% slippage condition. He discussed the direction of principal stress by the geometrical relation with observed slip-lines. Tanaka(1959) also measured the deformation of clay powder under undriven and driven lugged wheel with narrow lugs and with wider lugs. In case of narrow lugged wheel, he found that the clay powder behavior seemed the same in both single lug wheel and in multiple lugged wheel case.

Equal or Over Liquid Limit Condition

Wu *et al.*(1984) firstly measured the deformation of wet clay soil (37.5% moisture content) under a lug. They used small dot markers to trace the movement of clay soil in successive photos. They concluded that the passive soil resistance theory could not be applicable to soil behavior analysis under lug of lugged wheel. In subsequent paper, Wu *et al.*(1986) discussed the wedge formation under the lug plate.

Shao and Wong(1986) observed the soil deformation in the same way as in Wu *et al.*(1984) using Ottawa sand and silt clay with 35.5-37.5% moisture content. They confirmed that the previous cavity formed by the preceding lug significantly influenced the soil flow and the failure pattern of following lug.

As a systematic study on cage wheel blocking, Salokhe and Gee-Clough(1987a) measured the soil deformation under single lug of const-

ant sinkage condition with 50% slippage. They used Bangkok clay soil of 49% moisture content, whose LL was 46%. They also observed boundary wedge formation in soil under single lug (1987b) and multiple lug (1988) condition and concluded that there did not generally exist the boundary wedge in case of multiple lugged wheel. They also investigated the soil adhering behavior in terms of various lug surface treatments(1987c). One of their findings was that the shape of boundary wedge in single lug was elliptical, which was different from the observation of Wu *et al.*(1986).

Lu and Shao(1987) pointed out that the large wheel slippage (more than 49.6%) caused the elliptical boundary wedge in their experiments on wet cohesive soil.

There are few researches which observe the soil behavior under a lug of a lugged wheel with wet cohesive soil under the driven wheel experimental condition and employ the concurrent soil reaction measurement at soil-lug interface. Especially, as Gee-Clough(1984) mentioned, the effect of lug-lug interaction on thrust generation seems the most difficult but necessary problems which must intensively be studied. And in order to get enough information on slip lines, boundary wedges and flow patterns in wet cohesive soil, much efforts are needed in soil behavior analysis.

2.3 Theoretical Methods

For theoretical methods, there seems to be three approaches which have been applied in the soil-lug system problems such as Passive Soil Resistance Theory, Slip Line Method and Finite Element Method.

2.3.1 Passive Soil Resistance Theory

This analysis is mainly based on two famous works by Hettiaratchi and Reece(1974,1975) which were updated and refined version of prior paper by Hettiaratchi *et al.*(1966). Their principle lies in the extended idea of Terzaghi's famous bearing capacity formula with the combination of Sokolovski's idea of Rankine zone, Transition zone and Interface zone (Sokolovski, 1960). Mechanically speaking, the theory can be characterized as a limit equilibrium method in which the equilibrium condition on bounding fracture slip line only is considered.

Gee-Clough and Chancellor(1976) divided the action of lug plate into vertical and horizontal and they firstly calculated the reaction force by applying plate-sinkage theory which was originally proposed by M.G. Bekker for vertical soil failure and passive soil resistance theory by Hettiaratchi *et al.*(1966) for horizontal one. Although the idea that the action of lug could be divided into vertical and horizontal direction lacked the effect of lug rotation, the possibility of engineering calculation of lug forces with design example was shown (Gee-Clough,1978).

Zhang and Shao(1984) also applied this theory with side wall effects of lug plate to predict the single lug reaction and they claimed that calculated forces agreed well with experimental results from single lug tester.

The calculation of soil reaction by this method is very simple and practical, but the main demerit lies in the assumption that the free soil surface must be horizontal which cannot be admitted for the case of lugged wheel with multiple lugs and that the movement of lug consists only of translational component. And as this theory is based on the force equilibrium condition at the bounding slip line only, it

cannot deal with the velocity field within soil, i.e. soil behavior, at all. In this sense, there is the limit of the applicability for this method as a simulation tool for both soil behavior and soil reaction as long as the new concept or suitable modification is not employed, as many researchers pointed out (Wu *et al.*,1984; Salokhe *et al.*,1987b).

2.3.2 Slip Line Method

The slip line method is a popular theory both for steady-state metal forming analysis and for basic bearing capacity or embankment stability analyses in civil engineering problems. This method has clear mathematical backgrounds of Kötter's (or Hencky's) equation for stress field and of Geiringer's equation for velocity field. For some special cases with well presumed slip line and prior calculation of distribution of maximum principal stress direction within the soil, explicit solution can be obtained by finite difference method (Hill, 1950) or by constructing geometric relations (Pragar,1959) or by analytic methods of differential operators (Ewing,1967; Collins,1968).

Sakai *et al.*(1984) assumed the basic slip line field under a lug of lugged wheel and firstly solved the equilibrium equations assuming two cases of rigid-perfect plastic soil and soil with recovery of deformation. Their result showed that the calculated forces were in most cases greater than the experimental results. The deformed soil over the horizontal line and the rotation of lug plate were neglected in their analysis.

However, soil-lug interactions, in principle, belong to the group of unsteady state problems with complicated prior lug cavities where the initial and successive setup of slip line is very difficult.

Thus, the applicability of slip line method to soil-lug system problems is substantially limited.

2.3.3 Finite Element Method

Finite Element Method (or FEM) is the most popular tool for numerical simulation of both structural and non-structural problems in engineering. The review and current achievements can be seen in the textbook by Zienkiewicz(1977).

On the other hand, the application of FEM in soil-lug system problems is quite limited. The main reason for this drawback lies in the fact that the localized large deformation of soil is usually occurred under lug which is very hard to trace in standard elasto-plastic FEM.

To overcome this difficulty in elasto-plastic analysis and to analyze problems until relatively large deformation of soil, three approach may be considered and applied to soil-lug system interactions; (i) finite deformation formulation of elasto-plastic FEM, (ii) weakened condition models in standard elasto-plastic FEM, and (iii) limit analysis by FEM.

The finite deformation formulation might be possible in the analysis of soil-lug system problems, but the material constants and computation time must be paid attention in the application of elasto-plastic FEM.

The second group of models, one of which is called Rigid Body Spring Model (RBSM) and was developed by Kawai(1980), is a special stress model with weakened condition at elemental nodes in FEM. RBSM has been applied to upper bound analysis of basic problems such as tension of V-notched specimen, stability analysis of slope etc. Since

the formulation of RBSM is very simple, there is the possibility of application in reaction prediction of soil-lug system which is currently tried in this thesis.

Rigid Plastic FEM (or RPFEM), which belongs to the third group and was originated in the analysis of deformation in metal forming problems (Lee and Kobayashi,1973), became a popular simulation tool for plastic forming processes. Mahrenholtz and Dung(1987) presented the review of FEM in that field. In soil mechanics, Tamura *et al.* (1984) firstly formulated the limit analysis of soil structure by RPFEM for saturated clay, and some developments were achieved by following the same formulation (Asaoka and Ohtsuka,1986; Kikusawa and Hasegawa,1987). Asaoka(1988) reviewed the formulation and clarified the meaning of effective stresses in relation to von Mises yield criterion.

Tanaka and Nakashima(1987) tried RPFEM analysis of soil-lug interaction problems with wet cohesive soil condition and simple mesh configuration. Their results clearly showed that the soil behavior under lug could be analyzed by RPFEM.

One of the merit of RPFEM is its easy implementation of velocity condition on a lug, that is the both translation and rotation of lug plate can be taken into consideration once the proper velocity assumption is added and initial shape of prior lug cavity is given. Both passive soil resistance method and slip line method have the demerit that the initial guess of proper shape of slip line is necessary. But in RPFEM, the slip lines are the derived result of calculation.

Since RPFEM is based on the minimization of plastic energy dissipation in soil, no consideration is included on elastic loading in principle. This is why the analysis on combined elastic and plastic

region by RPFEM is not so effective.

2.4 Approach in This Research

In this thesis, the author stands on the unified approach of both soil reaction and soil behavior because the soil reaction and the soil deformation behavior interact each other in the real situation and they cannot be treated and simulated separately.

The term "interaction" means, in this thesis, the relation of action of lug to the soil and reaction from soil on lug at soil-lug interface. Thus, the observation of soil behavior corresponds to the visible sensing of the lug action, whereas the measurement of soil reaction means the detection of boundary resistance on a lug plate which is generated by the stresses within the soil under lug.

The soil used in this study is wet cohesive soil, since there are few studies as listed in the group of equal or over Liquid Limit in former sections, although the often use of lugged wheel can be seen in flooded condition. And the existence of hardpan is neglected in this study, since the author mainly puts emphasis on the analysis of successive lug interactions (i.e. small distance of lug-lug cavity case) by model wheel-type laboratory experiments with assumed homogeneous soil condition and the mechanical structure of hardpan in a soil box is very difficult to construct and control throughout experiments.

In order to simulate soil-lug interaction mechanics, the author employs two numerical models as summarized in the last section, namely Rigid Body Spring Model (RBSM) for simple reaction prediction and Rigid Plastic Finite Element Method (RPFEM) for more precise reaction and behavior simulation of soil-lug interactions.

Chapter 3 EXPERIMENTAL ANALYSIS OF SOIL REACTION ON A LUG OF LUGGED WHEEL

3.1 Introduction

From the survey of previous studies in Chapter 2, it is clear that the experimental approach in terms of concurrent observation for both soil reaction on lug and soil behavior under lug with the no confined sinkage condition and preceding lug trench existence should be adopted for the practical laboratory experiments under similar operational situation of lugged wheel. As the first attempt of experimental analysis in the current study, three experiments are done in order to experimentally analyze the effect of lug parameters such as lug angle, total number of lug and wheel slippage on soil reaction on a lug of lugged wheel on wet cohesive soil by considering the above stated points. First, soil reaction characteristics with lug angle of 30 deg are obtained by EXP-I experiment. Second, the effect of different lug angle on the soil reaction characteristics is clarified by EXP-II. Third, the relationship between the wheel load and average sinkage of lugged wheel is verified by EXP-III. Then, the average wheel sinkage and the sinkage variation in terms of the differences in lug angle are discussed by the experimental data of EXP-II and it is shown that the sinkage variation velocity can be approximated by a trigonometric function.

3.2 Experimental Apparatus and Condition

3.2.1 Experimental Apparatus

Schematic diagram of experimental apparatus which were used in all experiments EXP-I, EXP-II and EXP-III is shown in Fig.3-1. The difference in (A) and (B) in Fig.3-1 is not significant, although there exists the slight change of structure in Wheel Installing Frame (WIF)[3] and sinkage measurement devices. Model lugged wheel[4] has the diameter of 300 mm and the width of 155 mm by considering the easiness of handling in experiments. And this wheel consists of flat iron lug plate whose specifications are 50 mm in length, 155 mm in width and 3 mm in thickness. Total number of lug in a wheel n_L can be changed among 6, 9 and 12. The lug for reaction measurement has shorter width of 151.5 mm in order to avoid the frictional interference between the lug plate and the glass of soil box.

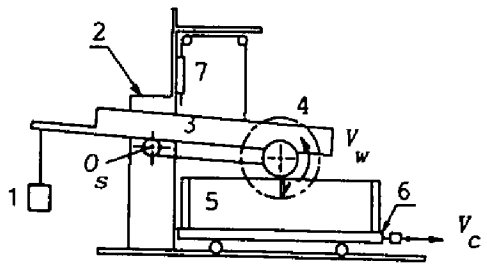

1 Counter Weight
2 Wheel Drive Unit
3 Wheel Installing Frame
4 Model Lugged Wheel
5 Soil Box
6 Soil Box Carrier
7 Sinkage Sensor

(A) Experimental Apparatus for EXP-I

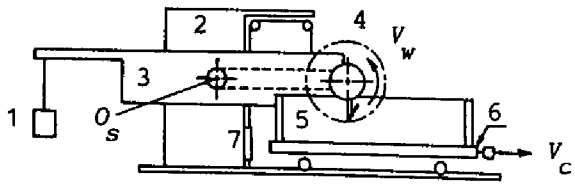

(B) Experimental Apparatus for EXP-II, EXP-III

Fig.3-1. Schematic diagram of experimental apparatus.

The lug angle α, which is the angle between the radial direction of the wheel at lug outer tip and the lug surface plane, can be changed by exchanging suitable lugs. WIF is only supported by the power transmitting shaft with the center O_s via pillow blocks, which permits the free movement in vertical direction.

The wheel load is applied by Counter Weight[1]. The measurement of wheel load was done when the position of WIF was horizontal. And the experiments were also done with nearly horizontal location of WIF so that the variation of moments around O_s which directly reflected the variation of wheel load became minimum as far as possible.

The soil box[5] has the inner specification of 880 x200 x200 mm with 5 mm glass on one side of it to observe the soil behavior concurrently. Detailed methods of observation will be explained in next chapter.

The wheel slippage i_w is determined by the relative velocity difference between the constant circumferential velocity of wheel V_w= 2.2 (cm/sec) which is assumed as in quasi-static condition and the travel velocity of Soil Box Carrier[6] V_c which is determined by the time measurement for fixed travel distance, which is expressed in Eq.(3.1).

$$i_w = \left(1 - \frac{V_c}{V_w} \right) \times 100 \quad (\%) \tag{3.1}$$

In this study, the slippage variation cannot be taken into account since V_c is also constant during experiments because of the principle of forced slippage mechanism of apparatus.

3.2.2 Lug Reaction Measurement System

Measurement Principle and Force System

The lug reaction on a lug from the soil is shown in Fig.3-2. The wheel is assumed to travel in x-axis direction with constant angular velocity ω around wheel shaft O_w in the figure.

The magnitude of soil reaction vector R can be decided by the measurement of normal component F_n and tangential component F_t of soil reaction on a lug plate as in Eq.(3.2).

$$R = \sqrt{F_n^2 + F_t^2} \tag{3.2}$$

The direction of reaction vector ζ to the local η-axis on lug can be expressed as;

$$\zeta = \tan^{-1}\left(\frac{F_t}{F_n}\right) \tag{3.3}$$

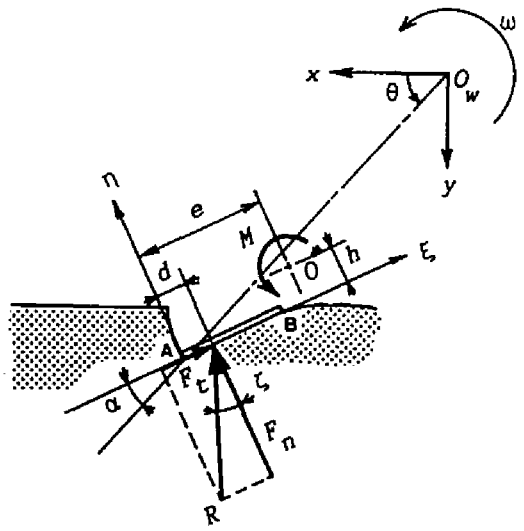

Fig.3-2. Soil reaction at soil-lug interface.

And the distance d from the lug outer tip A to the acting point of reaction vector is calculated by the moment equilibrium on an arbitrary moment measuring point O^* as;

$$d = e - \frac{M + F_t\, h}{F_n} \tag{3.4}$$

where e: distance of O^* and A in ξ-axis direction, h:distance of O^* and lug surface in η-axis direction, and M: reaction moment on O^*. For the sake of convenience, d is set to e when F_n=0 in Eq.(3.4) in order to avoid calculation error of zero division in Eq.(3.4).

Pull P of lug which means the lug traction and Lift L of lug which means the lug flotation can be obtained as the transformation of F_n and F_t to global Cartesian Coordinate System with the convention of positive signs in x-axis direction for P and in negative y-axis direction for L as in Eq.(3.5) with the rotational angle of wheel θ.

$$\begin{Bmatrix} P \\ L \end{Bmatrix} = \begin{pmatrix} -\cos(\theta - \alpha) & \sin(\theta - \alpha) \\ \sin(\theta - \alpha) & \cos(\theta - \alpha) \end{pmatrix} \begin{Bmatrix} F_t \\ F_n \end{Bmatrix} \tag{3.5}$$

The converted lug torque T_l on O_w can be expressed by Eq.(3.6),

$$T_l = F_n\,(R_0 \cos\alpha - d) - F_t\, R_0 \sin\alpha \tag{3.6}$$

where R_0 is the radius of lugged wheel (=15.0 cm). This torque implies the acting torque for the period from the first contact of measurement lug to the soil to the detachment of lug. Therefore one can get the estimated wheel toque T by the superposition of T_l with the angular shifts of lug interval. Likewise, the estimated wheel gross traction P_w can be calculated by the superposition of P with

corresponding lug interval shifts of lugged wheel. The reason of using T instead of measured data T^* is that there sometimes exists the friction interference between the side face of other lug plates and glass and the data T^* do not precisely express the wheel torque applied to the system.

The traction efficiency η_t of lugged wheel is defined as follows;

$$\eta_t = \frac{P_a V_c}{2\pi T_a n} \times 100 \quad (\%) \tag{3.7}$$

where P_a: average value of wheel gross traction P_w (N), T_a: average value of estimated wheel torque T (Ncm), and n: revolution speed of wheel (rps).

Developed Force Transducers

In order to measure fundamental reactions, F_n, F_t and M, the force transducer system was developed as shown in Fig.3-3. This system consists of 2-axial force transducer (Fig.3-3(ii)) which has the 4x4 mm sensing beam and two installing mounts [A] and [B] and the moment cell (Fig.3-3(iii)) which is attached between the 2-axial force sensor mount [C] and wheel flange. F_n is detected by strain gauges, 1-4, and F_t by those from 5 to 8 and M from 9 and 10. Each combination of gauges forms Wheatstone bridge circuit to detect signals strongly and accurately. The sign of each reaction is assumed positive as shown in Fig.3-2.

Data Flow in Measurement

Fig.3-4 illustrates the data flow diagram for each experiment.

In EXP-I, all the data were recorded by an electromagnetic oscillograph, whereas in EXP-II and EXP-III magnetic tape recorder was used and necessary data were later converted from analog signal to digital one with the sampling clock ϕ' which corresponded to 2 deg wheel rotation.

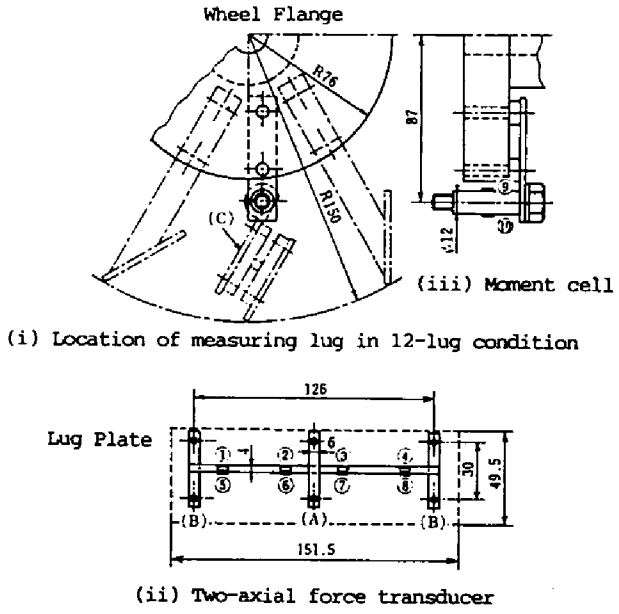

Fig.3-3. Transducers for soil reaction measurement.

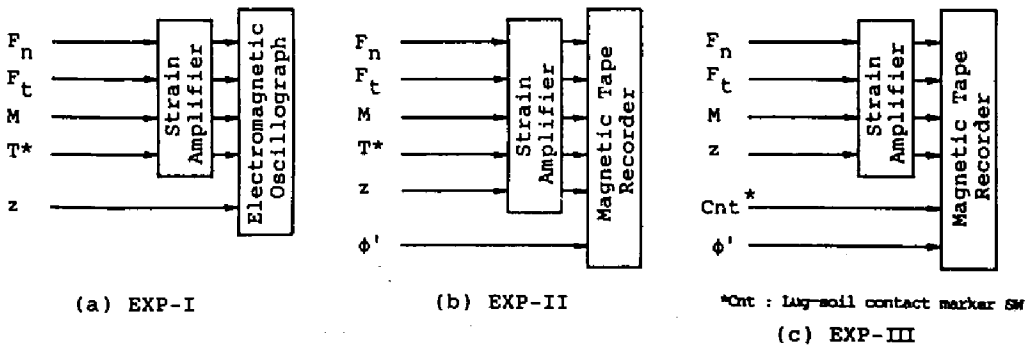

Fig.3-4. Data flow diagram in soil reaction experiments.

3.2.3 Experimental Conditions

Tables 3-1 to 3-3 show the combination of experimental conditions respectively. In EXP-I and EXP-II, wheel load was set to almost the same condition except for EXP-III experiment whose purpose was to observe the load-sinkage relation. Soil condition is listed in Table 3-4. The soil texture classification is based on USDA system (Kohnke, 1968).

Table 3-1. Experimental condition for EXP-I.

Number of Lug :	6, 9, 12
Lug Angle (deg):	30
Slippage (%) :	16.4, 30.1, 39.5
Wheel Load (N) :	52.4-54.9 (Average 53.7)

Table 3-2. Experimental condition for EXP-II.

Number of Lug :	6, 9, 12
Lug Angle (deg):	30, 45, 60
Slippage (%) :	13.8, 28.8, 43.1
Wheel Load (N) :	46.6-55.7 (Average 50.6)

Table 3-3. Experimental condition for EXP-III.

Number of Lug :	6, 9, 12	
Lug Angle (deg):	30, 45, 60	
Slippage (%) :	34.8	
Wheel Load (N) :	39, 51, 59	(Nominal)

Table 3-4. Used soil condition.

Experiment Series	EXP-I,-II	EXP-III
Soil Texture	Loam	Silt Loam
Sand (%)	40.0	24.5
Silt (%)	45.4	73.7
Clay (%)	14.6	1.8
Liquid Limit(%)	35.1	41.2
Plastic Limit(%)	25.0	24.5
Specific Gravity	2.61	2.76
Moisture Content(%)	38.5(I),36.5(II)	44.2

3.3 Result of Experiments and Discussion

3.3.1 Reaction Vectors and Lug Loci

In order to clarify the effect of total lug number of lugged wheel, lug angle and wheel slippage on geometrical behavior of soil reaction vectors, results of EXP-I and EXP-II are presented and discussed.

EXP-I

Figs.3-5, 3-6, 3-7 show typical examples of EXP-I result where the magnitude of reaction vectors are normalized by the maximum reaction (R_{max}). The cases for n_L=12 in Fig.3-5 and for n_L=9 in Fig.3-6 clearly show that R_{max} position (Δ) appears at about 30 deg after the contact for n_L=12 case and about 40 deg for n_L=9 case respectively. For the case of n_L=6 in Fig.3-7, R_{max} position appears at about 60 deg after contact for i_w=30.1% and i_w=39.5%. But for i_w=16.4% case, the position of R_{max} locates at rather smaller rotational angle. This might correspond to the remarkable change of lug loci in n_L=6 case, where the action of lug no longer continues until about 60 deg after the contact of lug to soil in case of i_w=16.4%.

The distance of acting point of soil reaction d, in general, shows similar tendency in each case. Maximum value of d (d_{max}) can be seen at the same position of R_{max} except for the case of n_L=6 and i_w=16.4% (Fig.3-7(c)). At the location where the lug dominantly applies the rotational action to the soil, d seems to move to the outer tip of lug, which is easily imagined from the result of measurement of soil pressure on rotational retaining wall (James and Bransby,1971).

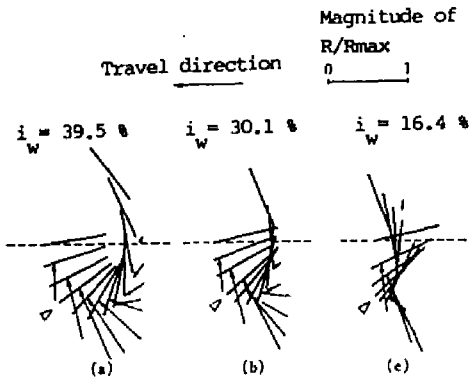

Fig.3-5. Result of reaction vector and lug loci for EXP-I (n_L=12).

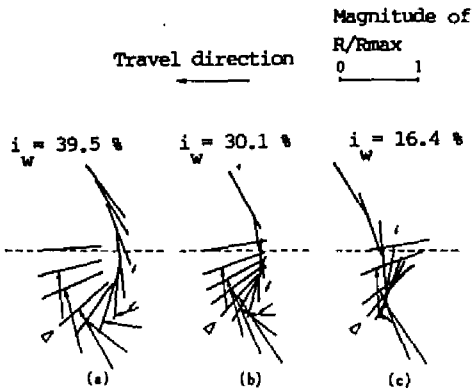

Fig.3-6. Result of reaction vector and lug loci for EXP-I (n_L=9).

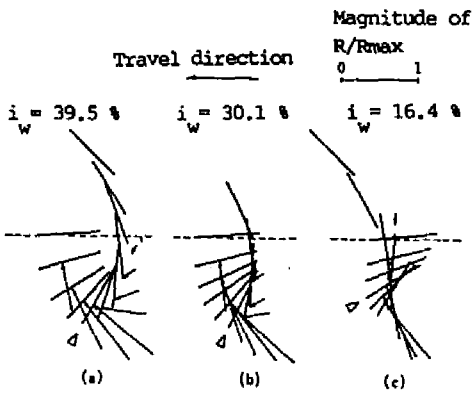

Fig.3-7. Result of reaction vector and lug loci for EXP-I (n_L=6).

EXP-II

Since the case of n_L=9 showed the intermediate tendency of n_L=6 and n_L=12 as in the former Fig.3-6, the results of n_L=12 and n_L=6 only are shown in Fig.3-8 and Fig.3-9 respectively as examples on the effect of lug angle change. Maximum soil reaction position will be listed in 3.3.2.

In both figures, the same tendency of location of generated maximum soil reaction is found as in the case of α=30 deg and n_L=12 of EXP-I. As α became large, remarkable change of d is observed. That is, the initial contact from inner tip of lug occurs in most cases of α=45 deg and α=60 deg as a result of decreasing wheel sinkage in such lug angles. It is clear that this phenomenon will bring the negative effects on wheel traction generation, since the inner tip contact of lug plate means the increase of rolling resistance of lugged wheel which is caused by the increase of overriding distance of soil in front of and below the wheel.

3.3.2 Pull and Lift Characteristics

EXP-I

Figs.3-10, 3-11, 3-12 are the result examples on pull and lift force characteristics of lug, calculated by Eq.(3.5).

In each figure, the maximum lift (L_{max}) shows nearly the same value in terms of n_L, owing to the constant wheel load condition. The rotational position of L_{max} appears at about 30 deg for n_L=12 and 40 deg for n_L=9 after the initial contact. But in case of n_L=6, the rotational position of L_{max} remains about 30 deg after the contact of lug to soil.

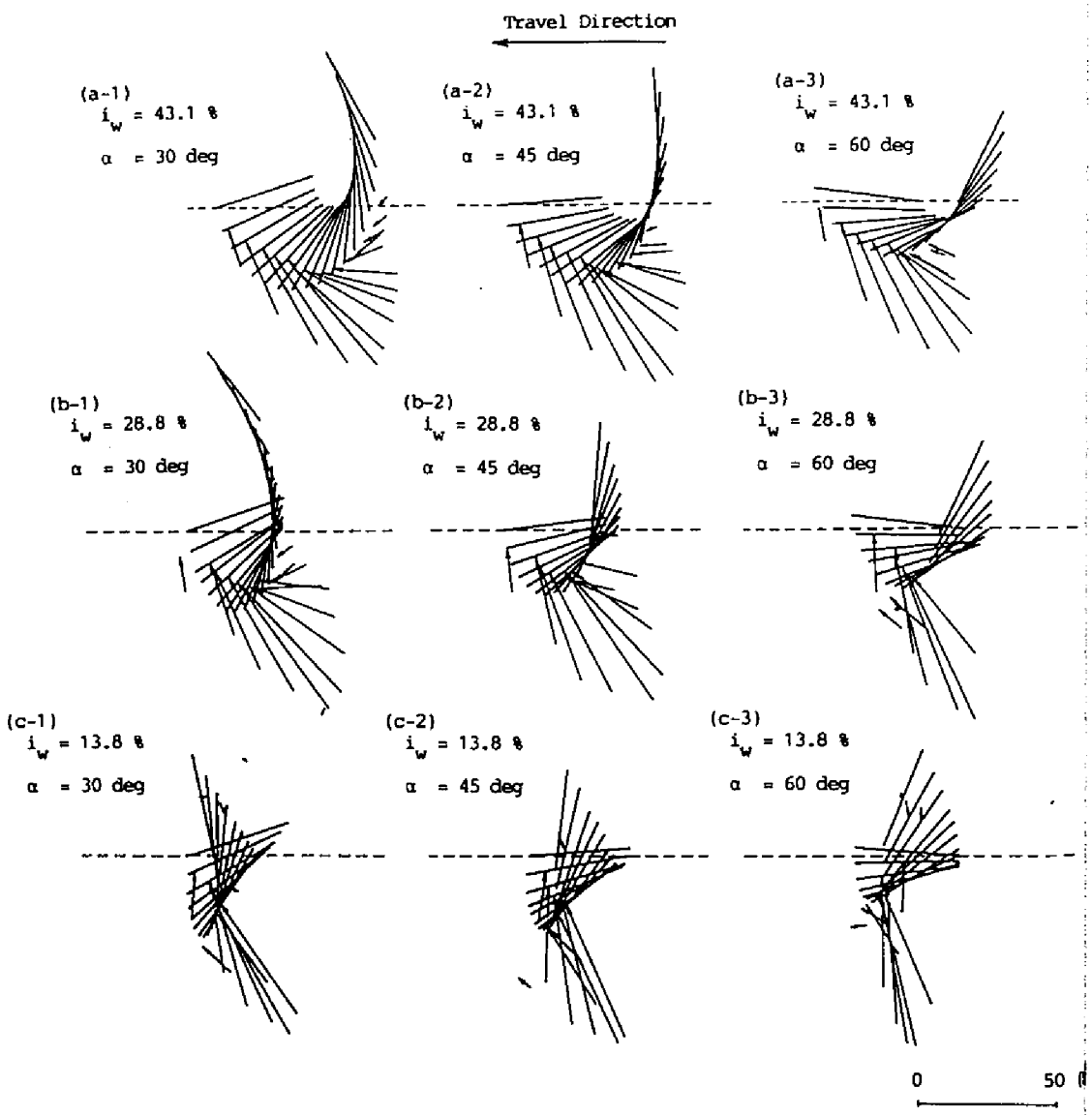

Fig.3-8. Result of soil reaction and lug loci for EXP-II (n_L=12).

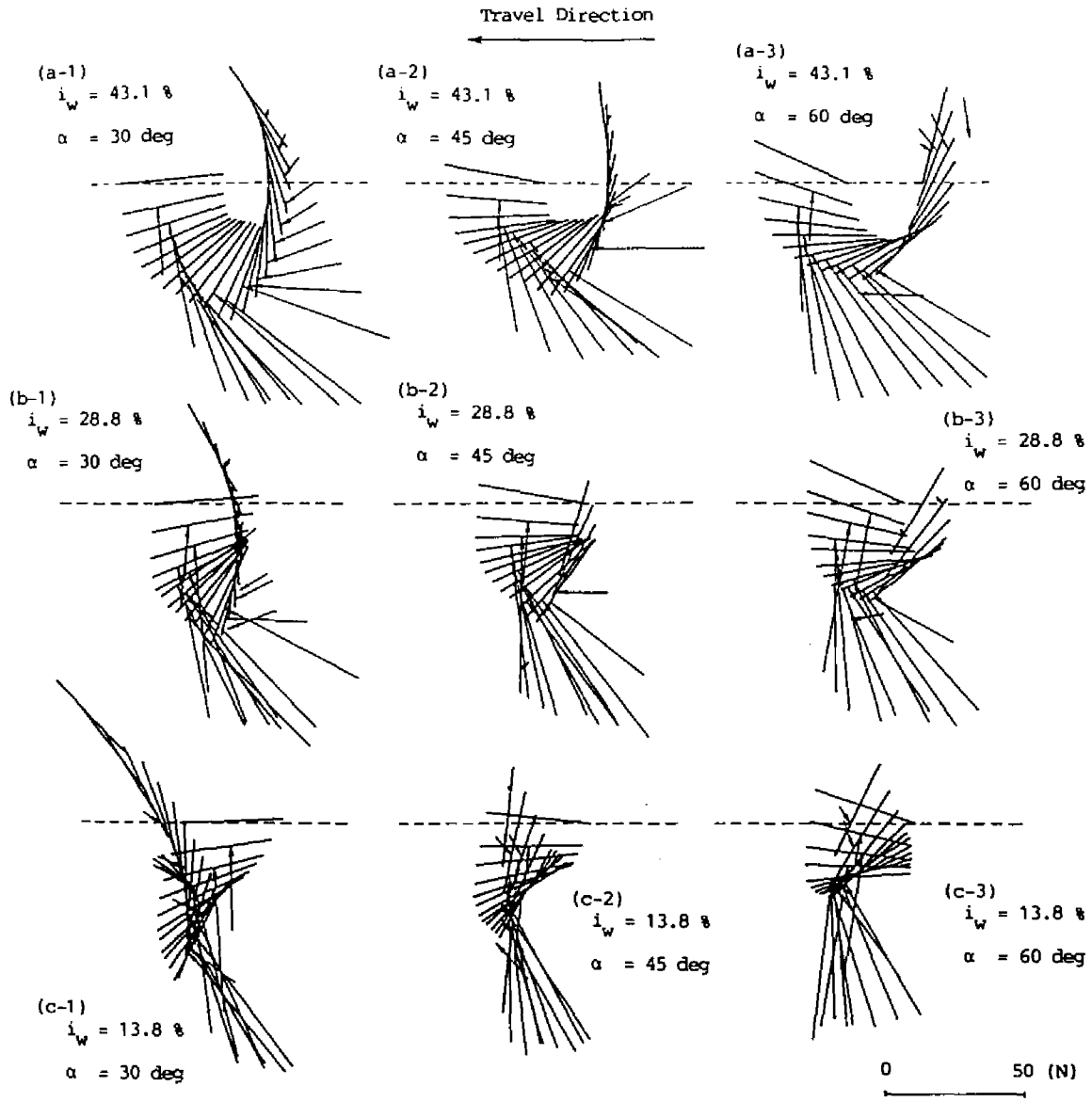

Fig.3-9. Result of soil reaction and lug loci for EXP-II (n_L=6).

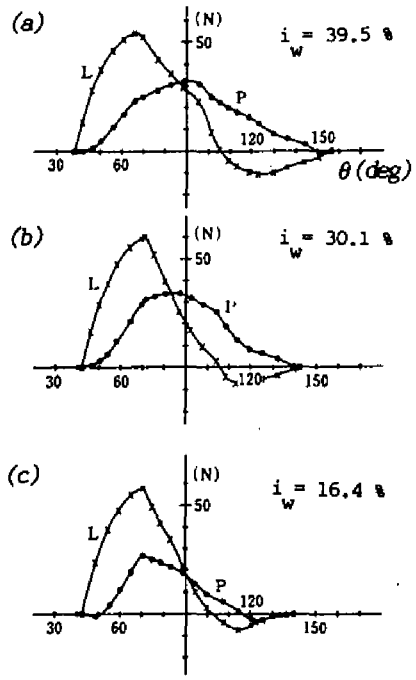

Fig.3-10. Pull and lift characteristics for EXP-I (n_L=12).

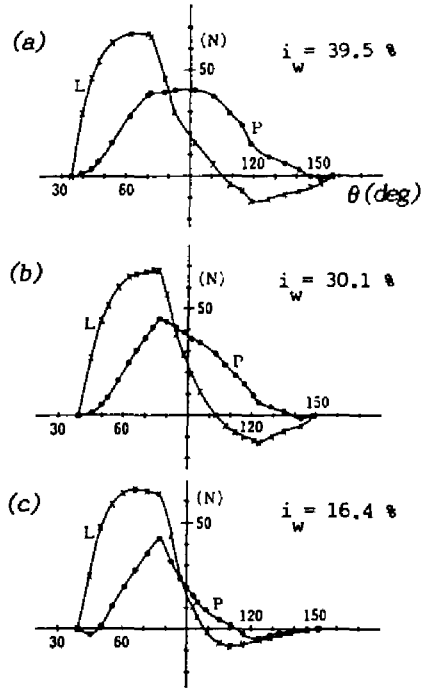

Fig.3-11. Pull and lift characteristics for EXP-I (n_L=9).

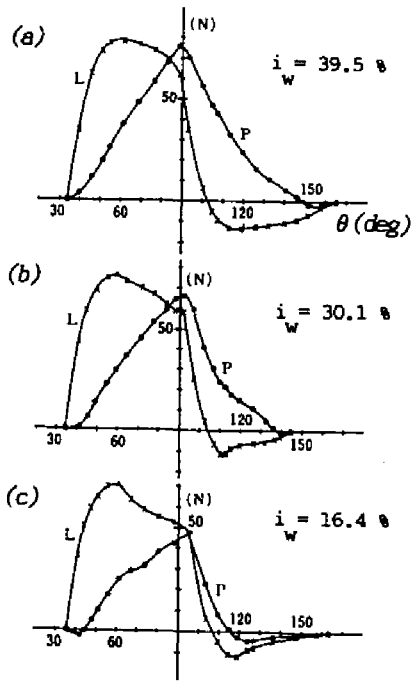

Fig.3-12. Pull and lift characteristics for EXP-I (n_L=6).

It is interesting to note that the large negative lift is observed for i_w=39.5% in all cases. This means that the soil is pulled upward which would be useless in terms of flotation of wheel. As for pull force, the rotational position where maximum value P_{max} is observed translates to small rotational angle position as i_w decreases in Fig.3-10 and Fig.3-11. But in Fig.3-12, P_{max} is always generated at nearly the lowest position of lug outer tip (θ=90 deg). Negative pull is seen in i_w=16.4% case in all figures. It means that the opposite surface of lug plate is in contact with soil and the so-called bulldozing effect of lug becomes large, which can be seen in the results of the former section.

EXP-II

Figs.3-13, 3-14 are the examples for n_L=12 and n_L=6 respectively. In general, the value of L_{max} is nearly the same in each lug angle case in terms of n_L, which is the same tendency as in EXP-I. On the other hand, the value of P_{max} is decreasing as lug angle increased. Precise behavior of average P and L will be observed in the next section.

The case of small lug angle and i_w=43.1% or i_w=28.8% in both figures shows the interesting latter half lug action where $L<0$ and $P>0$ which means the action of upward push of soil by lug plate. And the tendency of shorter period of lug contact to soil is remarkable when α becomes large, which is the result of decreasing wheel sinkage.

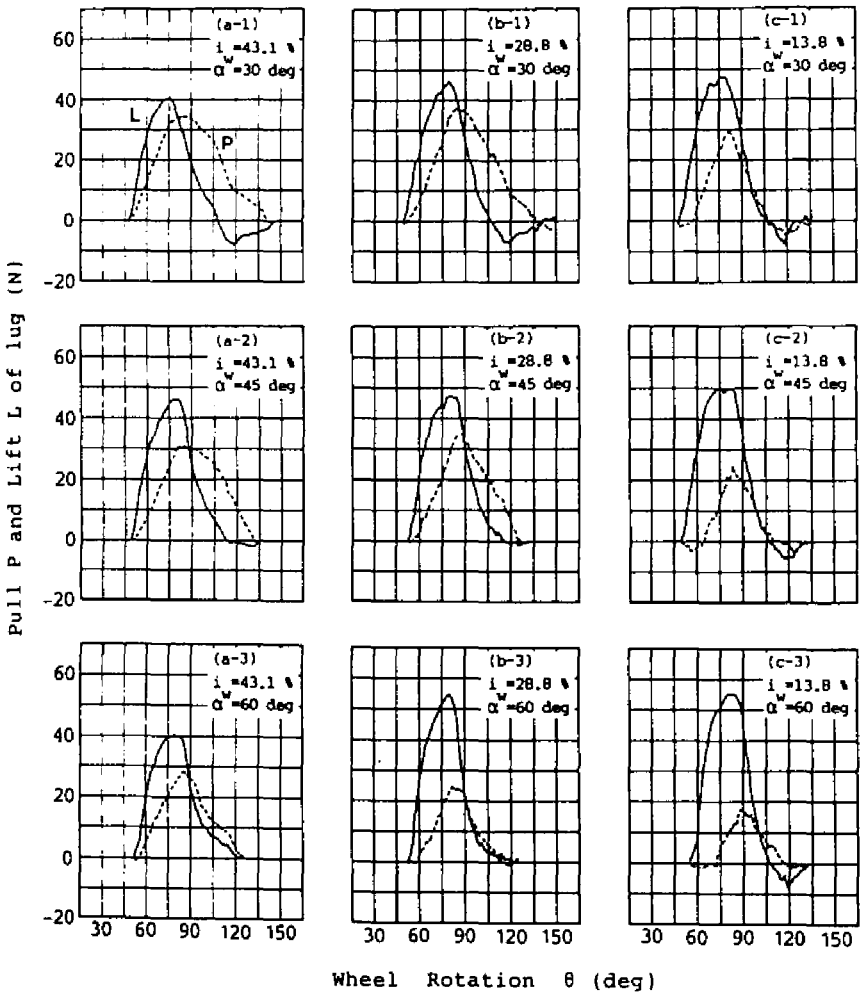

Fig.3-13. Pull and lift characteristics for EXP-II (n_L=12).

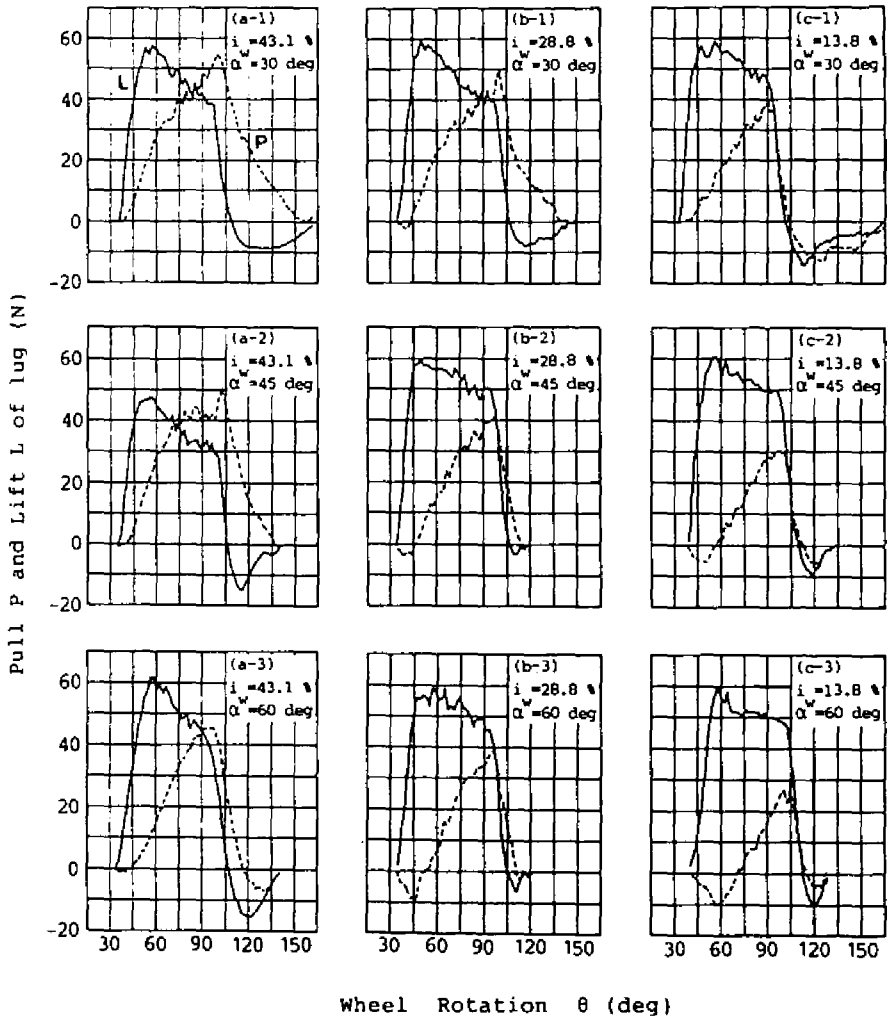

Fig.3-14. Pull and lift characteristics for EXP-II (n_L=6).

Angular position of R_{max} (θ_{rmax}) which is decided from the result is shown in Table 3-5 with the angle θ_{pmax} and θ_{lmax} where P becomes maximum and L becomes maximum respectively. From the table, in case of n_L=12, R_{max} and L_{max} are observed at the same rotational position which is independent of lug angle. As the slippage becomes small, positions of P_{max}, L_{max} and R_{max} become close one another.

Table 3-5. Rotational angle of R_{max}, P_{max} and L_{max} for EXP-II.

i_w (%)	n_L	α (deg)	θ_e *) (deg)	θ_{rmax} (deg)	θ_{pmax} (deg)	θ_{lmax} (deg)	ζ '**) (deg)	ϕ_{rmax} ***) (deg)
43.1	12	30	46.3	75.7	86.3	74.3	80.8	126.5
		45	48.4	80.8	82.8	80.8	87.4	123.2
		60	52.0	84.0	86.0	80.0	100.3	124.3
	9	30	40.8	72.8	87.8	67.8	81.1	123.9
		45	40.8	70.8	90.2	62.2	105.0	130.8
		60	45.0	74.0	86.0	68.0	103.7	117.7
	6	30	34.7	96.7	99.7	57.7	76.3	143.0
		45	36.0	76.0	102.7	56.0	108.5	139.5
		60	33.8	87.8	99.8	54.8	107.0	134.8
28.8	12	30	49.7	81.0	84.4	80.4	77.3	128.3
		45	51.4	82.7	85.4	81.4	87.0	124.7
		60	52.4	80.4	82.4	80.4	92.7	113.1
	9	30	41.5	73.5	88.2	66.8	77.3	120.8
		45	46.2	78.9	88.2	74.9	88.7	122.6
		60	43.5	71.5	84.5	67.5	95.0	106.5
	6	30	34.5	72.5	99.5	50.5	75.2	117.7
		45	34.5	95.9	98.5	53.2	80.7	131.6
		60	35.7	71.0	97.0	57.0	99.5	110.5
13.8	12	30	47.3	79.3	79.3	74.3	72.2	121.5
		45	50.7	83.3	84.0	77.3	77.1	115.4
		60	56.2	85.2	87.2	80.2	79.6	104.8
	9	30	43.9	72.5	85.2	64.5	73.8	116.3
		45	46.1	70.1	86.1	63.1	78.2	103.3
		60	50.3	76.3	91.6	72.9	79.9	96.2
	6	30	33.5	82.2	91.5	54.2	71.1	123.3
		45	36.6	55.9	97.3	55.9	78.4	89.3
		60	40.7	58.7	102.7	58.7	82.9	81.6

NB: *)Entry angle of lug into soil
**)Angle between R_{max} and lug plate defined from lug outer tip A
***)Angle between R_{max} and horizontal plane measured from travel direction

For the cases of n_L=9 and n_L=6, L_{max} is observed at about 20 deg rotation from the entry of lug into soil and P_{max} is generated at the rotational angle difference after contact of about 40 deg and about 60 deg respectively. The angle for R_{max} locates between θ_{pmax} and θ_{lmax} and remarkable influence of lug angle can not be seen.

Angle of R_{max} to horizontal line from travel direction (ϕ_{rmax}) decreases for each n_L case and α with the decrease in wheel slippage. This result might correspond to the tendency in slip-drawbar pull relation for tires where the larger drawbar pull is generated as the wheel slippage becomes large and the angle of reaction vector to horizontal line becomes large.

3.3.3 Effect of Lug Angle on Average Soil Reaction

Result of EXP-II is used to verify the effect of lug angle on behavior of average P and L. Average P (P_{ave}) and average L (L_{ave}) of lug were calculated by numerical integration whose graphical meaning was the division of surrounded area between the curve of P or L and zero reaction line and the angular period of contact of lug to soil.

Fig.3-15 shows the result of calculation. As can be seen in the figure, L_{ave} increases whereas P_{ave} decreases with the increase in lug angle. The reason of this is considered as the result of strong interrelation of the decrease in wheel sinkage as lug angle increases with the decrease in total effective area of lugs in contact with soil. This is different from single lug tester results with constant sinkage, where both P_{ave} and L_{ave} increase with the increase in α (for example, Gee-Clough *et al.*,1976). L_{max} is generally independent from lug angle for each n_L as in Figs.3-13 and 3-14. As for P_{ave}, the combined effect of the increase in P_{max} and in wheel sinkage with the

decrease of α might affect the increase of P_{ave} for i_w=43.1% and i_w= 28.8%. In i_w=13.8% case, P_{ave} seems to be almost constant with the variance of α in each n_L cases, since V_c becomes large and this might cause the shorter period of pull generation of lug, and thus results in weak pull generation at α=30 deg.

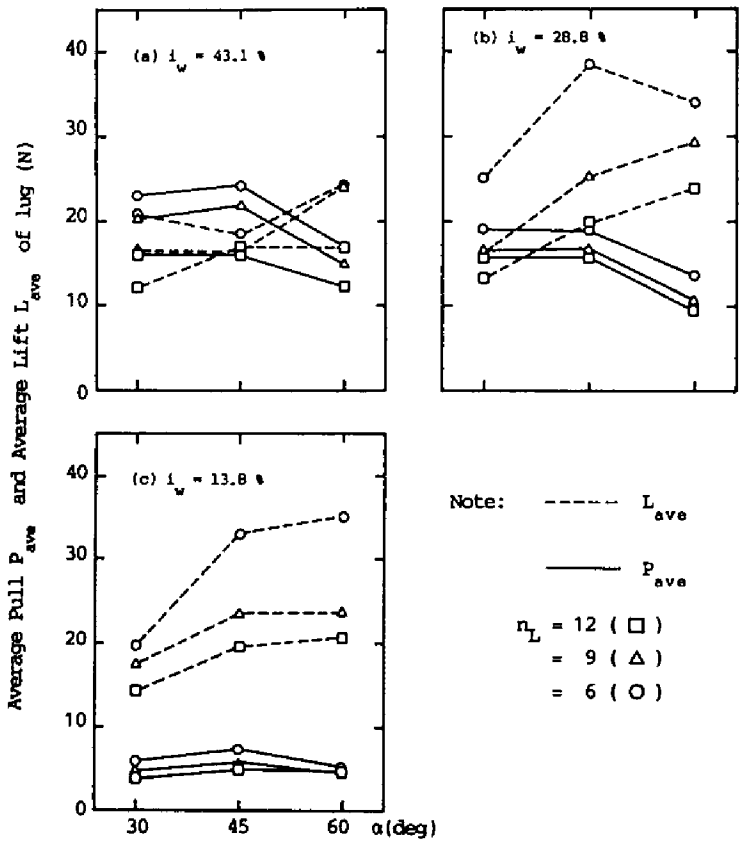

Fig.3-15. Relation of average pull and average lift.

3.3.4 Effect of Wheel Load and Lug Angle on Wheel Sinkage

Results of EXP-II and EXP-III are shown in Figs.3-16 and 3-17 respectively to clarify the effect of lug angle on wheel sinkage (Fig. 3-16) and the load-sinkage relationship of wheel (Fig.3-17). Wheel

load (WL) and wheel sinkage (Z) have in fact the meaning of average value in the lug-soil contact mechanism.

Wheel load fluctuates in principle from the variation in counter weight moment around O_s in Fig.3-1 caused by the instantaneous change of acting point of soil reaction on a lug. The given WL is in this sense the average value and this is verified by the numerical averaging of L by considering the lug spacing over lug contact period.

EXP-II

In Fig.3-16, it is obvious that lug angle has the clear influence on wheel sinkage, that is the increase in lug angle cause the decrease in wheel sinkage for all wheel sinkage cases. Dotted line in the figure is the regression equation;

$$Z = A_1 n_L + A_2 \alpha + A_3 \tag{3.8}$$

The calculated coefficients of Eq.(3.8) are listed in Table 3-6. Precise look on the coefficients reveals the interesting point that the wheel sinkage in i_w=13.8% case shows the relatively large effect of lug angle and this might be caused the strong negative action of lug to soil in α=30 deg which is regarded as bulldozing or soil cutting.

Table 3-6. Coefficients of regression analysis for Fig.3-16.

i_w(%)	A_1	A_2	A_3	R^2
43.1	-0.34333	-0.06190	10.37780	0.94635
28.8	-0.39104	-0.04852	10.07670	0.97083
13.8	-0.35813	-0.07583	10.87290	0.94860

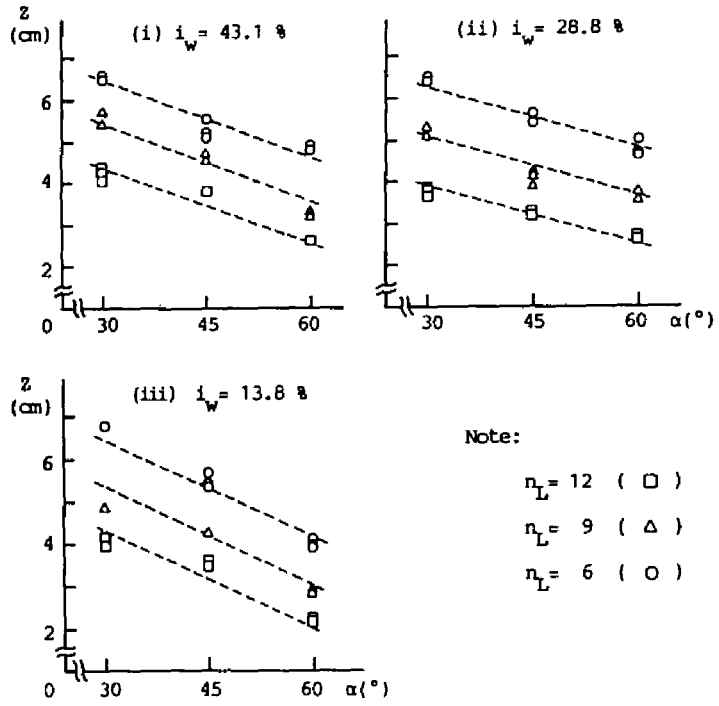

Fig.3-16. Relation of lug angle on wheel sinkage for EXP-II.

EXP-III

As shown in Fig.3-17, in all n_L cases, average sinkage Z_a becomes large in 30 deg lug angle. And for α=45 deg and α=60 deg, Z_a does not show large difference. It is also obvious that the relationship of wheel load and Z_a is almost linear, except for n_L=6 case. The sudden relaxation of gradient of graph for large WL in Fig.3-17(c) is regarded as the strong influence of the wheel flange contact to the soil which was occurred as the wheel sinkage increased.

By the regression analysis, the relation of wheel load and wheel sinkage with lug angle for each n_L can be expressed as follows;

$$Z = A_1\alpha + A_2WL + A_3 \tag{3.9}$$

Table 3-7 shows the coefficient list of Eq.(3.9). It is interesting to note that the coefficient for wheel load is rather large for n_L=6 case whereas that for lug angle becomes large for n_L=12 case.

Table 3-7. Coefficients of regression analysis for Fig.3-17.

n_L	A_1	A_2	A_3	R^2
12	-0.07414	0.07874	6.63536	0.94135
9	-0.06458	0.08498	6.89939	0.89735
6	-0.02541	0.13340	4.59717	0.83402

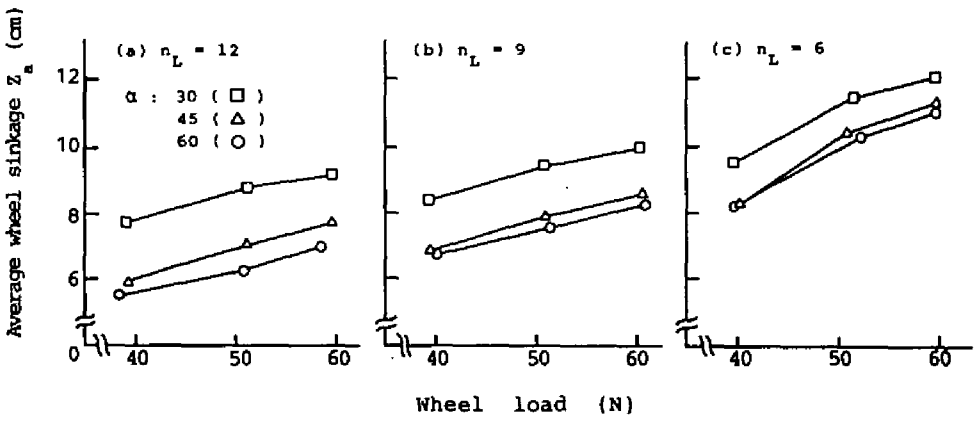

Fig.3-17. Relation of average wheel sinkage and average wheel load.

3.3.5 Traction Efficiency

Traction Efficiency η_t was calculated for the results of EXP-II and EXP-III and shown in Figs.3-18, 3-19. Calculation was done by using Eq.(3.7).

EXP-II

Multiple regression analysis was done for each wheel slippage with the data on lug angle and total lug number which were considered most significant factor for η_t. In Fig.3-18, the results of regression equation as follows are shown as dotted line for each i_w case;

$$\eta_t = A_1 n_L + A_2 \alpha + A_3 \tag{3.10}$$

The obtained coefficients for Eq.(3.10) are listed in Table 3-8. The clear tendency of increasing η_t with the decrease of α is seen in the figure, except for i_w=13.8%. And for i_w=43.1%, the effect of n_L is neglected though the data show ambiguity on linear relation. Current regression analysis is verified as follows; with R^2=0.29972, F-value for this regression becomes 6.8479 since the degree of freedom is 16 and lower limit F-value is 4.49 for the significance level of 0.05 (Kishine, 1974). The strong effect of n_L, instead of α, is shown in case of i_w= 13.8%. The reason of this behavior is explained by the insensitive influence of α on average pull of lug as shown in 3.3.3.

Table 3-8. Coefficients of regression analysis for η_t in EXP-II.

i_w(%)	A_1	A_2	A_3	R^2
43.1	0.00000	-0.25468	58.6220	0.29972
28.8	2.38496	-0.46288	51.5248	0.81742
13.8	2.33092	0.00000	20.2876	0.61677

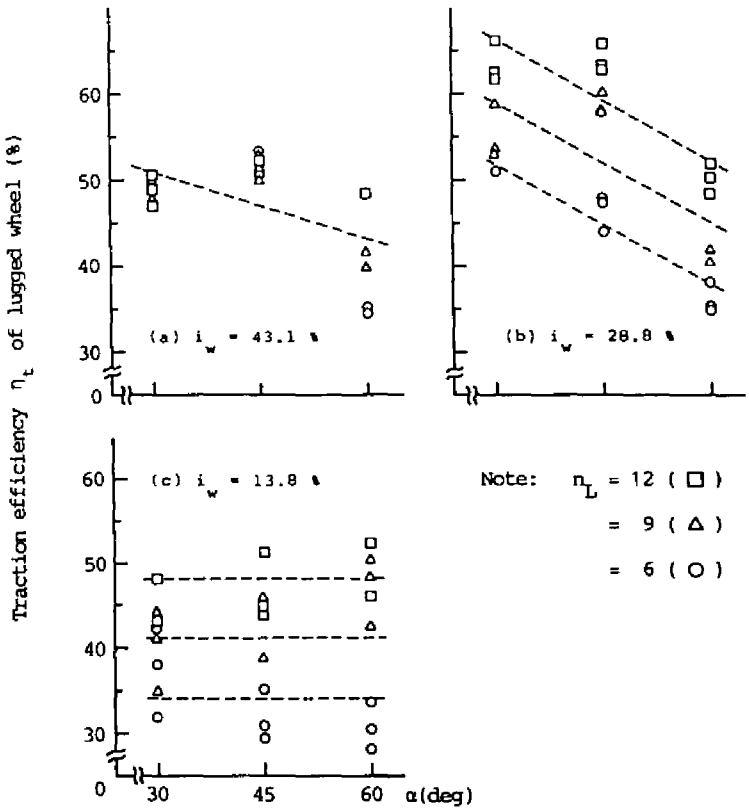

Fig.3-18. Result of traction efficiency for EXP-II.

EXP-III

It is clear, in Fig.3-19, that the large wheel sinkage which is caused by the large WL decreases η_t in all combination of α and n_L. Further precise look at the relation of n_L and η_t, however, shows the different tendency from the result of EXP-II. That is, the increase in n_L results in the decrease of η_t.

Table 3-9. Coefficients for η_t of EXP-III.

n_L	A_1	A_2	A_3	R^2
12	-0.39907	-0.55879	70.9329	0.81347
9	-0.38506	-0.26221	57.1535	0.77494
6	-0.57376	-0.54810	78.9098	0.88608

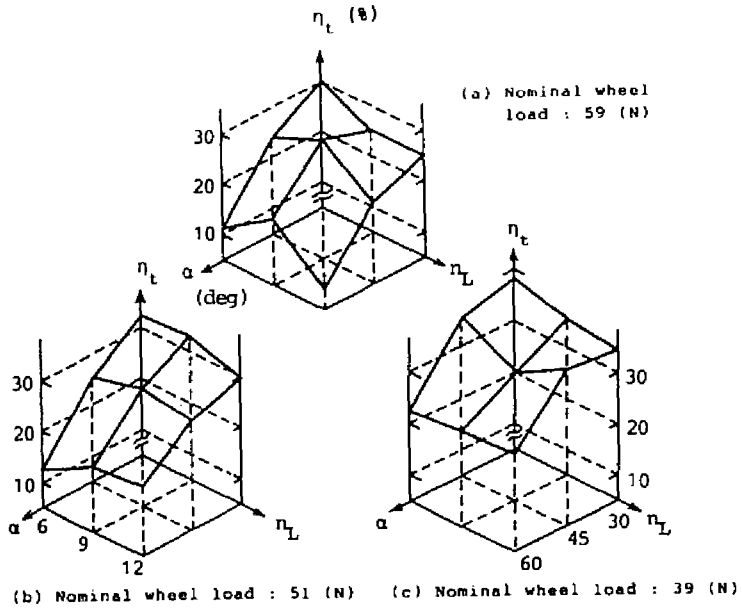

Fig.3-19. Result of traction efficiency for EXP-III.

In order to observe this in detail, the regression analysis was done with equation as follows;

$$\eta_t = A_1\alpha + A_2WL + A_3 \tag{3.11}$$

The coefficients list for Eq.(3.11) is shown in Table 3-9.

The reverse tendency of η_t in small lug angle case is obtained which is different from η_t in EXP-II. But, if it is observed in terms of n_L individually, the value of η_t by Eq.(3.11) clearly indicates the same tendency as in EXP-II that the traction efficiency becomes large as α decreases.

3.4 Sinkage Variation of Wheel

3.4.1 Assumption

In this experiment, the slippage is defined by Eq.(3.1) with V_w= 2.2 (cm/s) and average velocity of soil bin carrier V_c which was measured as the average speed of carrier prior to the experiment. This definition naturally involves the introduction of average wheel slippage, i.e. if the sinkage of wheel occurs in the real situation, V_c would vary with the magnitude of sinkage variation which is permitted in the present apparatus. Here, for the sake of easy understanding of behavior and implementation of later simulation, the variation of sinkage is assumed not to cause the severe effect on the slippage variation.

It is also assumed that the sinkage variation can be expressed as a simple trigonometric function of the form as follows;

$$Z = Z_0 \sin (\Omega t + \phi_0) + Z_a \qquad (3.12)$$

where Z_0 : amplitude of sinkage variation (cm)

Z_a : average sinkage (cm)

Ω : angular velocity which depends on n_L (rad/s)

ϕ_0 : phase shift at initial contact of lug to soil (rad)

Fig.3-20 shows two example data of sinkage variation of wheel and the result of approximation by Eq.(3.12). In the figure, the lateral axis is expressed in travel distance, although in Eq.(3.12) the function of Z is expressed for the time t, which was done for later use of Eq.(3.12). The expression of trigonometric function shows the well approximation of sinkage variation.

Obtained constants for Eq.(3.12) are listed in Table 3-10. Ω is

the value which depends on the total number of lug on a wheel, but slight variation is also seen in the figure because the resolution angle of A/D conversion clock was 2 deg wheel rotation. The effect of lug angle on Z_0 is not obvious in the table. The average sinkage Z_a varies with lug angle and wheel slippage.

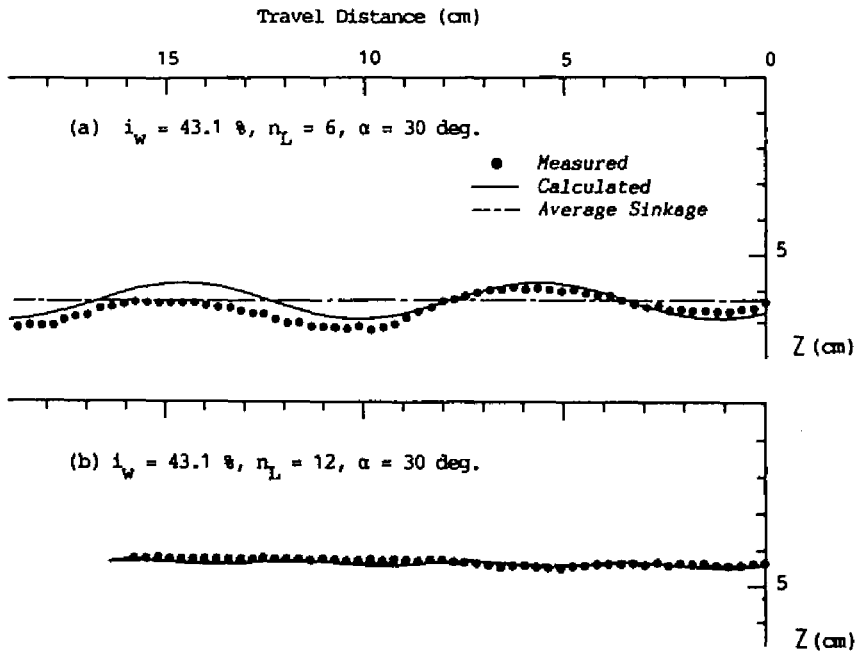

Fig.3-20. Example of sinkage variation of lugged wheel.

Table 3-10. Parameters for Equation (3.12) based on EXP II.

i_w	n_L	α	z_0	Ω	ϕ	z_a
43.1	12	30	0.088	1.8900	-0.2244	4.26
		45*	0.047	1.8900	-0.2244	3.75
		60	0.068	1.8900	-0.2244	2.47
	9	30	0.077	1.3230	0.3142	5.05
		45	0.283	1.3230	0.3142	4.76
		60	0.050	1.3230	0.3142	3.17
	6	30	0.487	0.88199	0.7330	6.31
		45	0.504	0.84524	0.7680	5.12
		60	0.224	0.85443	0.4582	4.71
28.8	12	30	0.123	1.8900	0.2244	3.63
		45	0.121	1.8900	0.2244	3.22
		60	0.132	1.8900	0.2244	2.52
	9	30	0.200	1.3230	0.4189	5.20
		45	0.185	1.3230	0.5236	4.18
		60	0.150	1.3230	0.6283	3.42
	6	30	0.564	0.85443	0.4516	6.35
		45	0.600	0.86362	0.7505	5.34
		60	0.246	0.88199	0.7330	4.58
13.8	12	30	0.086	1.8900	-0.2244	3.98
		45	0.093	1.8900	-0.2244	3.42
		60	0.093	1.8900	-0.2244	2.18
	9	30	0.135	1.3230	0.0000	4.75
		45	0.157	1.3230	0.0000	4.54
		60	0.132	1.3230	0.2094	2.73
	6	30	0.377	0.88199	0.3142	6.76
		45	0.475	0.88199	0.2443	5.26
		60	0.536	0.88199	0.2443	3.80

NB) i_w: wheel slippage (%)
n_L: total number of lug
α : lug angle (deg)
* : only one result data used

3.4.2 Equation for Velocity of Sinkage Variation and Lug Velocity

By differentiating Eq.(3.12) with respect to time t, the following sinkage variation velocity V_z can be derived.

$$V_z = \frac{dz}{dt} = z_0 \Omega \cos (\Omega t + \phi_0) \qquad (3.13)$$

Therefore, as shown in Fig.3-21, lug velocity at the lug outer

tip A can be calculated as the vector summation of V_C, V_W and V_Z at point A.

In general, for an arbitrary point P on a lug with distance d from A, x-and y-component of lug velocity V^P can be expressed as;

$$\begin{aligned} V_x^P &= V_C - V_w^P \sin(\theta + \lambda) \\ V_y^P &= V_z + V_w^P \cos(\theta + \lambda) \end{aligned} \qquad (3.14)$$

where

$$V_w^P = \frac{R_P}{R_0} V_w = R_P \omega$$

$$R_P = \sqrt{R_0^2 + d^2 - 2 R_0 d \cos\alpha}$$

$$\lambda = \tan^{-1}\left(\frac{d \sin\alpha}{R_0 - d \cos\alpha}\right)$$

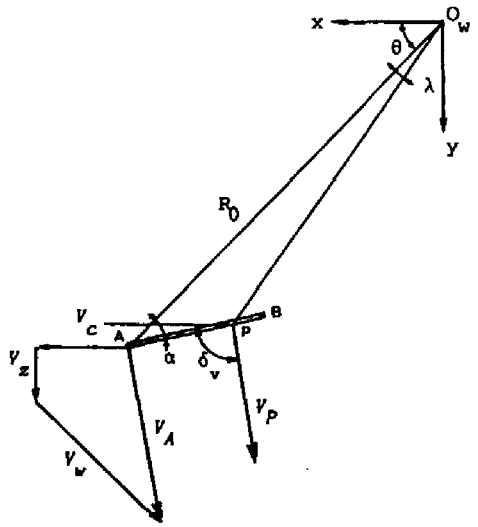

Fig.3-21. Representation of velocity vector of lug.

3.4.3 Relation of Velocity and Reaction Vector Direction

By calculating the velocity direction at R_{max} position on a lug, the relation of velocity and reaction vector is summarized as in Table 3-11, where δ_R corresponds to ϕ_{rmax} in Table 3-5.

Table 3-11. Acting direction of vectors V_{rmax} and R_{max}.

i_w (%)	n_L	α (deg)	v_x^R (cm/s)	v_y^R (cm/s)	δ_V (deg)	δ_R (deg)	$\Delta\delta$* (deg)
43.1	12	30	-0.7189	0.5508	142.5	126.5	16.0
		45	-0.7712	0.2073	165.0	123.2	41.8
		60	-0.8052	0.0328	177.7	124.3	53.4
	9	30	-0.6553	0.5000	142.7	123.9	18.8
		45	-0.7001	0.5777	140.5	130.8	9.7
		60	-0.8236	0.4557	151.0	117.7	33.3
	6	30	-0.7650	-0.0770	185.7	143.0	42.7
		45	-0.7068	0.2676	159.3	139.5	19.8
		60	-0.8948	0.1641	169.6	134.8	34.8
28.8	12	30	-0.4276	0.3290	142.4	128.3	14.1
		45	-0.4815	0.2329	154.2	124.7	29.5
		60	-0.5221	0.3924	143.1	113.1	30.0
	9	30	-0.3995	0.6508	121.5	120.8	0.7
		45	-0.4656	0.4329	137.1	122.6	14.5
		60	-0.4774	0.5501	131.0	106.5	24.5
	6	30	-0.4479	0.3805	139.6	117.7	21.9
		45	-0.4831	0.0339	176.0	131.6	44.4
		60	-0.4864	0.5132	133.5	110.5	23.0
13.8	12	30	-0.0812	0.3782	102.1	121.5	-19.4
		45	-0.1393	0.1898	126.3	115.4	10.9
		60	-0.2335	0.2273	135.8	104.8	31.0
	9	30	-0.0541	0.4622	96.7	116.3	-19.6
		45	-0.0546	0.3314	99.4	103.3	-3.9
		60	-0.1973	0.3002	123.3	96.2	27.1
	6	30	-0.0814	0.3576	102.8	123.3	-20.5
		45	0.1239	0.7177	80.2	89.3	-9.1
		60	0.0106	0.6245	89.0	81.6	7.4

*) $\Delta\delta = \delta_V - \delta_R$

In case of large wheel slippage, δ_V becomes larger than δ_R, which is considered as the result of combined influence of soil adhesion and interface friction. In i_w=13.8% case, especially at α=30 deg, negative angle difference ($\Delta\delta$) is seen. The effect of lug angle is

seen as the increase in $\Delta\delta$ with the increase in lug angle for every wheel slippage case. This increase in $\Delta\delta$ means the delay of the direction of reaction vector to the lug velocity vector and might be brought as the result of the change in friction condition at soil-lug interface.

Masuda *et al.*(1964) discussed the theoretical stress distribution on the lug surface based on Bekker's equation. According to their analysis, δ_R becomes larger than δ_V for sliding friction condition. Thus, above mentioned negative $\Delta\delta$ might be regarded as the effect of soil-lug interface slide and the increase of $\Delta\delta$ with lug angle in this sense means that the potential resistance against the sliding friction of lug becomes strong.

3.5 Conclusion

From some laboratory experiments for wet cohesive soil reaction on a lug of lugged wheel with non-confined wheel sinkage mechanism, several points were clarified as follows;

(1) Magnitude of soil reaction became maximum at about 30 deg after contact of lug to soil for the case of total lug number of 12. And for other total lug number cases, the rotational angle for maximum soil reaction located between the rotational angles for maximum pull and maximum lift for large wheel slippage, but the rotational angle for maximum soil reaction translated to that of maximum lift for small wheel slippage case.

(2) With almost the same wheel load condition, average pull increased and average lift decreased as lug angle became small in large wheel slippage. The increase in average lift for larger lug angle had the

relation with the decrease in average sinkage and thus effective area of lugs of lugged wheel in contact with soil. In case of small slippage of 13.8%, lug angle showed no remarkable effect on average pull for each total number of lug case.

(3) Wheel sinkage was verified to depend on total number of lug and lug angle for constant wheel load condition and on wheel load and lug angle for load-sinkage experiment. Clear influence of wheel slippage on wheel sinkage could not be found, except for the obvious dependency on lug angle for small wheel slippage case.

(4) Defined traction efficiency increased with the decrease in lug angle for each total lug number, except for small wheel slippage.

(5) Sinkage variation could be approximated by a trigonometric function as follows;

$$Z = Z_0 \sin(\Omega t + \phi_0) + Z_a$$

(6) The absolute direction angle of lug velocity vector measured from the travel direction of wheel at the acting position of maximum soil reaction on a lug became larger than the absolute direction angle of R_{max} vector except for small wheel slippage and small lug angle case where the effect of the sliding friction between lug and soil might be strong.

Chapter 4 EXPERIMENTAL ANALYSIS OF SOIL BEHAVIOR UNDER A LUG OF LUGGED WHEEL

4.1 Introduction

Soil behavior under a lug of lugged wheel is experimentally investigated in order to get the information on effects of lug parameters on soil deformation and on relation of the soil behavior which is the result of the action from lug and soil resistance, which was measured in Chapter 3, as the reaction from soil. First, the behavior of sand is investigated as the preliminary experiment(PRE). Second, the concurrent observations of wet cohesive soil behavior in EXP-I and EXP-II experiments of last chapter are done and the results are discussed in relation with soil reaction results of Chapter 3.

4.2 Experimental Condition and Apparatus

4.2.1 Experimental Condition

First, preliminary experiments were done using the standard sand with air-dried moisture condition. Table 4-1 shows the experimental condition on this investigation. Second, the serial experiments for wet cohesive soil behavior observation were done with soil reaction experiments on Tables 3-1 and 3-2 in Chapter 3.

Table 4-1. Experimental condition for PRE.

Number of Lug :	6, 9, 12
Lug Angle (deg):	30
Slippage (%) :	15.0, 26.0, 40.0
Wheel Load (N) :	19.6

4.2.2 Experimental Apparatus

For preliminary experiments, the facility was constructed as shown in Fig.4-1. The forced slippage with free sinkage principle was also adopted. Lugged wheel was 30 cm in diameter and 12 cm in width with the lug of 4 x12 x0.4 cm. Main experiments (EXP-I, EXP-II) were concurrently done in the former reaction experiments with the same facility as in Fig.3-1 of Chapter 3.

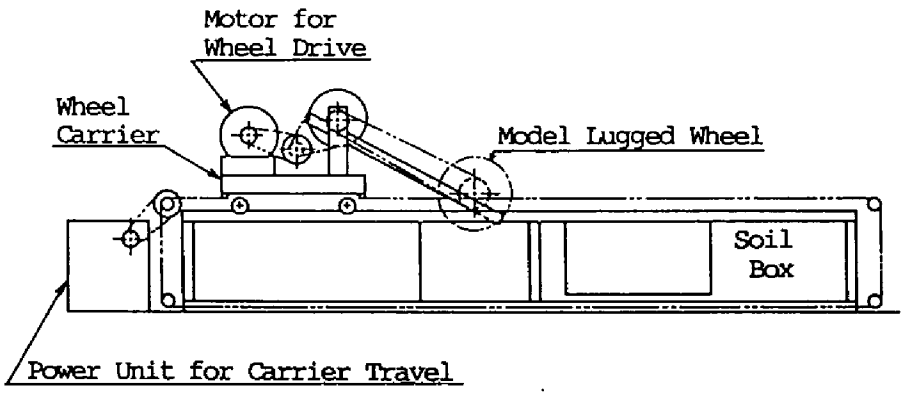

Fig.4-1. Schematic diagram of apparatus for PRE.

4.2.3 Visualization of Soil Deformation and Data Processing

Preliminary Experiment for Sand

The behavior of sand was visualized by drawing horizontal parallel flow line for every 2 cm interval with white or red chalk powder beforehand. The scale of length was supplied by attaching the ruler on the glass of soil box. At the experiment, successive photos were taken by a camera with motor drive unit and they are reproduced in B6 size (128 x182 mm) later. The flow line and boundary shape were

traced to get the information on behavior of sand under a lug. An example of PRE result is shown in Fig.4-2.

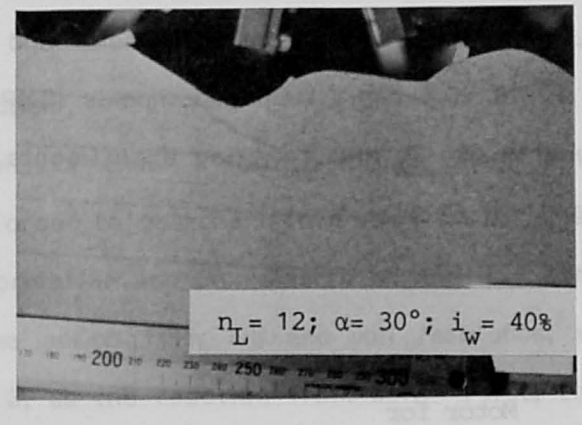

Fig.4-2. Example of sand behavior under a lug.

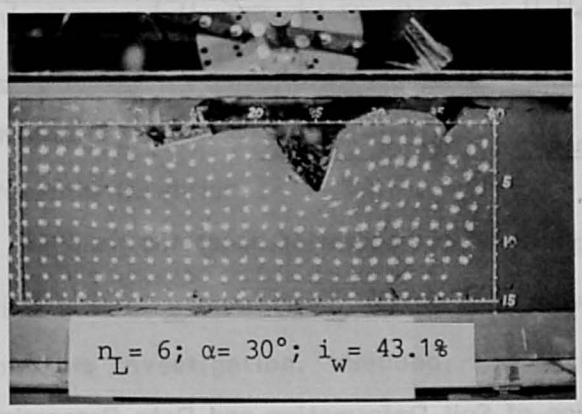

Fig.4-3. Example of loam behavior under a lug.

Experiments for Wet Cohesive Soil

For deformation investigation of wet cohesive soil, the white dot markers of 3 mm diameter were drawn on the side of soil with 1.5 x1.5 cm spacing.

Successive photos were taken manually (EXP-I) by a camera or automatically by a camera with motor drive unit (EXP-II). The photos were also reproduced in B6 size to trace the movement of markers, lug and free soil surface. Physical scaling of length could be checked by the scale units which were drawn on the glass.

To understand the deformation within soil visually, the regular quadrilateral grid was drawn in the data reading process by connecting the surrounding four markers. Thus, serial expression of soil deformation could be obtained by tracing the same dot markers. The meaning of grid line deformation is as follows; when the horizontal grid lines sink or rise from the original position, then the soil is mobilized downward or upward respectively and either backward or forward deformation of vertical grid lines implies the corresponding traction or bulldozing effect which was generated by a lug of lugged wheel. An example of EXP-II is shown in Fig.4-3.

4.3 Result of Soil Behavior and Discussion

In this section, results from PRE on sand and from EXP-II on wet loam soil are mainly used and the difference of soil flow under a lug is clarified.

4.3.1 Preliminary Result of Sand Behavior

Figs.4-4, 4-5, 4-6 and 4-7 show typical results of PRE for sand. Lug angle was fixed to 30 deg and the wheel traveled on the sand surface without contacting the glass of soil box in order to avoid frictional soil reaction which might cause the unusual wheel sinkage. Therefore, each lug cannot be seen except for the inner tip and wheel

flange, by which estimated lug position is obtained and shown in dotted lines in the figures.

40% wheel slippage

In Fig.4-4 for n_L=12 case, the first flow line below the sand surface shows the downward swell which corresponds to the downward action of lug in Fig.4-4(a). This swell line finally creates the fold point in Fig.4-4(e) with upward rise of the interim part between low-

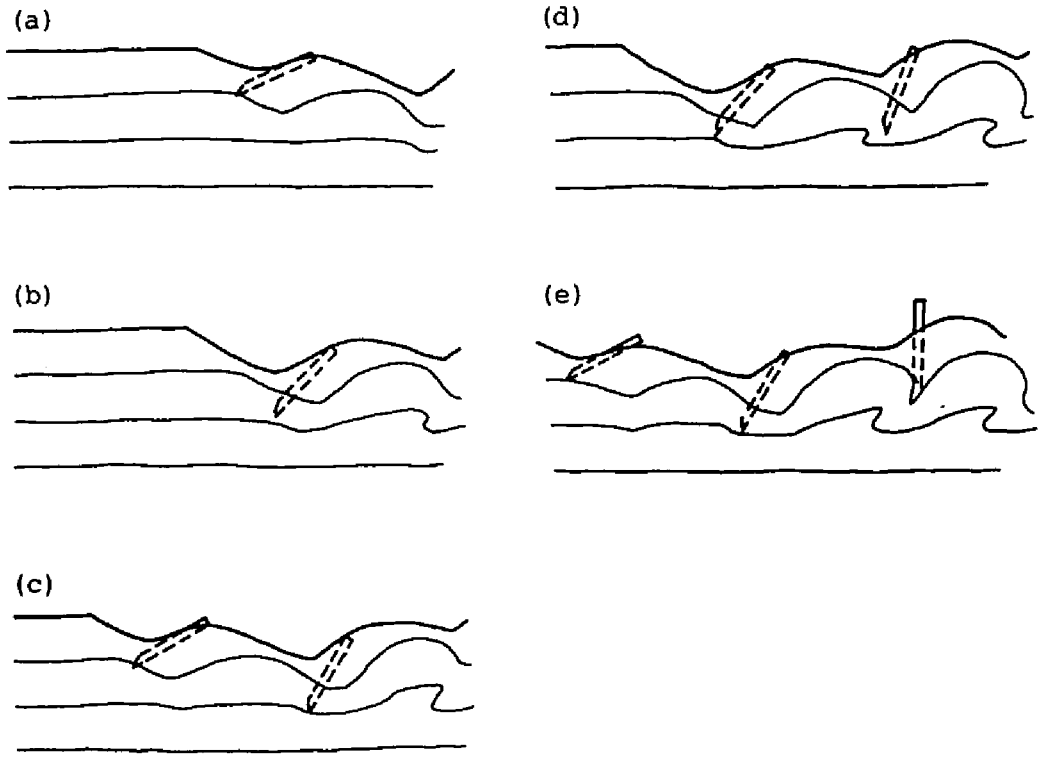

Fig.4-4. Result of sand behavior for n_L=12 and i_w=40%.

est points of flow line. Second flow line below the surface shows more interesting behavior of wave-like swelling generation which might be caused by the subsequent lug action on the sand which was confined by the preceding lug. It should be noted that the lug cavities are successively buried by the sand which flows in from the frontal sand surface. And no discontinuity in flow lines can be observed, which might be the result of the non-contact setting of lugs to the glass.

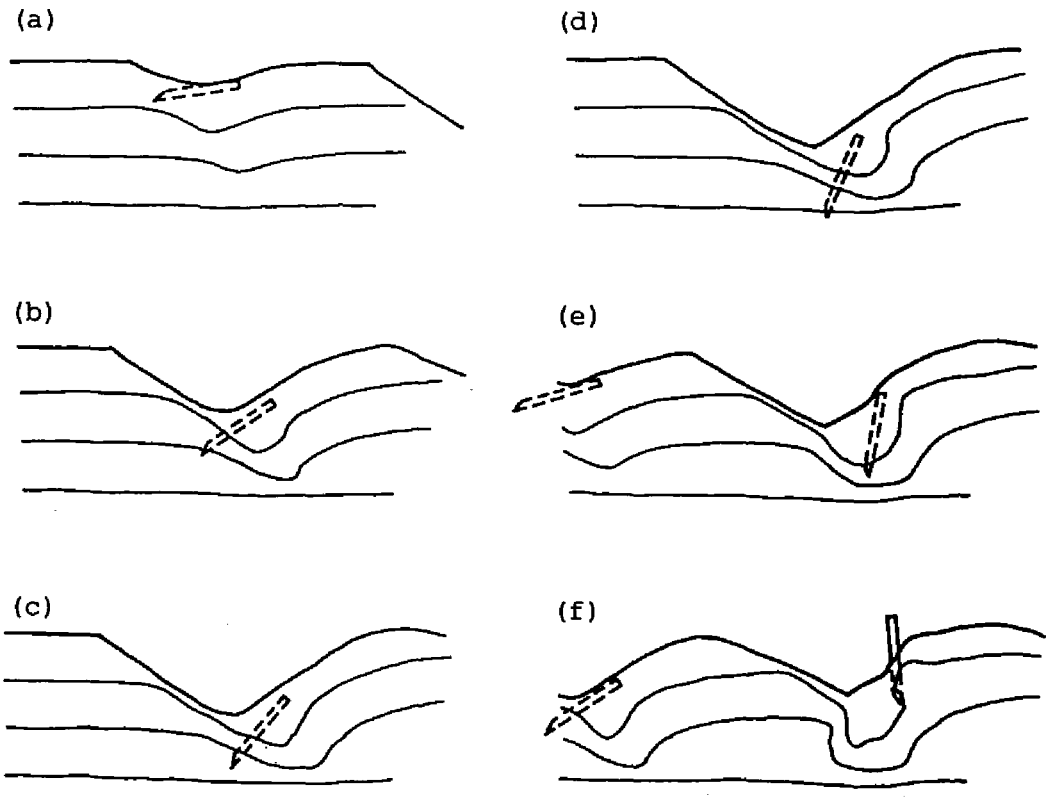

Fig.4-5. Result of sand behavior for n_L=6 and i_w=40%.

For n_L=6 case as in Fig.4-5, above stated phenomenon of inflow of sand which lies in front of lug to the lug trench is remarkable and continues until the lug reaches the rotational angle of 90 deg. After that angle, the action of lug is changed to upward and the first flow line shows the upward change of shape. Clear wave-like swellings are not seen in the second flow line. And no discontinuity in flow lines can also be observed in this case.

15% wheel slippage

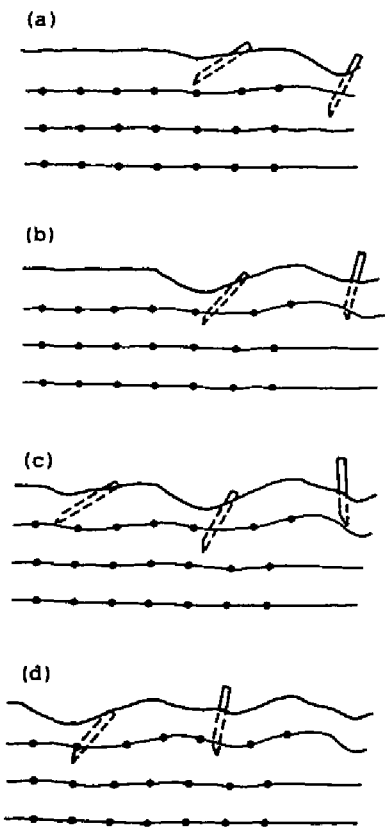

Fig.4-6. Result of sand behavior for n_L=12 and i_w=15%.

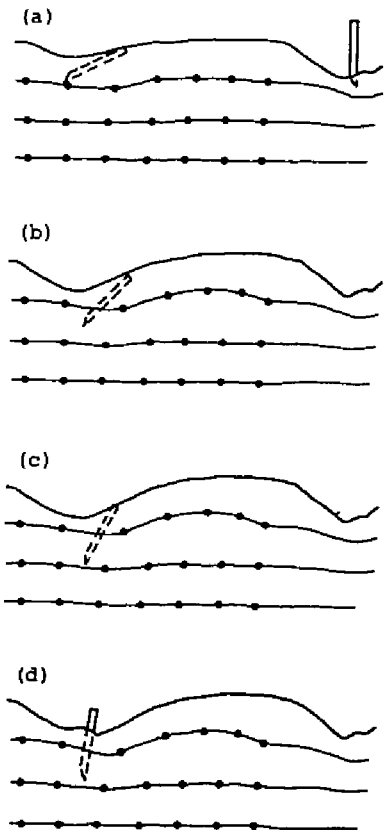

Fig.4-7. Result of sand behavior for n_L=6 and i_w=15%.

Figs.4-6 and 4-7 are the result of n_L=12 and n_L=6 respectively. In these figures, the flow lines are observed in detail by adding the discontinuous chalk marks for every 2 cm distance.

In Fig.4-6, after the entry of lug into soil, the sand which exists at the first flow line under surface between successive lugs is only mobilized by the action of lugged wheel. Except for the area below the lug plate, severe downward deformation of flow line cannot be seen. And as in the former slippage case, the self burying phenomenon of lug cavity by sand is also seen.

In Fig.4-7, the same tendency can be stated as in Fig.4-6. Additional upward rise became evident in the first flow line.

4.3.2 Result of Wet Cohesive Soil Behavior

The typical results on wet loam behavior under a lug in EXP-II are shown from Fig.4-8 to Fig.4-17. Intermediate experimental conditions such as n_L=9, i_w=28.8% and lug angle of 45 deg are selectively omitted. Dotted lines in those figures are estimated lug cavities which could not be observed because of soil adhesion to glass. And the lug with force measurement sensors is expressed in black line with the symbols **A** and **B**.

43.1% wheel slippage

Fig.4-8 is the result of n_L=12, i_w=43.1% and α=30 deg. Remarkable change of distances between neighboring marker dots which are considered as discontinuities in velocity field cannot be observed. And the action of lug is localized to the soil which locates between successive lugs, where the upward elongation of grid is remarkable especially at the latter part of lug rotation.

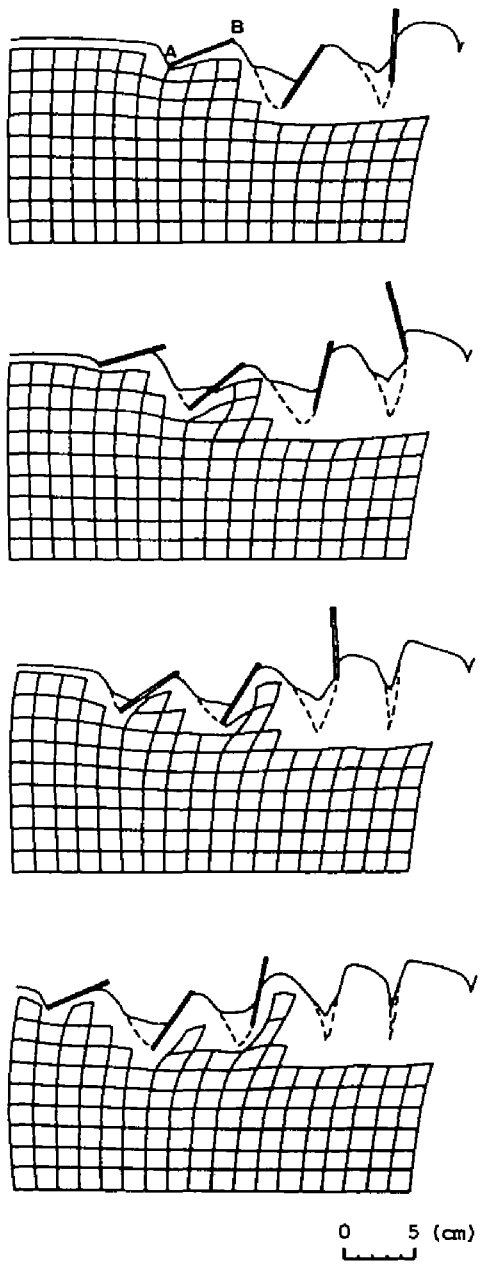

Fig.4-8. Wet loam behavior for n_L=12, α=30 deg and i_w=43.1%.

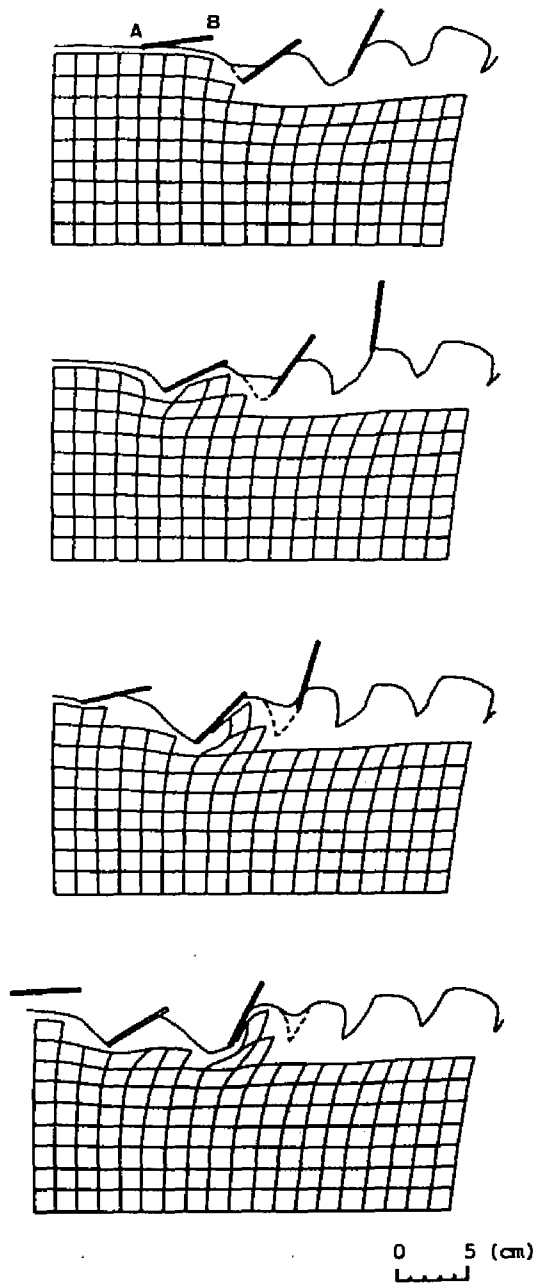

Fig.4-9. Wet loam behavior for n_L=12, α=45 deg and i_w=43.1%.

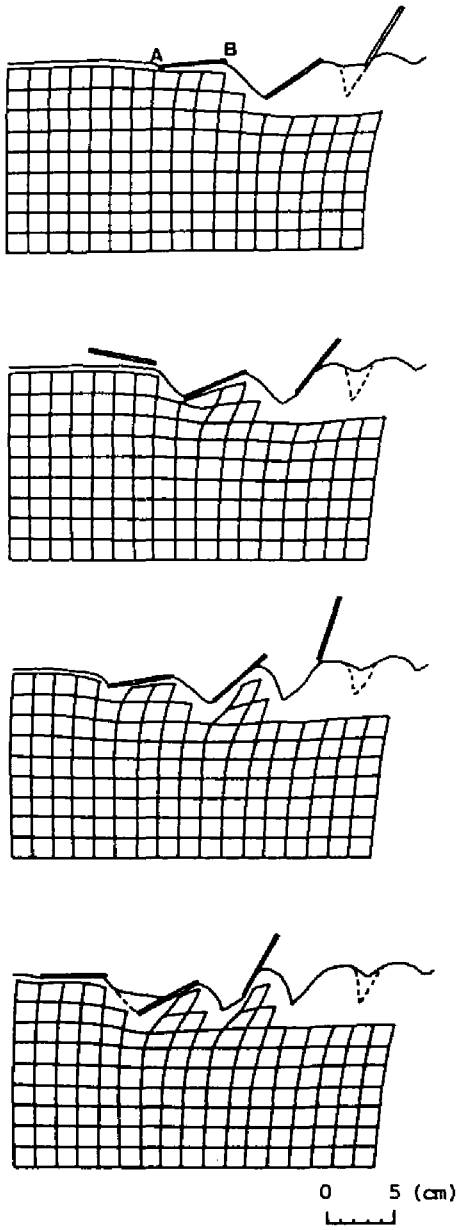

Fig.4-10. Wet loam behavior for n_L=12, α=60 deg and i_w=43.1%.

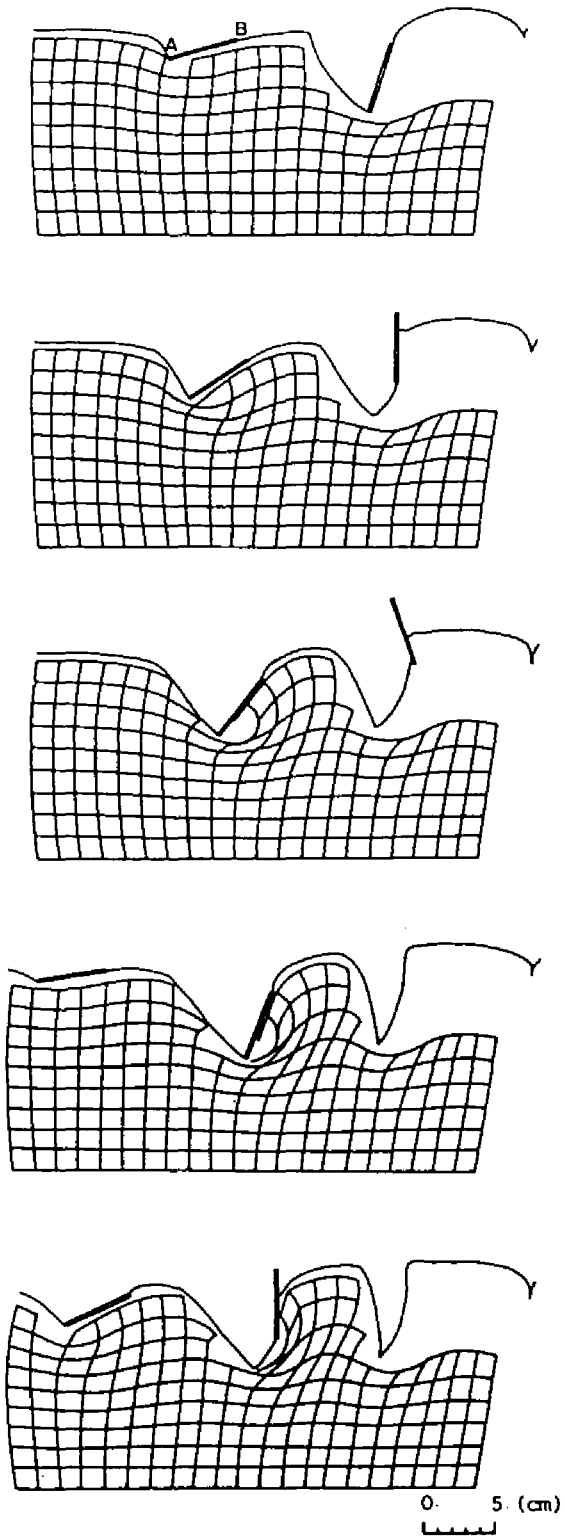

Fig.4-11. Wet loam behavior for n_L=6, α=30 deg and i_w=43.1%.

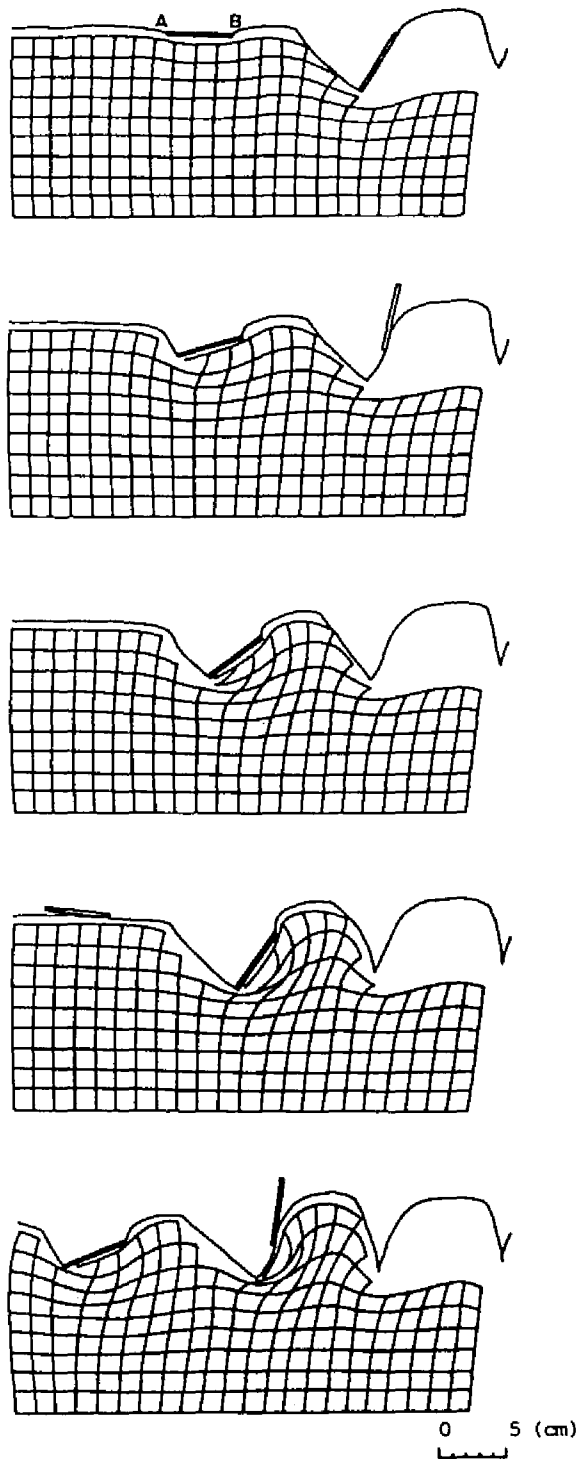

Fig.4-12. Wet loam behavior for n_L=6, α=45 deg and i_w=43.1%.

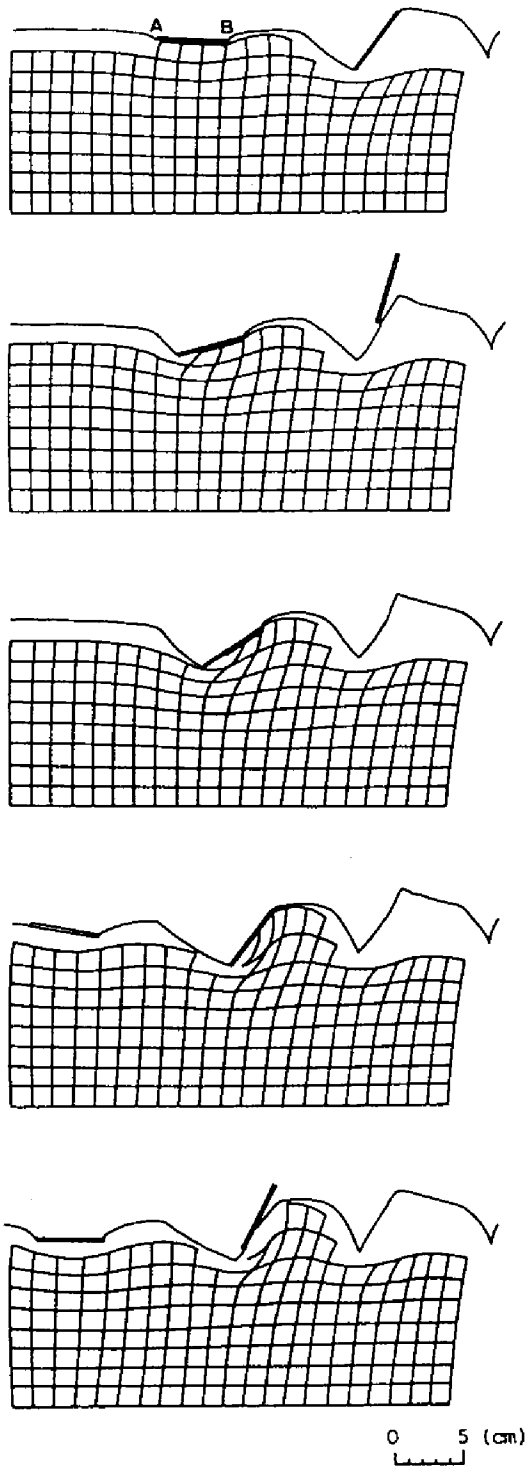

Fig.4-13. Wet loam behavior for n_L=6, α=60 deg and i_w=43.1%.

Fig.4-9 is the result of n_L=12, i_w=43.1% and α=45 deg case. Same tendency can be stated as in Fig.4-8.

Fig.4-10 is the result of n_L=12, i_w=43.1% and α=60 deg. Slightly different behavior of grid deformation can be observed, where the backward push of soil by lug plate becomes very weak. This would be expressed as the weakened backward bending of vertical grid lines just after the lug.

Fig.4-11 shows the result of n_L=6, i_w=43.1% and α=30 deg. At the initial contact, there is the vertical forward displacement of grid lines, which means that the soil is slightly pushed forward as the engagement of lug into soil. At the same time, the soil is pushed downward and then backward as the wheel rotates. Two things is especially noted; one is that the soil just below the lug plate does not deform until the lug passes about 90 deg wheel rotation angle. This non-deforming region may be called "boundary wedge", as shown by Wu *et al.*(1984). The other thing is that there exists the severe deforming region just below the boundary wedge and this is regarded as insufficient or localized slip line which does not reach to the free soil surface. Except for this severe deformation, the deformation behavior of grids is generally not excessive.

Fig.4-12 represents the result of n_L=6, i_w=43.1% and α=45 deg. Same tendency is observed for this case as in Fig.4-11.

Fig.4-13 depicts the case of n_L=6, i_w=43.1% and α=60 deg. In this figure, the grid deformation between successive lugs becomes clearly weakened, with the same tendency for localized deformation just below the lug plate.

13.8% wheel slippage

Fig.4-14 shows the result of n_L=12, i_w=13.8% and α=30 deg. The soil is mobilized forward by the back side of lug plate when the lug rotation becomes larger than about 100 deg, which is visualized by the clear forward deformation of vertical grid lines near the left side of lug plate in attention. And backward push of lug becomes very weak and localized at some part of soil between lugs. Severe deformation of grids on soil which locates between lugs which is seen as in Fig. 4-11 never appears in this case.

Fig.4-15 shows the result of n_L=12, i_w=13.8% and α=60 deg. Both forward and backward action of lug is no more remarkable than the case in Fig.4-14.

Fig.4-16 is the case for n_L=6, i_w=13.8% and α=30 deg. The combined effect of soil slip on the lug plate and the scratching up of soil by back side of lug generates the remarkable soil free surface deformation. As already stated in the case of n_L=12, strong backward push behavior of lug and the severe localized deformation of grids do not appear.

Fig.4-17 describes the result of n_L=6, i_w=13.8% and α=60 deg. In this case, there only exists the weakened action of lug for both backward and downward as in Fig.4-15.

4.3.3 Discussion

As shown in 4.3.1 and 4.3.2, the sand behavior is totally different from the wet cohesive soil behavior. That is, the phenomenon of self burying of lug cavity is the typical character of wind-dried sand behavior. For wet loam soil, such behavior never appears and free soil surface changes its shape with the wheel rotation, as Wu *et al.*

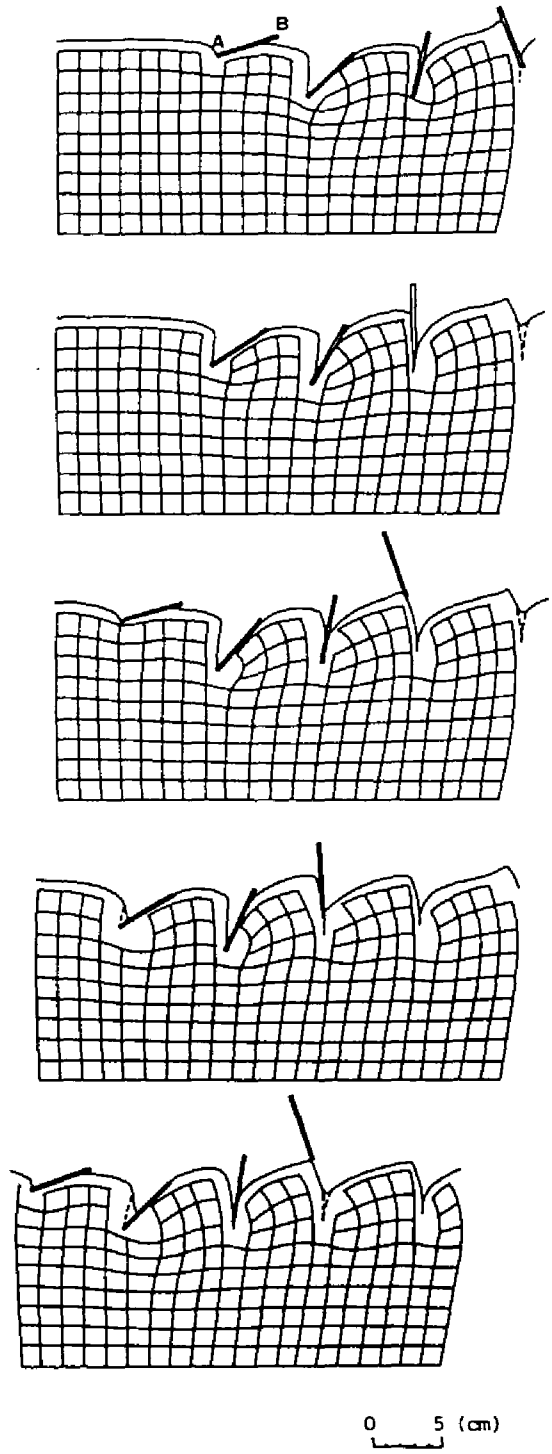

Fig.4-14. Wet loam behavior for n_L=12, α=30 deg and i_w=13.8%.

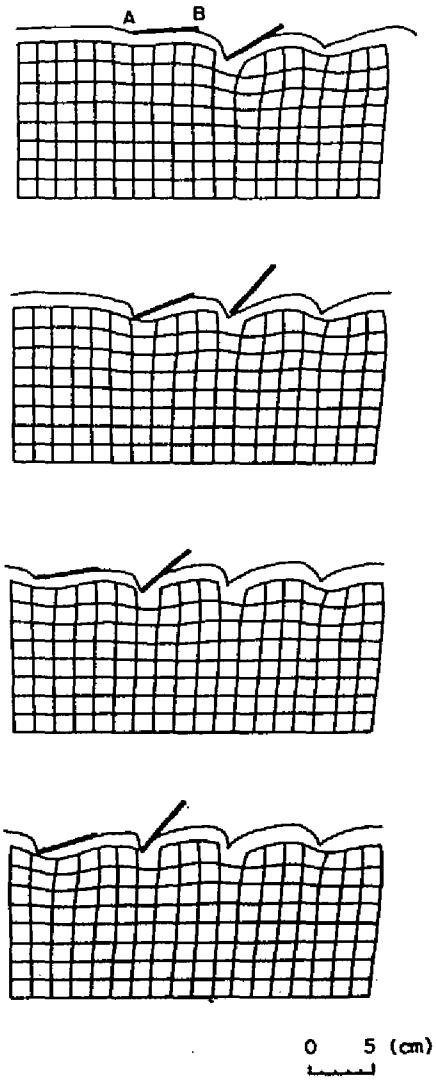

Fig.4-15. Wet loam behavior for n_L=12, α=60 deg and i_w=13.8%.

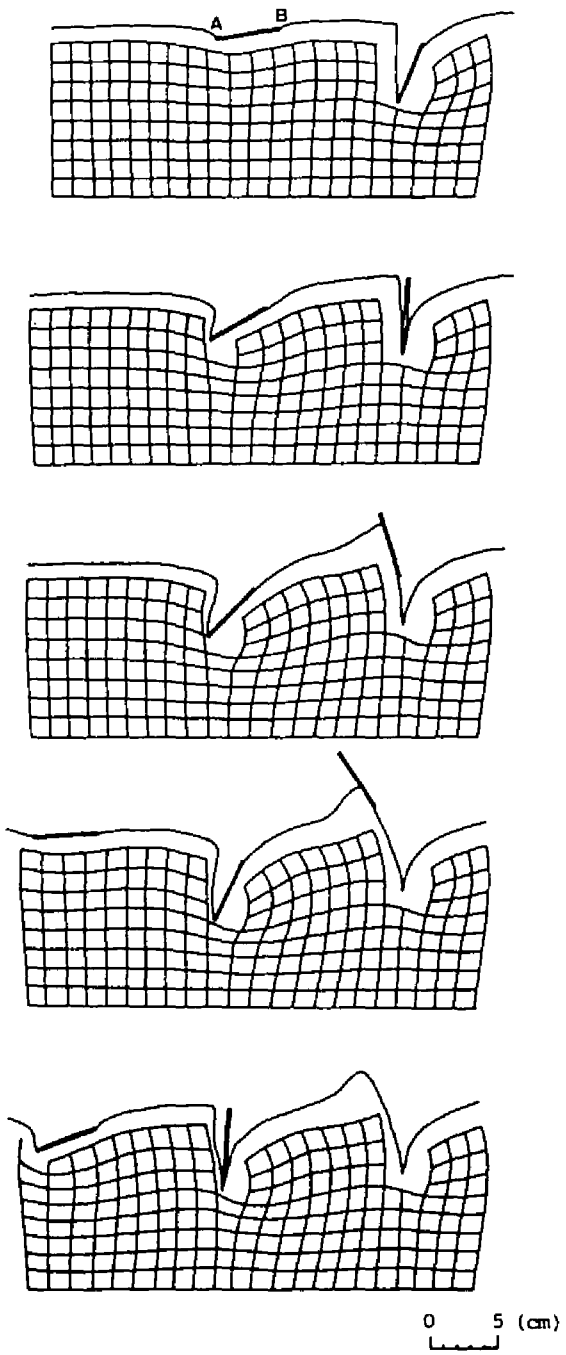

Fig.4-16. Wet loam behavior for n_L=6, α=30 deg and i_w=13.8%.

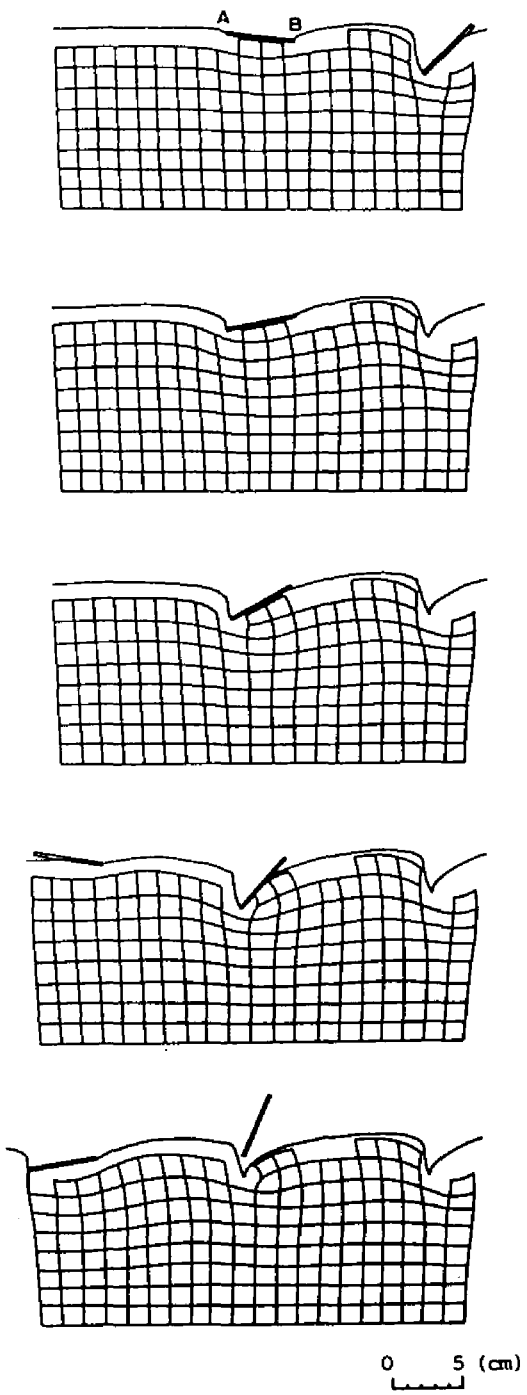

Fig.4-17. Wet loam behavior for n_L=6, α=60 deg and i_w=13.8%.

(1984) pointed out. Thus, the study of behavior for wet soil condition is very important to observe the practical soil flow under lug.

The effect of slippage on soil behavior is easily understood by the change in horizontal and vertical grid lines between lugs. In i_w= 43.1%, the component of backward displacement exists for both lug outer tip loci and inner tip loci. Therefore, the soil under lug suffers the backward push action from the lug, which is visualized as the rightward expansion of vertical grid lines for both n_L=12 and 6 condition. For i_w=13.8% case, the lug outer tip creates the slight backward displacement, whereas the inner tip of lug no longer shows the backward displacement in its loci as in Fig.3-8 or in Fig.3-9. Thus, the expansion of vertical grid lines in the right becomes weakened and the increase in bulldozing resistance will cause the useless expenditure of input energy for wheel traction. Downward swelling of horizontal grid lines is proportional to the wheel sinkage. If the wheel sinkage is large as in Fig.4-11, then the input energy from wheel shaft might be used for soil compression and overriding of soil just below the lug and this work will increase as the wheel sinkage becomes large. Thus, as stated in Chapter 3, the traction efficiency becomes small for large wheel sinkage case. Upward expansion in horizontal grid lines implies the result of upward push of soil by lug. This action is especially obvious for i_w=43.1% and 30 deg lug angle cases, where resulting negative lift of lug is seen as in Figs.3-13 and 3-14. The action of lug to soil becomes weak as the wheel sinkage decreases for lug angle of 60 deg cases.

As summarized in Chapter 2, the wet soil behavior has been studied successively (Wu *et al.*,1984; Shao *et al.*,1986; Salokhe *et al.*,1987a,1987b,1988). The experimental apparatus in this study is

based on the forced wheel slippage method with non-confined wheel sinkage. Thus, the strict mechanism of the action of lugged wheel to soil might be different from the already published studies. But qualitatively speaking, the behavior of wet cohesive soil in this study turned out to be almost the same as in the observation by Wu *et al.*(1984). Especially, there exists the obvious non-deforming region which may be called boundary wedge under the lug plate as in Fig.4-11.

The shape of boundary wedge is currently under study, since Salokhe *et al.*(1987a) proposed the elliptic shape which is different from conventional prism-like shape (Wu *et al.*,1986). From the result obtained in this chapter, the shape is found to be very close to ellipse, although the precise investigation is impossible since the grid spacing of 1.5 cm is rather large compared with that of 0.5 cm (Salokhe *et al.*, 1987a). Recently, Lu *et al.*(1987) reported that the emergence of elliptic boundary wedge was observed for large wheel slip of 49.6% or larger. On the other hand, Salokhe *et al.*(1988) insisted that boundary wedge was not observed on successive lug in multiple lugs experiments. Further investigation is needed on this fundamental point, since this is one of the basic assumption which must be decided in advance in the application of conventional passive soil resistance theory and slip line method to soil-lug problems.

From the investigation, the deformation of each grid could be regarded as the deformation without volume change, or area change for two dimensional case. That is, as seen in Fig.4-18 for example, the grid unit under upward elongation will follow the lateral shrink, and *vice versa*. This behavior supports the assumption that nearly saturated wet cohesive soil under the action of lug approximately deforms or flows with undrained condition, which is different from the

soil compression behavior observed for rather dried and unsaturated moisture content of soil (Tanaka, 1958).

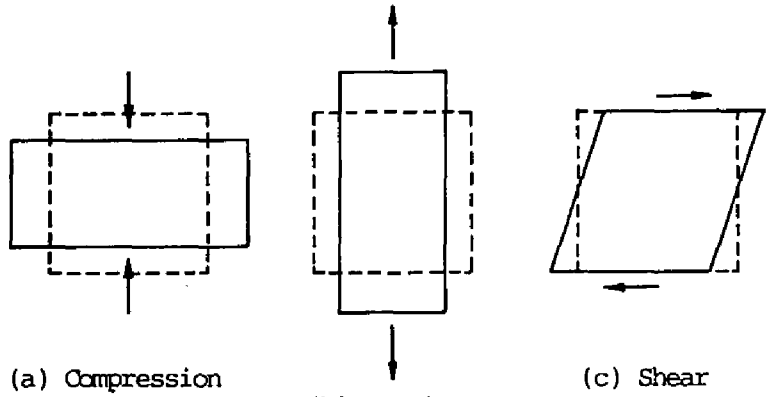

Fig.4-18. Possible basic deformation pattern of grid without volume change.

In the wet cohesive soil, distinct slip lines which were defined by the discontinuous lines in velocity field could not be observed. Instead, at the region near the lug outer tip, severe localized distortion of grid was evident. This distortion can be considered as the insufficient shearing line which does not reach to the soil surface since other part of soil showed no severe deformation. Therefore, the direct application of slip line theory, for example, will result in the poor estimation of soil reaction for wet cohesive soil unless any new assumption of the prior estimation of virtual slip line is not employed.

4.4 Conclusion

By results of the soil behavior under lug of lugged wheel which was observed concurrently with the laboratory experiments on soil reaction in Chapter 3, following points were clarified;

(1) By comparing with the result on preliminary experiments on sand behavior, the wet cohesive soil behavior was verified to be totally different from the sand behavior. And no self burying phenomenon in sand appeared in wet cohesive soil behavior.

(2) Behavior of wet cohesive soil showed the strong effect of lug angle, total number of lug and wheel slippage, since the lug loci varied with such lug parameters.

(3) Approximation of soil deformation with no volume change was verified by observing each grid behavior. And this means that the soil deforms with the undrained condition, which is different from the low moisture content case.

(4) The cohesive soil behavior showed the severe localized deformation at the lug outer tip which did not reach to the soil free surface. This result suggests the necessity of proper assumption of slip line fields for currently popular passive soil pressure theory and slip line method when they are applied to the soil-lug system interactions.

(5) There existed the so-called boundary wedge where the soil did not suffer deformation until 90 deg rotational angle of wheel. The shape of wedge was approximately similar to ellipse, though the precise shape could not be measured by the current visualization method.

Chapter 5 SOIL REACTION ANALYSIS BY RIGID BODY SPRING MODEL

5.1 Introduction

In Chapter 2, it was clear that the analytic methods such as the slip line method have the difficulty in constructing the proper slip lines *a priori* from which the exact solution can be derived in the complex free boundary surface of soil at soil-lug system. Instead of analytic methods, numerical methods have the flexibility in the analysis of various structures whose behavior shows not only elastic response but also plastic one. Following two chapters deal with the application of FEM to soil-lug system in two levels; (i) the first level quick prediction of soil reaction (Chapter 5), (ii) the second level precise prediction of both soil reaction and soil behavior at soil-lug interface (Chapter 6). In these methods, the important condition of both translation and rotation of lug plate is included.

As the first level quick prediction method in order to roughly understand the soil reaction only in terms of change in lug parameters, a simple FEM model which is called Rigid Body Spring Model (RBSM) is applied to soil-lug interaction problems and its applicability is discussed. It is assumed that no distinct displacement at the adjacent boundary between elements appears and that the soil behaves elasto-plastically with well-known Mohr-Coulomb yield criterion.

5.2 Rigid Body Spring Model and Formulation

5.2.1 Model Description

RBSM was developed as the special elements for strong non-linear

problems in Finite Element analysis (Kawai,1980). The fundamental idea of RBSM is based on the weakened condition of continuity at each elemental nodes in conventional FEM. In RBSM, the continuity condition is only satisfied at the centroids of neighboring elements. And the element of RBSM is not deform, but the normal and tangential springs distributed over the boundary of adjacent elements only transmit the force information. In this sense, it is easy to include the discontinuity condition, such as slip lines, compared with the friction or interface elements in general FEM (Zienkiewicz, 1977).

The above mentioned characteristics also suffer the demerit of this model that the initial proper guess of slip line is necessary as in Slip Line Method and that the rigid element assumption causes the lack of information on Poisson's ratio, which means that RBSM calculates the upper bound solution just like the limit analysis of structure with no reliability on elastic deformation data.

5.2.2 Formulation

Based on the formulation by Kawai(1980), the outline of fundamental formulation is summarized as below. Superscript T means the transpose of matrix or vector.

Let I and II be two adjacent triangle elements as shown in Fig. 5-1. The displacement of an arbitrary point P(x,y) on the boundary between two elements $\mathbf{U}$ can be expressed by the displacement of centroid of elements I and II $\mathbf{U}_i$ as in Eq.(5.1),

$$\mathbf{U} = \mathbf{G}\ \mathbf{U}_i \tag{5.1}$$

where $U^T = (u_I \;\; v_I \;\; u_{II} \;\; v_{II})$

$U_i^T = (u_I \;\; v_I \;\; \theta_I \;\; u_{II} \;\; v_{II} \;\; \theta_{II})$

$$G = \left[\begin{array}{ccc:ccc} 1 & 0 & y-y_{gI} & & & \\ 0 & 1 & x_{gI}-x & & O & \\ \hdashline & & & 1 & 0 & y-y_{gII} \\ & O & & 0 & 1 & x_{gII}-x \end{array}\right]$$

x_{gI}, y_{gI} : x, y coord. of centroid on element I

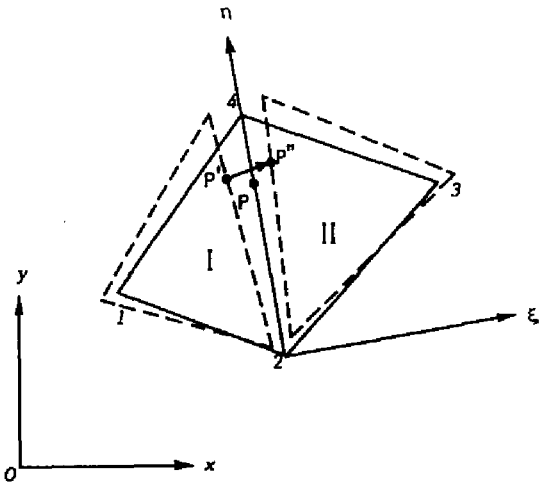

Fig.5-1. Relative displacement in adjacent elements I and II.

Relative displacement vector δ of a point P which is shown in Fig.5-1 as P'P" becomes as in Eq.(5.2) in terms of displacement of centroids expressed in local coordinate system U.

$$\delta = M_r \, \bar{U} \qquad (5.2)$$

where $\delta^T = (\delta_n \;\; \delta_s)$

$$M_r = \begin{bmatrix} -1 & 0 & 1 & 0 \\ 0 & -1 & 0 & 1 \end{bmatrix}$$

$$\bar{U}^T = (\bar{U}_I \quad \bar{V}_I \quad \bar{U}_{II} \quad \bar{V}_{II})$$

By the coordinate transformation matrix J, the relation between global x-y coordinate system and the local ξ-η system can be expressed as follows;

$$\bar{U} = J \quad U \tag{5.3}$$

where

$$J = \begin{bmatrix} l_1 & m_1 & \vdots & \\ l_2 & m_2 & \vdots & O \\ \cdots & \cdots & \cdots & \cdots \\ & O & \vdots & l_1 \quad m_1 \\ & & \vdots & l_2 \quad m_2 \end{bmatrix}$$

$$l_1 = \cos(\xi,x) \qquad m_1 = \cos(\eta,x)$$

$$l_2 = \cos(\xi,y) \qquad m_2 = \cos(\eta,y)$$

Therefore, the relative displacement δ of an arbitrary point P on the element boundary after the deformation can be obtained by using the displacement vector on the centroid U_i as in Eq.(5.4),

$$\delta = B_r \quad U_i \tag{5.4}$$

where $B_r = M_r \; J \; G$. This B_r-matrix corresponds to general B-matrix in conventional FEM.

Strain vector ε on ξ- and η-axis is defined by the relative displacement vector δ with the distance H in ξ-axis direction between centroids as in Eq.(5.5).

$$\varepsilon = \frac{1}{H} \delta \tag{5.5}$$

where $\varepsilon^T = \{ \varepsilon_n \quad \varepsilon_s \}$

$H = H_I + H_{II}$

From Eqs.(5.4) and (5.5), the relation of strain vector ε and displacement vector of centroids U_i is expressed as in Eq.(5.6).

$$\varepsilon = \frac{1}{H} B_r \quad U_i \tag{5.6}$$

Stress-strain relation has the well-known form as follows;

$$\sigma = D \quad \varepsilon \tag{5.7}$$

where $\sigma^T = \{ \sigma_n \quad \tau_s \}$

$$D = \begin{bmatrix} \frac{(1-\nu)E}{(1+\nu)(1-2\nu)} & 0 \\ 0 & \frac{E}{1+\nu} \end{bmatrix} \quad \text{for plane strain}$$

In Eq.(5.7), E stands for Young's Modulus and Poisson's Ratio is expressed in ν. σ_n is assumed to be positive in case of tension.

Spring constants K_n and K_s which are assumed to be distributed on n-axis and can be expressed by the combination of diagonal components of D-matrix in Eq.(5.7) and H as in Eq.(5.8).

$$K_n = \frac{(1-\nu)E}{(1+\nu)(1-2\nu)H}$$

$$K_s = \frac{E}{(1+\nu)H} \tag{5.8}$$

Therefore, the strain energy which is stored in the distributed spring system on the boundary 2-4 in Fig.5-1 for unit thickness can be expressed as follows;

$$\Phi = \frac{1}{2}\int_{\ell_{24}} \varepsilon^T D\ \varepsilon\ dS = \frac{1}{2}\ U_i^T \int_{\ell_{24}} \frac{1}{H^2} B_r^T D\ B_r\ dS\ U_i \tag{5.9}$$

Thus, by Castigliano's theorem, the force-displacement relation on the boundary 2-4 can be obtained as in Eq.(5.10).

$$P = \frac{\partial \Phi}{\partial U_i} = K_r\ U_i \tag{5.10}$$

where $P^T = \{P_{xI}\ \ P_{yI}\ \ M_{cI}\ \ P_{xII}\ \ P_{yII}\ \ M_{cII}\}$

K_r = Symmetric stiffness matrix (6 x 6)

For plastic behavior, Mohr-Coulomb yield criterion of Eq.(5.11) is adopted for distinction of elastic-plastic states.

$$f = \tau_s^2 - (C - \tan\phi\ \sigma_n)^2 \tag{5.11}$$

D-matrix for plastic state (i.e. D_p) becomes as follows;

$$D_p = D - S_m \tag{5.12}$$

where

$$D = \begin{bmatrix} D_1 & 0 \\ 0 & D_2 \end{bmatrix} \quad ; \text{ as in Eq.(5.7)}$$

$$S_m = \frac{1}{f_s}\begin{bmatrix} S_{11} & S_{12} \\ S_{21} & S_{22} \end{bmatrix}$$

$$S_{11} = D_1^2[(C - \sigma_n \tan\phi)\tan\phi]^2$$

$$S_{22} = D_2^2 \tau_s^2$$

$$S_{12} = S_{21} = D_1 D_2 \tau_s (C - \sigma_n \tan\phi)\tan\phi$$

$$f_s = D_2 \tau_s^2 + D_1[(C - \sigma_n \tan\phi)\tan\phi]^2$$

Therefore, the reaction in plastic state (f=0) can be calculated by using Eq.(5.12) in the update formulation of stress-strain relation (Zienkiewicz,1977).

The crack generation is not considered in this study, since for soil with high moisture content no crack is created within the soil mass.

5.2.3 Program Flow

Fig.5-2 shows the program flow of RBSM which was programmed by the author. Original Fortran program list with macro instructions is presented in the text of Kawai(1980).

The main character of RBSM program is the simplicity of analysis. And the calculation may be executed by personal computer because the total program size of current program includ ng working area is rather small (about 400 kB).

For elasto-plastic analysis by RBSM, the updated formulation with well-known r_{min} method (Yamada *et al.*,1968) is employed, with limited prescribed displacement condition which is corresponding to 2 deg wheel rotation. In this sense, the method employed in this chapter may be called confined limit analysis.

5.3 Preparation of Analysis

5.3.1 Lug Displacement Condition

The velocity condition of lug, which was derived in Chapter 3, is transformed into displacement data by multiplying the small time increment and decomposed into translational component and rotational component. Easy inclusion of rotational condition of lug displacement

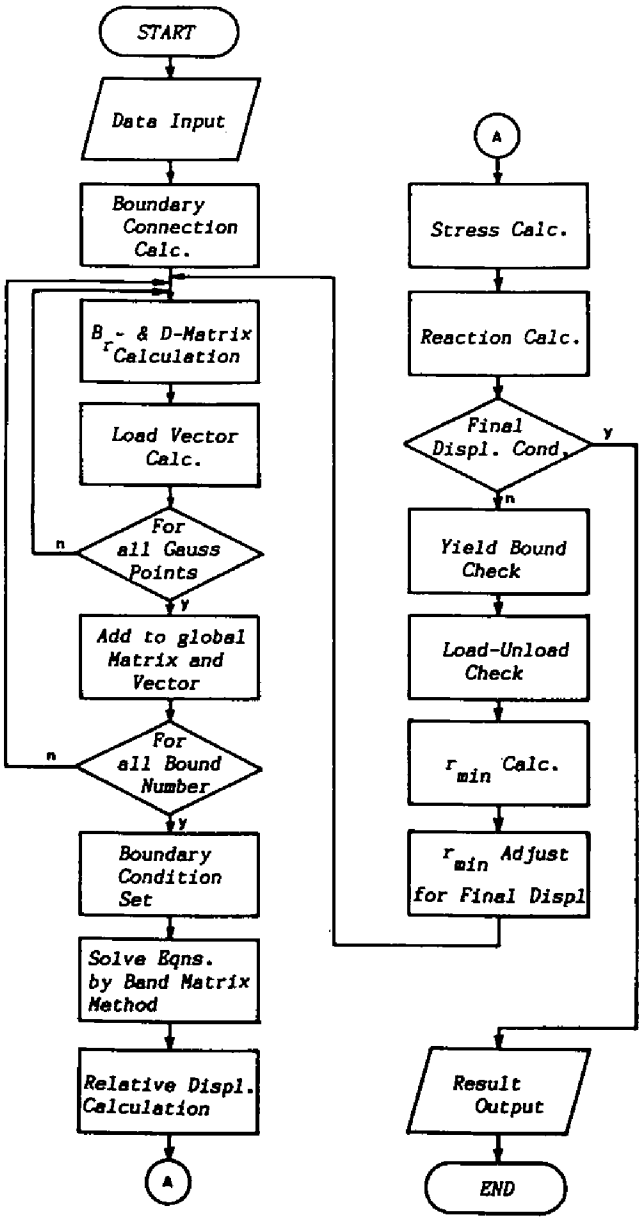

Fig.5-2. Program flow of RBSM analysis.

is the merit of discrete analysis as RBSM. The initial and successive lug position must also be given in advance as the information of mesh division. This preparation is done by considering the experimental soil behavior and lug loci as shown in Chapters 3 and 4.

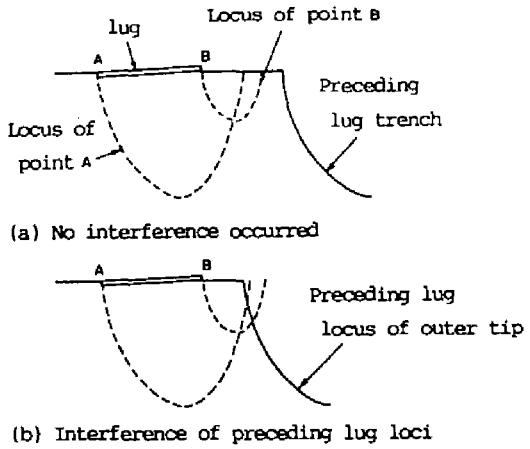

Fig.5-3. Interference of preceding lug loci on the lug of interest.

And no interference of preceding lug loci on the lug plate as in Fig.5-3 is assumed throughout the numerical analysis, since the condition for lug displacement must be simple in terms of quick prediction.

With the prescribed displacement condition, the calculation will be executed and the limit reaction load of three components (P, L and M_C) at the lug element centroid will be obtained.

5.3.2 Material Constants

In principle, material constants must be measured by uni-axial test etc. But RBSM is a special model with the ideal boundary springs which lack the mechanical structure in the physical meaning. Thus,

necessary material constants of E and ν are assumed, considering the incompressibility of soil for plastic flow. The cohesion C is measured as the undrained shear strength C_u by indoor vane shear device with considering the shear velocity of lug on the wet cohesive soil (Tanaka *et al.*,1988). Angle of internal friction is assumed to be 0 deg to ensure the incompressibility of wet cohesive soil. Used values are summarized in Table 5-1.

Table 5-1. Used material constants in RBSM analysis.

Cohesion	C	: 0.88	(kN/m^2)
Angle of internal friction	ϕ	: 0.0	(deg)
Specific weight of soil	γ	: 17.64	(kN/m^3)
Young's Modulus	E	: 490.0	(kN/m^2)
Poisson's Ratio	ν	: 0.49	

5.3.3 Mesh Configurations

It is well known that the upper bound solution is obtained in RBSM. This means that the initial guess of proper slip line field is required. Some improvements on this initial guess can be seen in Kim *et al.*(1987) with the automatic adjustment of mesh coordinates by minimization of elastic potential. But in this study, no procedures on optimization of slip line construction are included for simplicity of program.

As is well known, RBSM has no reliability on deformations since the formulation is based on the rigid-body assumption of elements. Thus, approximate method for the tracing of deformation at soil boundary surface must be added. In this study, the constant volume

condition which was evident in Chapter 4 is applied to define the subsequent mesh divisions by calculating the area of each mesh and changing the coordinates of specified nodes on the boundary of lug trench. And as stated in 5.3.1, current analysis holds for the cases of weak lug-lug interactions where the lug loci of preceding lug will not intersect with the current lug loci.

5.4 Result of Analysis and Discussion

Three lug angles for n_L=6, i_w=43.1% were analyzed, i.e. CASE-I for α=30 deg, CASE-II for α=45 deg and CASE-III for α=60 deg. Calculation was done at the interval of 8 or 9 steps for rotational angles in each case.

Soil Reaction

Figs.5-4, 5-5 and 5-6 show the results of soil reaction calculation based on RBSM analysis for CASE-I,-II and -III respectively. For reference, typical experimental result is also shown in each figure.

In Fig.5-4, the calculated lift of lug takes the maximum value at the first step, whereas the pull of lug becomes minimum at the same step. Negative P at the first step is the remarkable difference from the experimental data. The difference of angle for P_{max} becomes 2 deg and that for L_{max} is 18 deg. In this sense, the calculation was qualitatively done well, except for the first step of displacement condition, the magnitude of P_{max} or L_{max} and the large negative value of L after 90 deg rotation.

Fig.5-5 and Fig.5-6 also show the same tendency as stated above. The angle differences in P_{max} and L_{max} for Fig.5-5 are 4 deg and 16 deg respectively and those for Fig.5-6 are 14 deg and 12 deg.

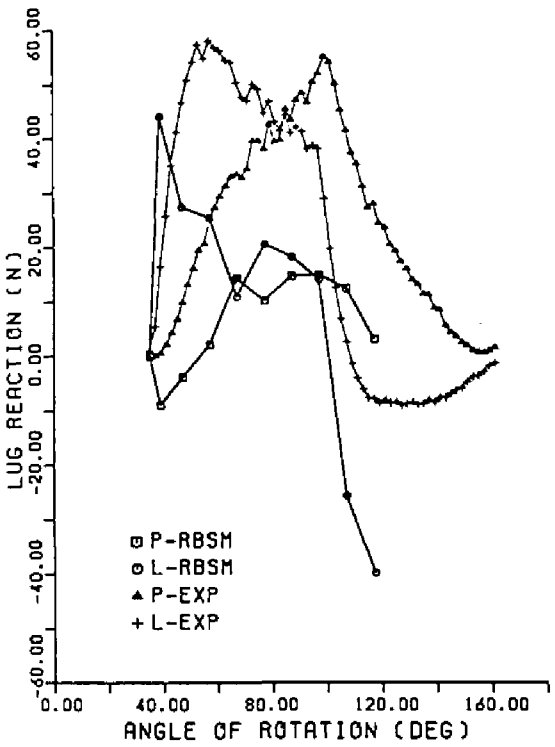

Fig.5-4. Soil reaction for CASE-I.

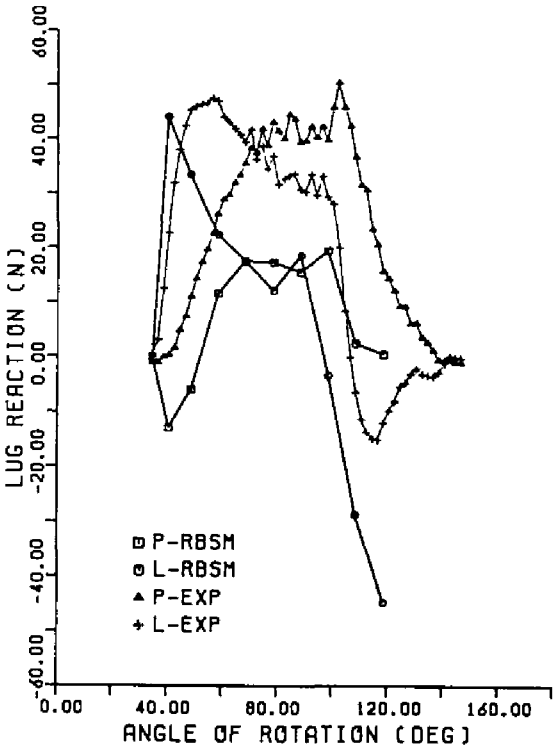

Fig.5-5. Soil reaction for CASE-II.

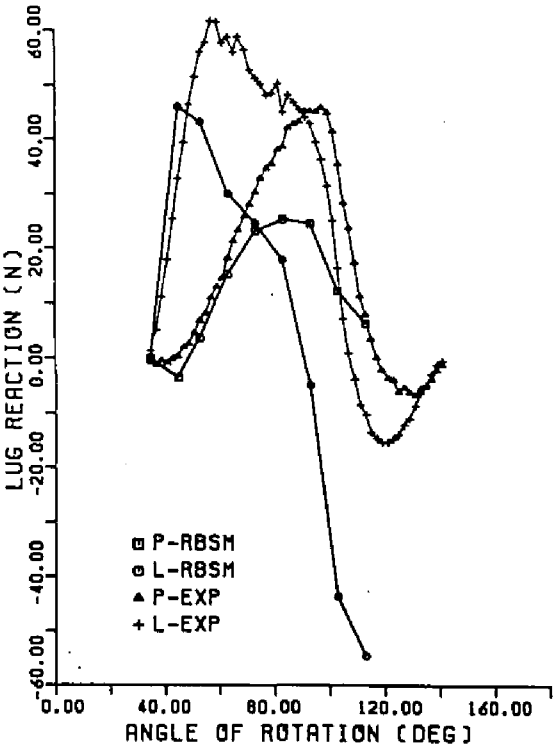

Fig.5-6. Soil reaction for CASE-III.

The error order of calculated P and L in all figures is found to be within 50 N, which means the validity of calculation process where firstly plane strain analysis of two dimensional problem is assumed and solved and later the effect of lug width is considered as the linear multiplication of lug width (Gee-Clough *et al.*,1976). Thus, it is obvious that the qualitative characteristics of pull and lift of lug can be simulated by RBSM analysis as the first level rough but quick simulation.

The main reasons for the angle and magnitude difference in P_{max} and L_{max} are considered as follows; first, the used soil constants might be inadequate and second, the assumed initial mechanism and soil boundary surface might not be proper.

The first reason is inherent in RBSM, since there is no established method for determination of normal and tangential spring constants. And in current analysis, Young's modulus also plays an important role for determining the soil reaction for prescribed displacement condition, since the normal strain and tangential strain suffer the influence of magnitude of E which in turn confines the stress state and the reaction. But E is also difficult to fix for deformable soil such as wet cohesive soil. For further application of RBSM to soil-lug system, this point should also be studied intensively.

The second reason is also inevitable for RBSM as stated in 5.2.1. The reaction calculation by RBSM depends on the properly assumed slip lines with the smallest reaction force. Therefore, to derive the minimum value of reaction, the iteration for modification of slip mechanism is required whose process is not employed in current program. This fact implies that the prediction of soil reaction might be varied as the degree of experience for determining the initial slip

mechanism. There also exists the difficulty of soil boundary shape assumption. In this analysis, as shown in next item, the soil free surface behaves translation only without any rotational movement of mobilized soil which was observed in Chapter 4. As the slip mechanism is clearly influenced by the soil shape at free soil surface, the inherent limitation of RBSM or other type of upper bound methods must be well understood in reaction prediction. Further discussion on this yielding mechanism is done in the next item.

The effect of lug parameters, especially lug angle, is not quantitatively evident from the current RBSM analysis. The negative tendency of P_{max} value in terms of lug angle by RBSM simulation is seen where P_{max} also increases with the increase of lug angle, which is different from the experimental results as shown in Figs.5-4, 5-5 and 5-6.

Yielding Mechanism

Figs.5-7, 5-8 and 5-9 show the RBSM results for yielded bounds. Yielded boundaries are expressed by dot symbols in each figure. And as the boundaries are shown with no displacement result, the mesh configuration for each step is also shown in the figure.

From Fig.5-7, during the former part of lug contact until Fig.5-7(f) yielding mechanism is in general properly analyzed by RBSM. However, the latter part from Fig.5-7(g) to Fig.5-7(i) shows the complex mechanism of yielding.

Yielding mechanism at the first step in Fig.5-8 and Fig.5-9 shows the clear difference as lug angle increases. That is, in those figures lug plate contact with soil from the lug inner tip and the initial step shows the combined mechanism of backward slip lines and

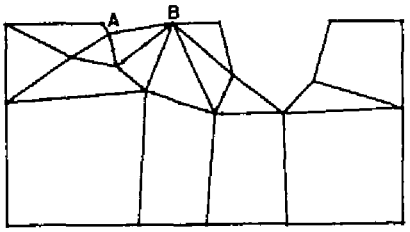

(a) Step 1 (θ=39.2 deg)

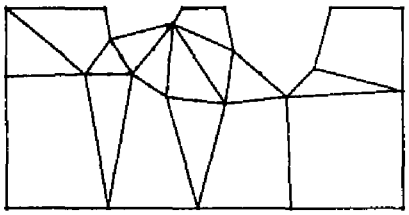

(b) Step 2 (θ=47.2 deg)

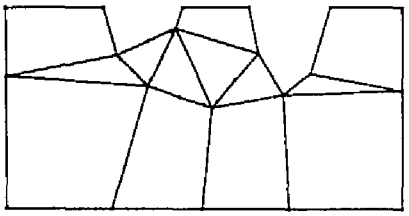

(c) Step 3 (θ=57.2 deg)

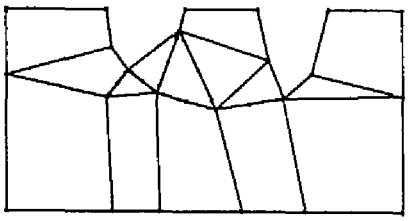

(d) Step 4 (θ=67.2 deg)

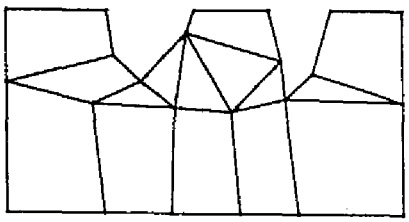

(e) Step 5 (θ=77.2 deg)

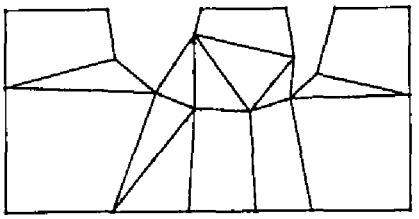

(f) Step 6 (θ=87.2 deg)

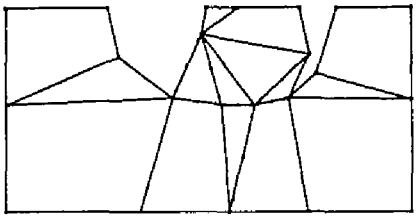

(g) Step 7 (θ=97.2 deg)

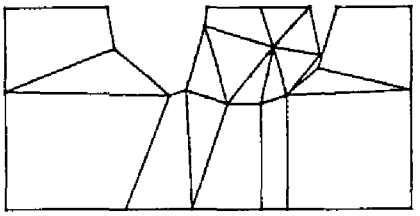

(h) Step 8 (θ=107.2 deg)

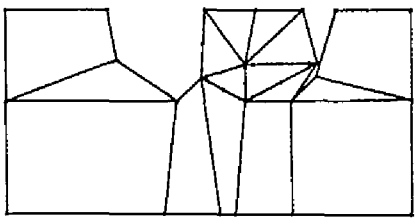

(i) Step 9 (θ=117.2 deg)

Fig.5-7. Yielding boundaries for CASE-I.

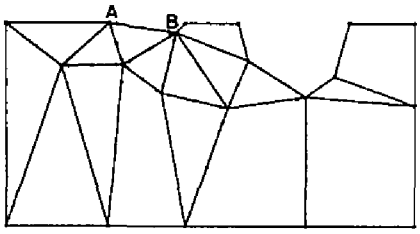

(a) Step 1 (θ=40.5 deg)

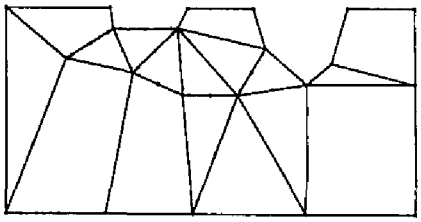

(b) Step 2 (θ=48.5 deg)

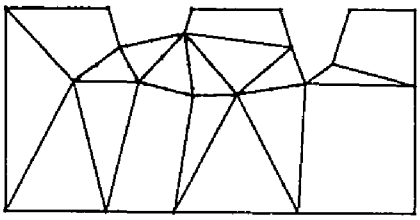

(c) Step 3 (θ=58.5 deg)

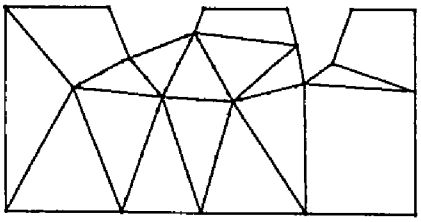

(d) Step 4 (θ=68.5 deg)

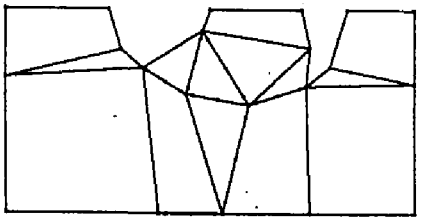

(e) Step 5 (θ=78.5 deg)

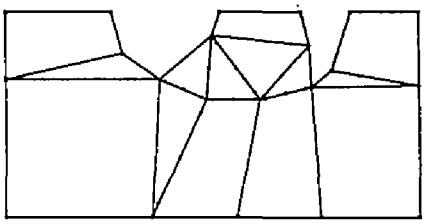

(f) Step 6 (θ=88.5 deg)

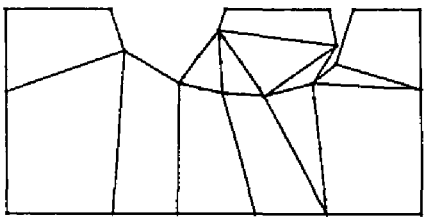

(g) Step 7 (θ=98.5 deg)

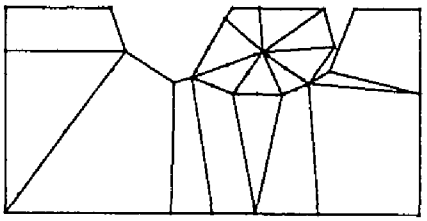

(h) Step 8 (θ=108.5 deg)

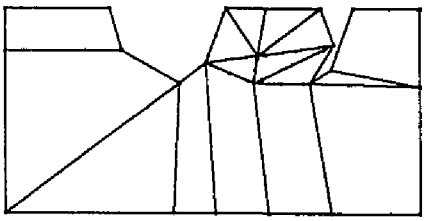

(i) Step 9 (θ=118.5 deg)

Fig.5-8. Yielding boundaries for CASE-II.

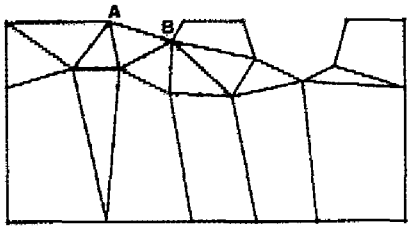

(a) Step 1 (θ=44.8 deg)

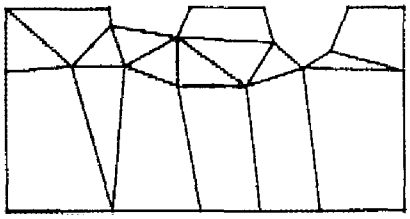

(b) Step 2 (θ=52.8 deg)

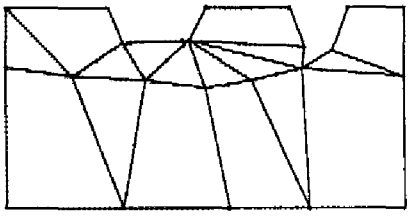

(c) Step 3 (θ=62.8 deg)

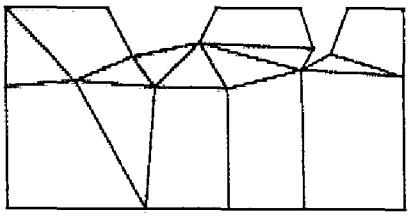

(d) Step 4 (θ=72.8 deg)

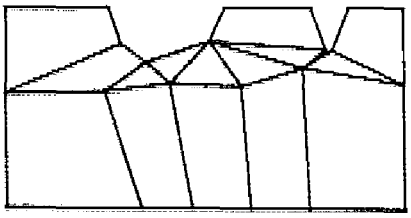

(e) Step 5 (θ=82.8 deg)

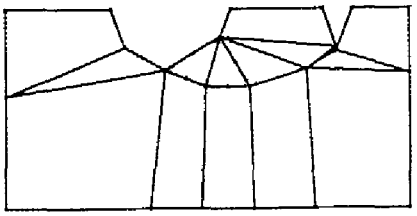

(f) Step 6 (θ=92.8 deg)

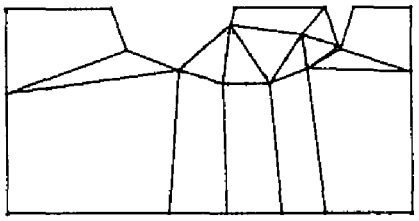

(g) Step 7 (θ=102.8 deg)

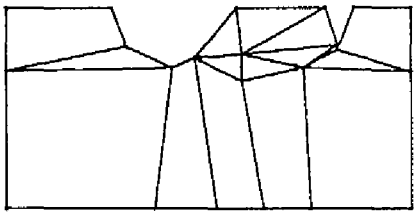

(h) Step 8 (θ=112.8 deg)

Fig.5-9. Yielding boundaries for CASE-III.

partly forward slip line as in Fig.5-8(a) which would rather be similar slip lines as seen in bearing capacity problems in civil engineering and which cannot be dealt with by the well-known passive soil resistance theory(Hettiaratchi *et al.*,1974). But from the experimental soil behavior, marker grids which locate in front of lug plate do not suffer from deformation at the early stage of lug action. Therefore, the soil-lug contact condition might affect the above stated mechanism generation, since in current RBSM analysis soil-lug interface parameters such as adhesion and interface friction angle are replaced by cohesion and internal friction angle. Other steps show the same tendency as in Fig.5-7.

From these figures on yielding mechanism, the importance of latter part of lug action after the rotational angle of about 90 deg is confirmed. The large difference in lift in soil reaction calculation by RBSM is clearly considered as the result of insufficiently assumed slip lines. However, the initial guess for such part is very difficult even for well-trained engineers, since the direction of lug action changes in each displacement step and the soil-lug interaction problem in nature belongs to the unsteady state problems where exact slip line fields cannot be constructed with ease. Thus, systematic mechanism generation method must be developed with the consideration of interface contact information so that RBSM analysis becomes a versatile simulation tool for soil reaction in soil-lug system.

No Boundary Rotation Result

In order to understand the importance of rotational information at soil-lug boundary, the calculation without rotational displacement condition is done for CASE-II and the result of soil reaction is shown

in Fig.5-10 and yielding mechanism in Fig.5-11.

From Fig.5-10, the tendency is the same as in Fig.5-5 until 60 deg rotational angle and also the magnitude is almost the same in that part. But after that angle, the graph of L becomes different from that in Fig.5-5 and takes smaller value until the final step, whereas the graph of P shows moderately similar behavior with Fig.5-5. The reason of the same tendency in the early stage of calculation would be related with the fact that the main action of lug to soil at that period consists of translation and the same yielding mechanism is

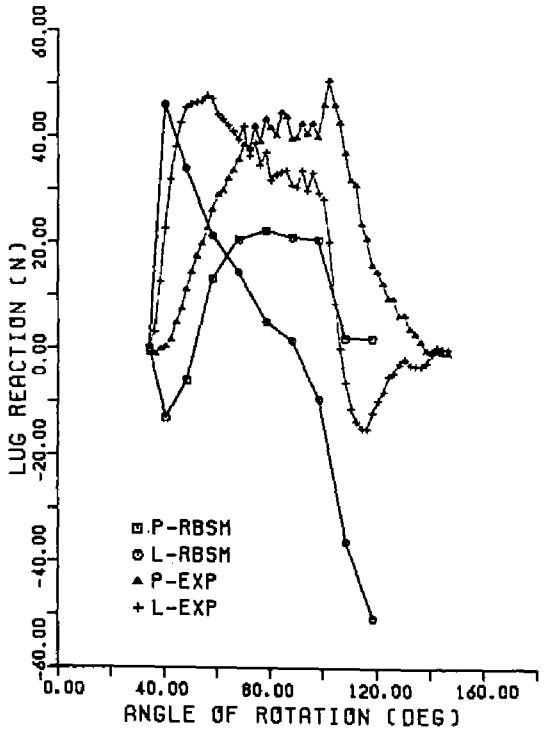

Fig.5-10. Soil reaction without rotational condition for CASE-II.

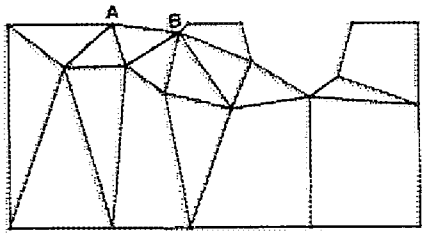

(a) Step 1 (θ=40.5 deg)

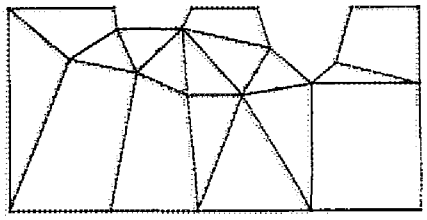

(b) Step 2 (θ=48.5 deg)

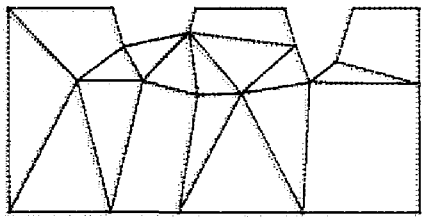

(c) Step 3 (θ=58.5 deg)

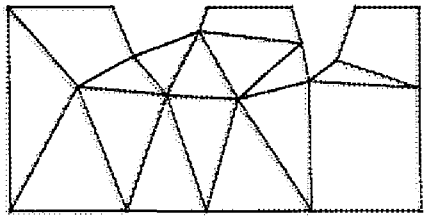

(d) Step 4 (θ=68.5 deg)

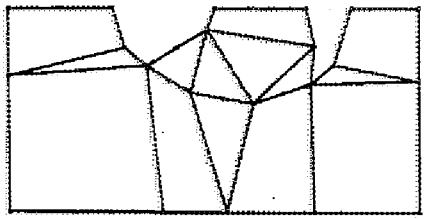

(e) Step 5 (θ=78.5 deg)

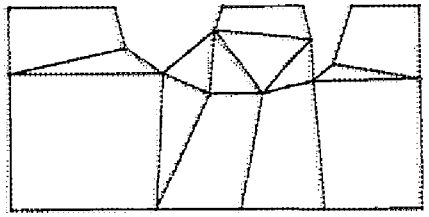

(f) Step 6 (θ=88.5 deg)

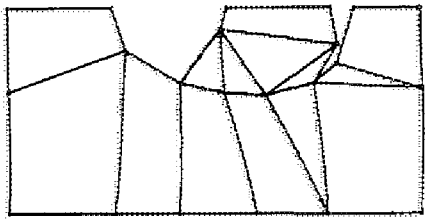

(g) Step 7 (θ=98.5 deg)

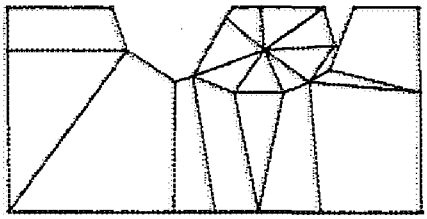

(h) Step 8 (θ=108.5 deg)

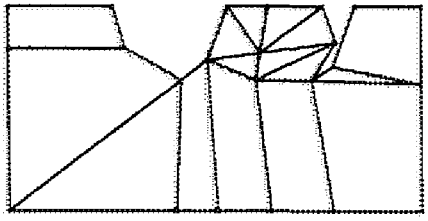

(i) Step 9 (θ=118.5 deg)

Fig.5-11. Yielding boundaries without rotational condition for CASE-II.

generated as in the case of rotational lug boundary condition. But for the latter part of rotational angle, the yielding mechanism would be different from the case of rotational boundary condition which is shown in Fig.5-11. Therefore, the graph of L shows the result of non-optimized slip mechanism and the new yielding mechanism must be assumed for no rotational boundary condition. This in turn suggests the importance of rotational boundary condition which must be taken into consideration for lug reaction prediction.

5.5 Conclusion

As the first level analysis of soil reaction on a lug, Rigid Body Spring Model was applied to soil-lug system and the following several points were clarified;

(1) With the constant volume condition and Mohr-Coulomb yield criterion with no internal friction angle, RBSM could be used as the qualitative first level soil reaction prediction at soil-lug interface for no prior lug loci interference case. But the effect of lug angle on soil reaction could not be cleared by the current RBSM program. For more precise reaction prediction, some important points such as material constants, initial slip mechanism and free boundary shape must be remarked and well prepared.

(2) The combined procedure of two dimensional plane strain analysis and linear multiplication of lug width brought the permissible result of calculation under current method of RBSM analysis.

(3) Yielding mechanism for larger lug angle at the first step of displacement condition turned out to be different from that of the case for 30 deg lug angle. And the complex mechanism of the latter

part of lug action after 90 deg rotational angle confirmed the necessity of some systematic mesh generation method with soil-lug interface information so that RBSM could become the versatile simulation tool.

(4) The difference of yielding mechanism for rotational lug boundary became evident by comparing the result of no rotational boundary condition. It was verified the necessity that upper bound analysis had to take the rotational effect of lug into consideration for more realistic analysis.

Chapter 6 SOIL REACTION AND BEHAVIOR ANALYSIS BY RIGID PLASTIC FINITE ELEMENT METHOD

6.1 Introduction

The soil under a lug showed the combined behavior of localized deforming region near the lug tip and non-deforming region in soil in Chapter 4. In this chapter, to precisely predict both soil behavior under a lug and soil reaction on a lug of lugged wheel as the second level analysis, Rigid Plastic Finite Element Method (RPFEM) which has been developed in metal forming processes is applied to soil-lug interaction problems and its validity is discussed in comparison with experimental results which were obtained in Chapter 3.

6.2 Formulation and Program Flow

6.2.1 Penalty Formulation

The implementation of RPFEM with conventional Lagrange Multipliers (Lee *et al.*,1973; Tamura *et al.*,1984) generates the singular coefficient matrix in simultaneous equations. To avoid zero entry in diagonal term of coefficient matrix and to shorten the calculation time of solver, the penalty formulation which was firstly proposed by Zienkiewicz *et al.*(1975) is adopted.

A functional with the constraint of constant volume can be expressed by adopting a large positive penalty number K as in Eq.(6.1).

$$\Psi_p = \int_V D(\dot{\varepsilon}_{ij})\, dV - \int_V W_i \dot{u}_i\, dV - \int_{S_f} R_i \dot{u}_i\, dS + \frac{K}{2}\int_V (\dot{\varepsilon}_{kk})^2 dV \quad (6.1)$$

where $D(\dot{\varepsilon}_{ij}) = \sigma_{ij}\dot{\varepsilon}_{ij}$: internal plastic energy dissipation

σ_{ij} : stress on the yield surface

$\dot{\varepsilon}_{ij}$: strain velocity for σ_{ij}

$\dot{u}_i$: displacement velocity

W_i : body force for unit volume

R_i : surface traction for unit boundary area

$\dot{\varepsilon}_{kk}$: volumetric strain velocity

Stationary condition of Eq.(6.1) will be given by the partial differentiation with respect to nodal velocity $\dot{u}_i$ only without any additional constraint conditions.

In order to describe the behavior of rigid perfectly-plastic body, following vectors and matrices are introduced for 4-node iso-parametric element with the relation on Mises yield stress $\sigma_0 = \sqrt{2}\, C_u$ (Tamura,1986). Superscript T means the transpose of matrix or vector and subscript e stands for an arbitrary element.

Nodal velocity vector

$$\dot{u}_e^T = \{\dot{u}_1 \ \dot{v}_1 \ \dot{u}_2 \ \dot{v}_2 \ \dot{u}_3 \ \dot{v}_3 \ \dot{u}_4 \ \dot{v}_4\}$$

Elemental strain velocity vector

$$\dot{\varepsilon}_e^T = \{ \dot{\varepsilon}_x \ \ \dot{\varepsilon}_y \ \ 2\dot{\varepsilon}_{xy} \} = B\, \dot{u}_e$$

Differential operator for strain velocity

$$B = \{ B_1 \ \ B_2 \ \ B_3 \ \ B_4 \}$$

$$B_n = \begin{bmatrix} \dfrac{\partial N_n}{\partial x} & 0 \\ 0 & \dfrac{\partial N_n}{\partial y} \\ \dfrac{\partial N_n}{\partial y} & \dfrac{\partial N_n}{\partial x} \end{bmatrix} \qquad n : \text{Node Index}$$

Elemental volumetric strain velocity

$$\dot{\varepsilon}_{ve} = \dot{\varepsilon}_x + \dot{\varepsilon}_y = L_v \dot{u}_e$$

Differential operator for volumetric strain velocity

$$L_v = \{ L_1 \quad L_2 \quad L_3 \quad L_4 \}$$

$$L_n = \left\{ \frac{\partial N_n}{\partial x} \quad \frac{\partial N_n}{\partial y} \right\} \qquad n : \text{Node Index}$$

Elemental plastic energy dissipation

$$D(\dot{u}_e) = \dot{\varepsilon}_e^T \sigma_e = \dot{\varepsilon}_e^T s_e$$

Constant coefficient matrix

$$Q = \begin{bmatrix} 1 & 0 & 0 \\ 0 & 1 & 0 \\ 0 & 0 & 1/2 \end{bmatrix}$$

Elemental equivalent strain velocity

$$\bar{\dot{\varepsilon}} = \sqrt{\dot{u}_e^T B^T Q B \dot{u}_e}$$

Elemental deviatric stress vector

$$s_e = \frac{\sigma_0}{\bar{\dot{\varepsilon}}} Q \dot{\varepsilon}_e$$

Therefore, the functional of Eq.(6.1) for an arbitrary element with volume V_e becomes as in Eq.(6.2).

$$\Psi_{p_e} = \int_{V_e} \dot{\varepsilon}_e^T s_e \, dV - \int_{V_e} \dot{u}_e^T W \, dV - \int_{S_{f_e}} \dot{u}_e^T R \, dS + \frac{K}{2} \int_{V_e} (L_v \dot{u}_e)^2 dV \quad (6.2)$$

From the stationary condition with respect to nodal velocity $\dot{u}_e$, we can derive Eq.(6.3) which is the non-linear equilibrium equation as;

$$\sigma_0 \int_{V_e} \left\{ \frac{B^T Q B \dot{u}_e}{\bar{\dot{\varepsilon}}} + \frac{K(L_v^T L_v \dot{u}_e)}{\sigma_0} \right\} dV = \int_{V_e} W \, dV + \int_{S_{f_e}} R \, dS \quad (6.3)$$

Eq.(6.3) can be changed to linear equation by substituting $\dot{u}_e = \dot{u}_e + \Delta\dot{u}_e$ into Eq.(6.3) and by ignoring higher order terms of the small

perturbations $\Delta\dot{u}_e$ as in Eq.(6.4).

$$\sigma_0 \int_{V_e} \{ A^* - B^* + C^* \} \, dV \, \Delta\dot{u}_e$$

$$= \int_{V_e} W \, dV + \int_{S_{f_e}} R \, dS - \sigma_0 \int_{V_e} \{ A^* + C^* \} \, dV \, \dot{u}_e \quad (6.4)$$

where $$A^* = \frac{B^T Q \, B}{\bar{\dot{\varepsilon}}}$$

$$B^* = \frac{B^T Q (B\dot{u}_e)(B\dot{u}_e)^T Q B}{\bar{\dot{\varepsilon}}^3}$$

$$C^* = \frac{K \, L_V^T L_V}{\sigma_0}$$

Thus, by summing up Eq.(6.4) over all elements, the final form of Rigid Plastic Penalty Finite Element equations can be obtained.

Newton-Raphson Method with relaxation coefficient β=0.1 to 0.9 is employed to protect the excessive adjustment of updated value of $\dot{u}$ (Tamura,1986).

6.2.2 Treatment of Large Deformation

Soil behavior observation in Chapter 4 revealed that the severe deformation of soil occurred below the lug outer tip. To continue the numerical calculation in distorted mesh configurations, remeshing technique is adopted (Gelten *et al.*,1982; Oh *et al.*,1984; Cheng *et al.*,1986). In this analysis, simple stage number criterion is used as in Fig.6-1, instead of time consuming adaptive scheme (Kikuchi,1986).

The deformation of soil is traced by the same idea of soil behavior visualization as in Chapter 4. Firstly the initial marker grids are allocated on the initial mesh configuration. Then the relation of marker nodes and the global finite element nodes is calculated via

local triangulation technique. After the deformation of global mesh, the new marker node positions are updated with the displacement information on three nodes of global nodes and centroid. This method is similar to spatially fixed elements (Mori *et al.*,1983).

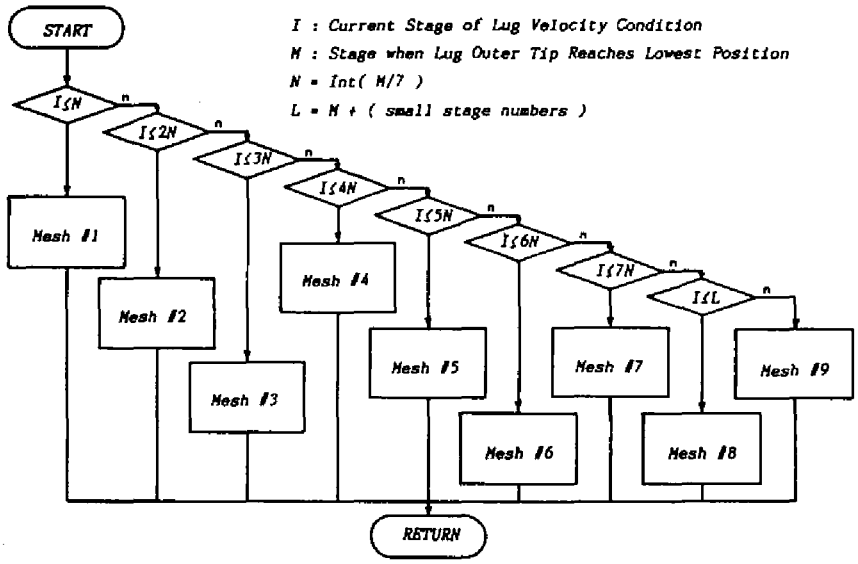

Fig.6-1. Rezoning strategy in current RPFEM analysis.

6.2.3 Program Flow

Fig.6-2 shows the program flow of RPFEM. Mesh division part has the following 6 steps;

(a) Selection of boundary nodes;

(b) 8-node superelement mesh division of given region;

(c) 4-node isoparametric mesh generation (Durocher *et al.*,1979);

(d) Boundary nodes and lug nodes detection;

(e) Renumbering of node numbers by Collins Algorithm (Collins,1973);

(f) Smoothing of element coordinates by weight of surrounding elements' area.

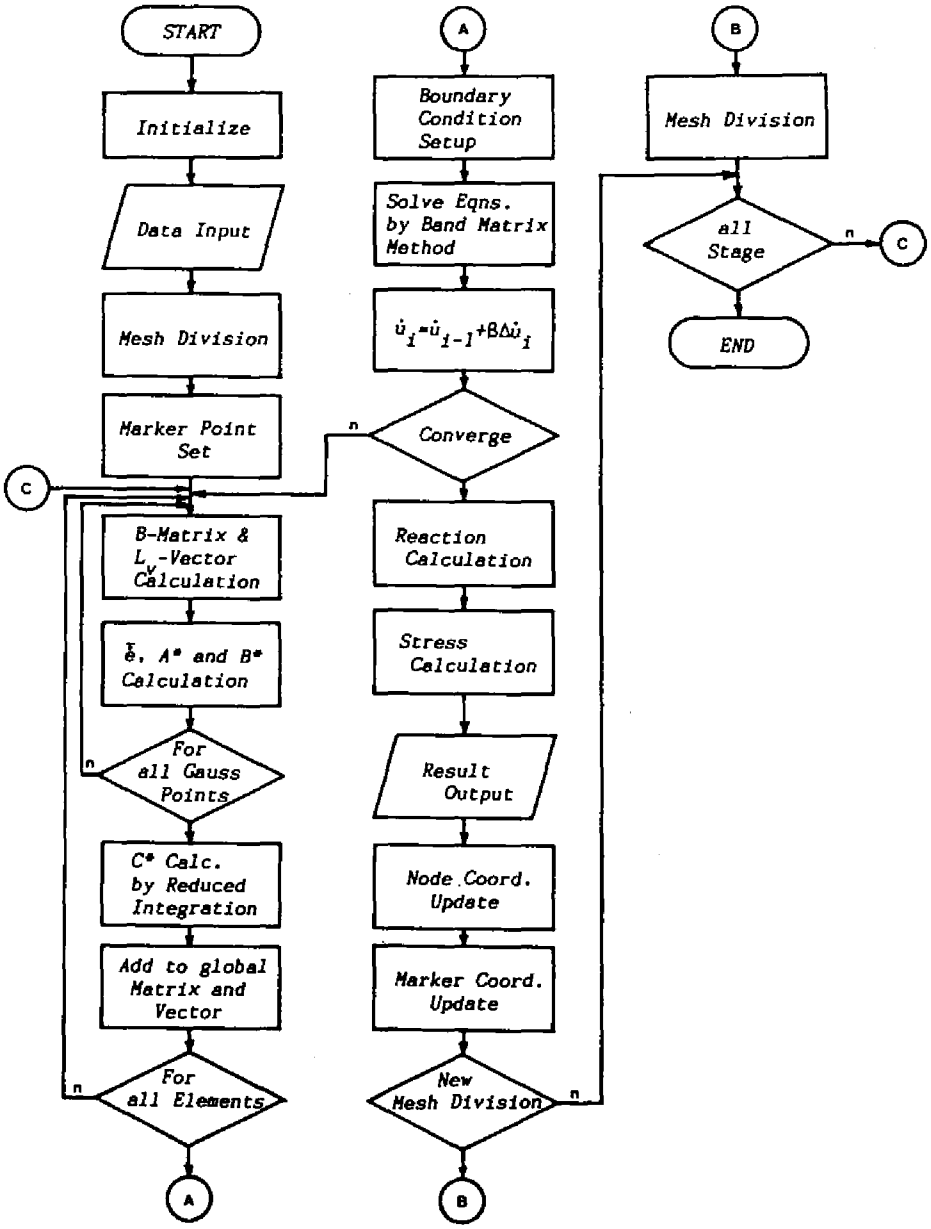

Fig.6-2. Program flow of RPFEM analysis.

The step (f) is to ensure the arbitrariness of mesh division. This plays an important role for rezoning process.

As is shown in 6.2.1, the velocity field is calculated through the minimization process of plastic energy dissipation. After the convergence of velocity field is obtained, i.e. calculated velocity field becomes very close or nearly equals to the exact velocity distribution within soil, then the stress field is calculated and the soil reaction on a lug can be evaluated.

Total necessary memory area including working area is about 1.5 MB with the maximum nodes of 180 and maximum elements of 130. Calculation is done by Fujitsu FACOM M-780 system of Data Processing Center, Kyoto University. Average solver time by conventional Band Matrix Method is about 0.5 sec in one lug velocity condition with about 30 iterations for each velocity step with the convergence criterion of $\|\Delta \dot{\mathbf{u}}_i\| / \|\dot{\mathbf{u}}_i\| < 0.0001$. And total calculation time of RPFEM is found to be about 210 sec for a given case of analysis.

6.3 Preparation of Input Data

6.3.1 Lug Velocity Condition

The basic data of lug velocity are calculated in advance which are based on the fundamental velocity conditions and the wheel sinkage velocity variation condition, as shown in Chapter 3. Time increment between each velocity condition is 0.2375 sec which corresponds to 2 deg wheel rotation. This velocity condition is added to analysis as the prescribed velocity condition on the lug boundary in the iteration of calculation (Osakada,1983). And the coordinates of nodes are updated by the explicit Euler method as $\mathbf{x}_i = \mathbf{x}_{i-1} + \dot{\mathbf{u}}_i \, t$ (Tomita,1987).

6.3.2 Material Constants

Cohesive soil with high moisture content--equal or over LL--can be regarded as nearly saturated soil and to deform with undrained shear condition since there is not enough time of drainage of internal pore water when the action of running devices is applied. Thus the deformation must occur without any volume change in the soil. In order to express this incompressibility, the well-known Levy-Mises rigid-plastic material law is adopted (Tamura *et al.*,1984). Therefore, required material constants are undrained shear strength C_u and specific weight of soil γ. In general, C_u depends on the shear velocity of soil. As in Chapter 5, indoor vane shear test was conducted to get the proper value of C_u (Tanaka *et al.*,1988). Used material constants are listed in Table 6-1. Penalty number K is decided to be 10^8 by preliminary calculation.

Table 6-1. Used material constants in RPFEM analysis.

Undrained shear strength	C_u	: 0.88	(kN/m^2)
Specific weight of soil	γ	: 17.64	(kN/m^3)

6.4 Result of Analysis and Discussion

Three cases of n_L=6 and i_w=43.1% are analyzed where the soil under a lug becomes mobilized largely, namely CASE-I for α=30 deg, CASE-II for α=45 deg and CASE-III for α=60 deg as in RBSM analysis. Used mesh rezoning patterns for each case are shown in Figs.6-3, 6-4 and Fig.6-5 respectively. In Fig.6-3, the smoothing of generated mesh is done until mesh pattern 5 and after that no smoothing scheme is adopted in order to avoid the excessive smoothing result of generated mesh.

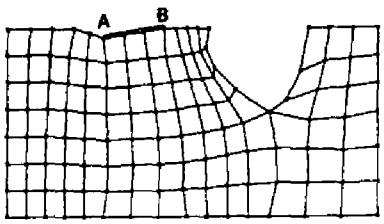

(a) Mesh #1 at Step 1

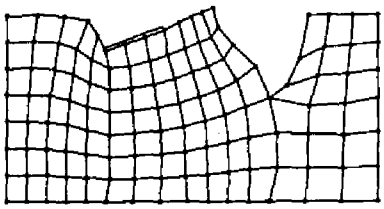

(b) Mesh #2 at Step 6

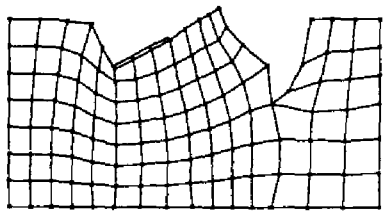

(c) Mesh #3 at Step 10

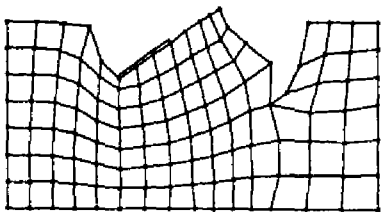

(d) Mesh #4 at Step 14

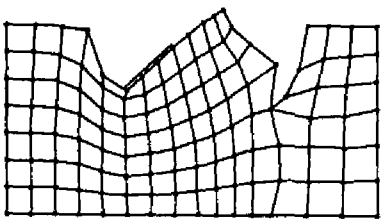

(e) Mesh #5 at Step 18

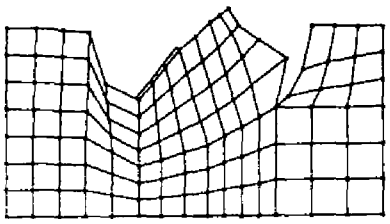

(f) Mesh #6 at Step 22

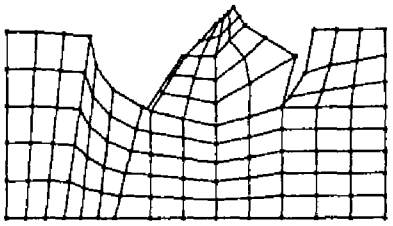

(g) Mesh #7 at Step 26

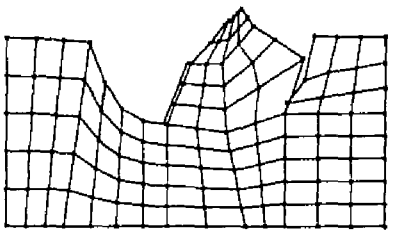

(h) Mesh #8 at Step 32

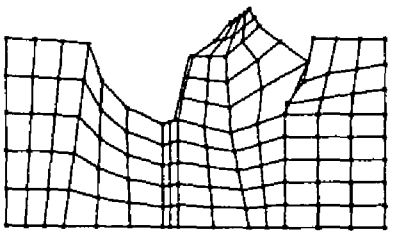

(i) Mesh #9 at Step 36

Fig.6-3. Mesh rezoning patterns for CASE-I.

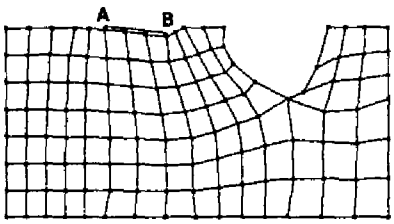

(a) Mesh #1 at Step 1

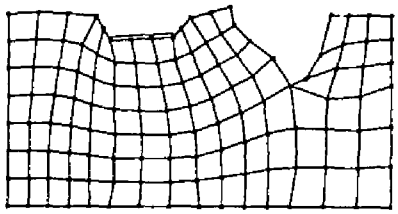

(b) Mesh #2 at Step 6

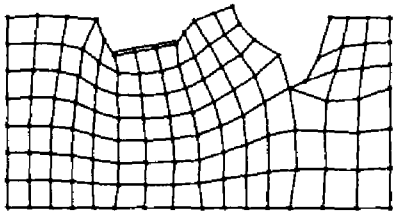

(c) Mesh #3 at Step 10

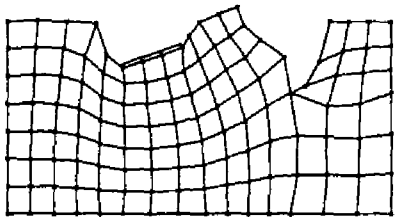

(d) Mesh #4 at Step 14

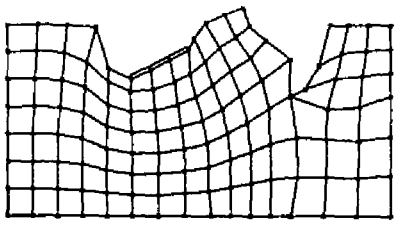

(e) Mesh #5 at Step 18

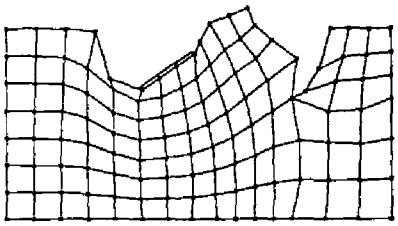

(f) Mesh #6 at Step 22

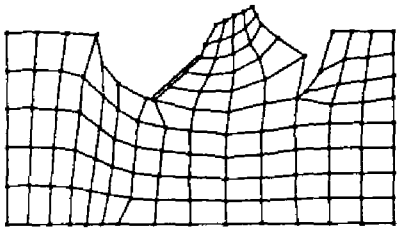

(g) Mesh #7 at Step 26

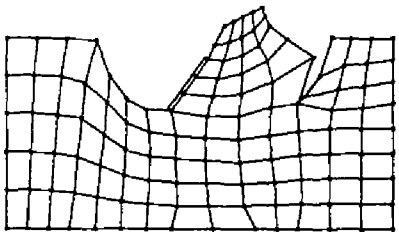

(h) Mesh #8 at Step 32

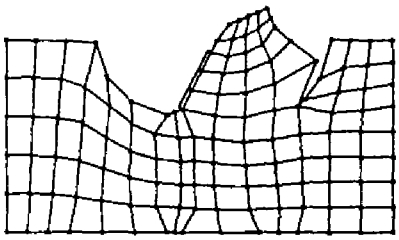

(i) Mesh #9 at Step 36

Fig.6-4. Mesh rezoning patterns for CASE-II.

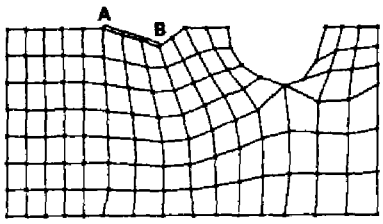

(a) Mesh #1 at Step 1

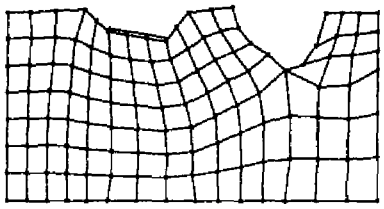

(b) Mesh #2 at Step 5

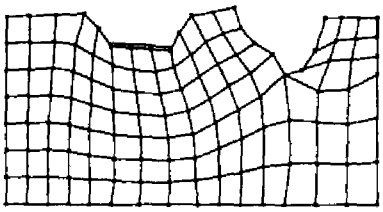

(c) Mesh #3 at Step 8

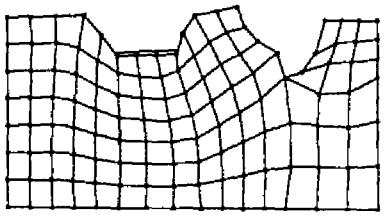

(d) Mesh #4 at Step 11

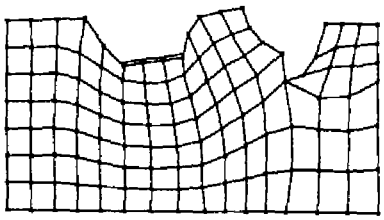

(e) Mesh #5 at Step 14

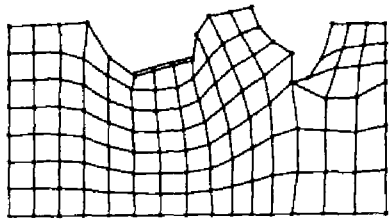

(f) Mesh #6 at Step 17

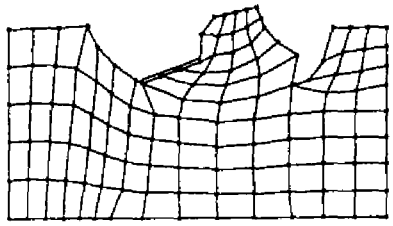

(g) Mesh #7 at Step 20

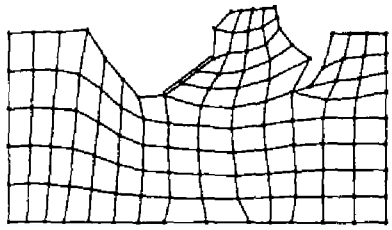

(h) Mesh #8 at Step 28

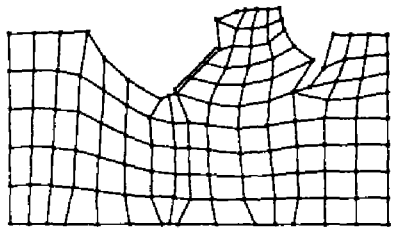

(i) Mesh #9 at Step 32

Fig.6-5. Mesh rezoning patterns for CASE-III.

6.4.1 Soil Behavior Analysis and Discussion

CASE-I

The result of analysis by RPFEM is shown in Fig.6-6. From the figure, the transition of boundary outline with the movement of lug mostly reflects the similar transition tendency of experimental result in Fig.4-11. The mobilized region of soil under lug becomes large and the interesting behavior of contact of left side of prior lug trench to the right side at the latter part of lug action is also remarkable which implies the excessive evaluation of soil deformation in RPFEM. By the assumption of no sliding friction at the lug surface, the non deforming region of marker grids exists especially in the former part of lug action until θ=90 deg. If one assumes the excessive deformation of marker grids at the lug outer tip is "slip line", then this slip line remains at the adjacent region of lug outer tip without extending up to the soil free boundary. This also presents the reproduction of similar behavior of experimental result in Chapter 4 by RPFEM. And the excessive effect of adhesion is observed at the final step of lug action, which is the result of no inclusion of detachment condition in the analysis.

CASE-II

In Fig.6-7, the result for 45 deg lug angle case is shown. In this case, the contact behavior of preceding lug trench becomes weakened by the combined effect of lug angle and the decrease in wheel sinkage. Deformation of marker grids also verifies the reduction in the influence region of lug action. Other points show the similar tendency as in the result of CASE-I.

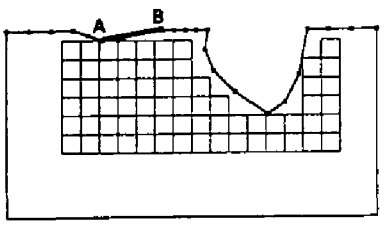

(a) Step 1 (θ=39.2 deg)

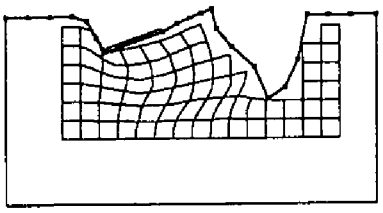

(b) Step 6 (θ=49.2 deg)

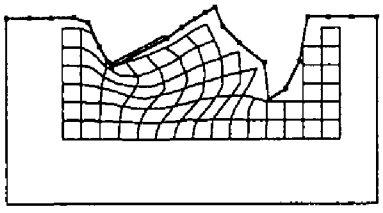

(c) Step 10 (θ=57.2 deg)

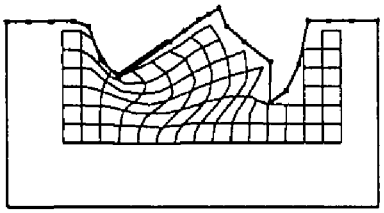

(d) Step 14 (θ=65.2 deg)

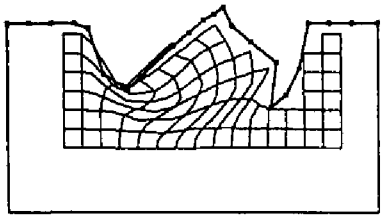

(e) Step 18 (θ=73.2 deg)

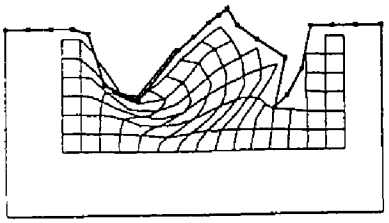

(f) Step 22 (θ=81.2 deg)

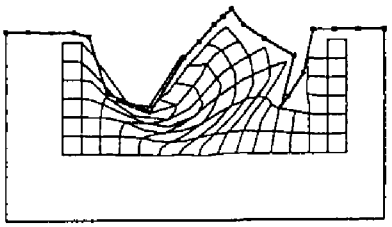

(g) Step 26 (θ=89.2 deg)

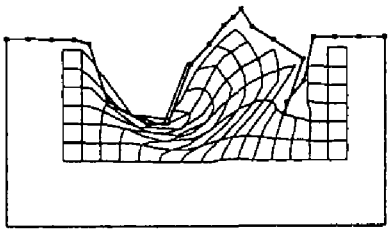

(h) Step 32 (θ=101.2 deg)

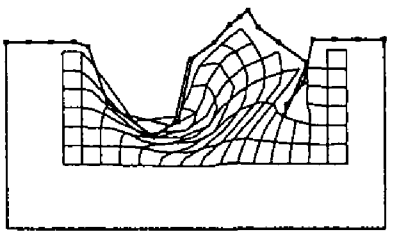

(i) Step 36 (θ=109.2 deg)

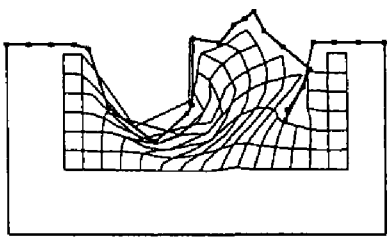

(j) Step 42 (θ=121.2 deg)

Fig.6-6. Soil behavior by RPFEM for CASE-I.

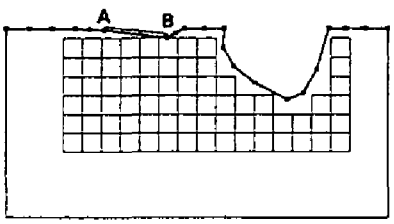

(a) Step 1 (θ=40.5 deg)

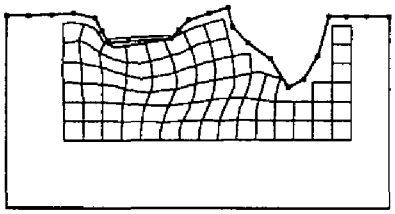

(b) Step 6 (θ=50.5 deg)

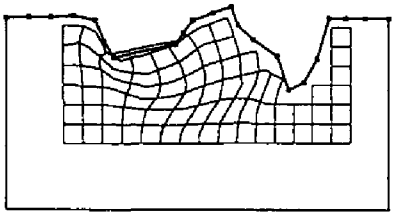

(c) Step 10 (θ=58.5 deg)

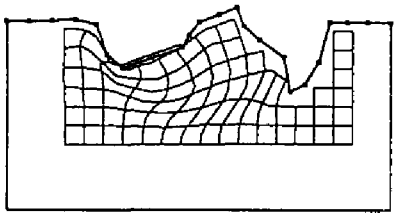

(d) Step 14 (θ=66.5 deg)

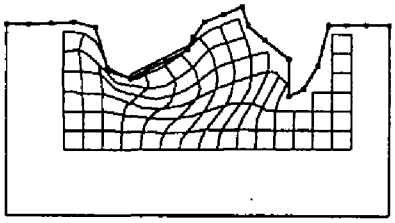

(e) Step 18 (θ=74.5 deg)

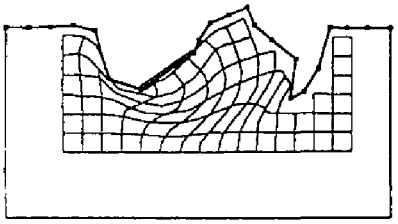

(f) Step 22 (θ=82.5 deg)

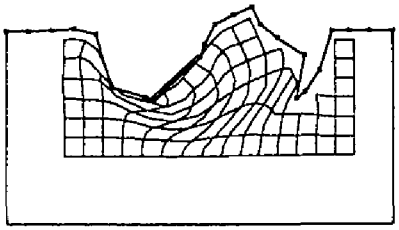

(g) Step 26 (θ=90.5 deg)

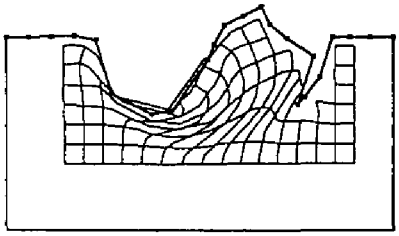

(h) Step 32 (θ=102.5 deg)

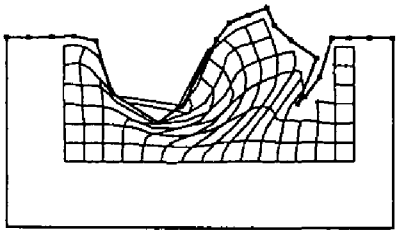

(i) Step 36 (θ=110.5 deg)

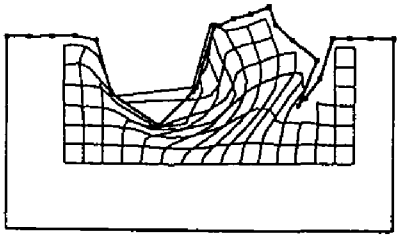

(j) Step 42 (θ=122.5 deg)

Fig.6-7. Soil behavior by RPFEM for CASE-II.

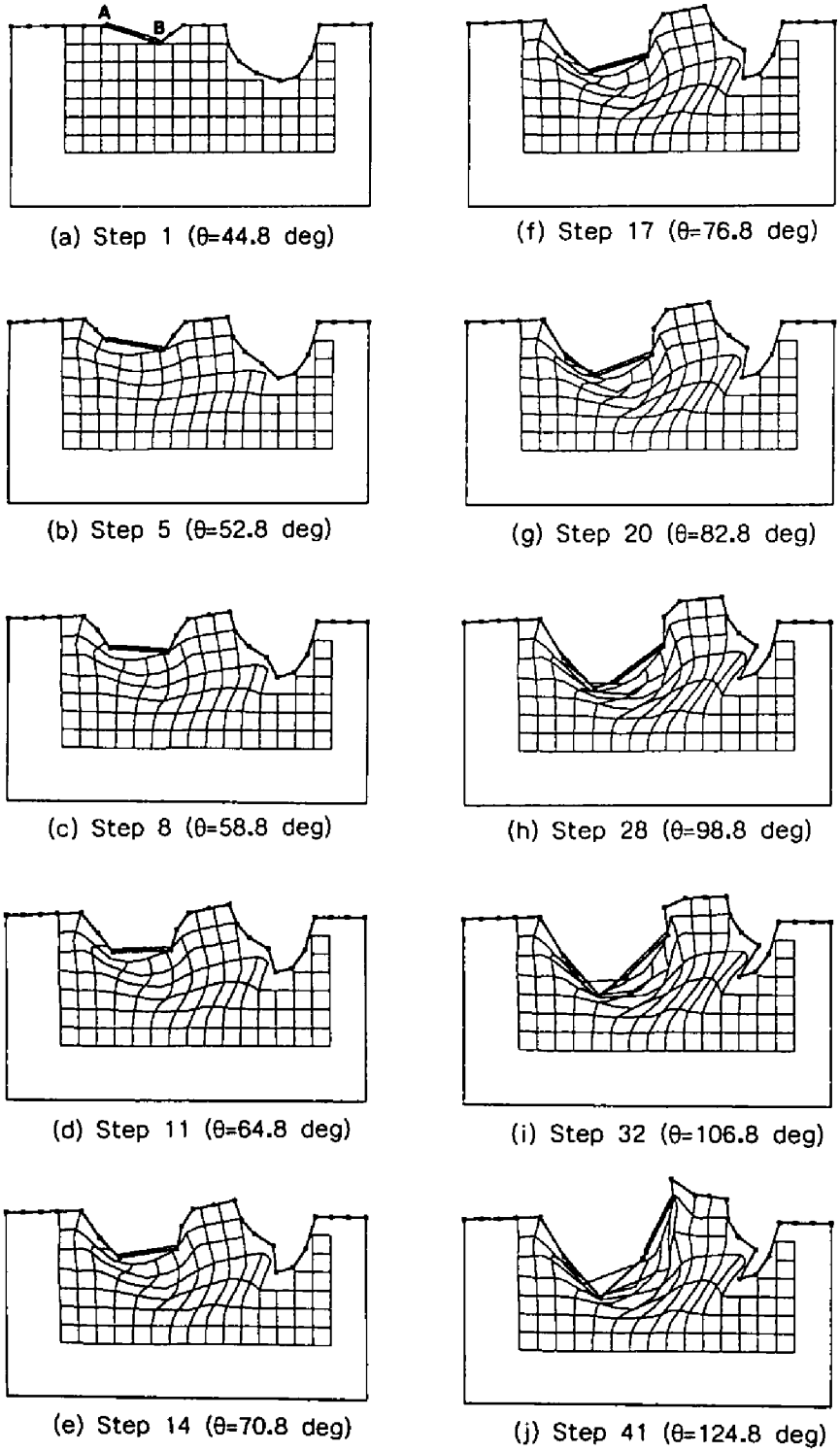

Fig.6-8. Soil behavior by RPFEM for CASE-III.

CASE-III

Fig.6-8 shows the result of 60 deg lug angle case. In this case, the action of lug to soil becomes weaker than other cases, which is observed as the less mobilized region of soil under lug in terms of rotational mobilization and the degree of behavior of left side of preceding lug trench. The marker grids deformation below the lug plate also supports the weakened influence of lug action, which would be the combined effect of the decrease in wheel sinkage.

Discussion

In general, the present analysis has the merit of capability in soil behavior analysis which cannot be done by RBSM or other limit analysis method. And the results qualitatively show the applicability of RPFEM as the second level precise simulation tool for soil behavior analysis.

In all cases, it is noted that the action of lug causes the slightly larger mobilized region involvement, which becomes remarkable at the latter part of rotational angle after 90 deg. That is, the action of lug in the upward direction causes the excessive downward soil boundary displacement which is the natural result of the assumption of incompressibility of soil. The experimental results in Chapter 4 show the interesting fact that the soil boundary at the lug tip moves with the lug action within the lug loci and the soil outside lug loci shows almost no displacement. In this sense, current analysis results in the overestimation of mobilized region of soil under lug. In order to express the soil behavior more precisely, the special element such as singular element (Mori *et al.*,1983) must be placed near the lug outer tip.

6.4.2 Soil Reaction Analysis and Discussion

CASE-I

Fig.6-9 shows the result of soil reaction calculation by RPFEM. It is easily understood that the smoothed line for the lift curve of RPFEM resembles the experimental lift curve, although the absolute value of RPFEM shows the lower result and the sudden change of value at the beginning of rezoning is also noticeable. And also the negative part of pull curve at the first step is seen whose absolute value is rather large compared with the same result of RBSM in Chapter 5. The rotational angle of P_{max} of 28.6 N is 87.2 deg and that of L_{max} of 36.4 N is 55.2 deg. The rotational angle positions for L_{max} and P_{max} are different from the experimental result, but the difference in the angle shows rather small value than that of RBSM in case of L_{max}.

CASE-II

From Fig.6-10, the same tendency as in CASE-I is confirmed. In this case, the negative value of pull at the first step becomes larger in absolute value than that of former case. In this sense, it reflects the better simulation of the effect of lug angle than RBSM. In the lift graph, there exists the large difference of sudden change of curve which corresponds to the step when newly rezoned mesh is adopted. L_{max} of 45.7 N is appeared at 48.5 deg and P_{max} is 25.1 N at 96.5 deg. The angles of rotation for L_{max} and for P_{max} in RPFEM become close to the experimental result.

CASE-III

In this case, general shift in reaction graph is almost similar

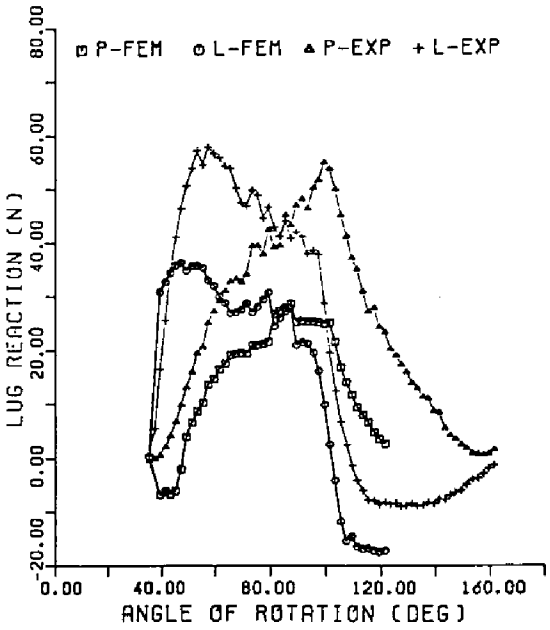

Fig.6-9. Soil reaction by RPFEM for CASE-I.

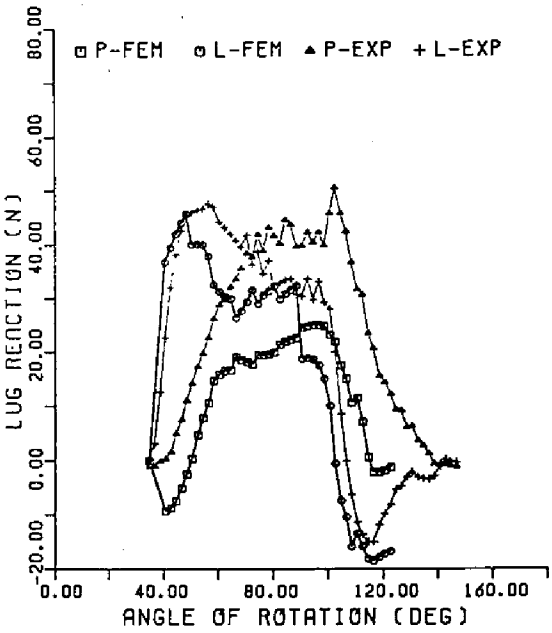

Fig.6-10. Soil reaction by RPFEM for CASE-II.

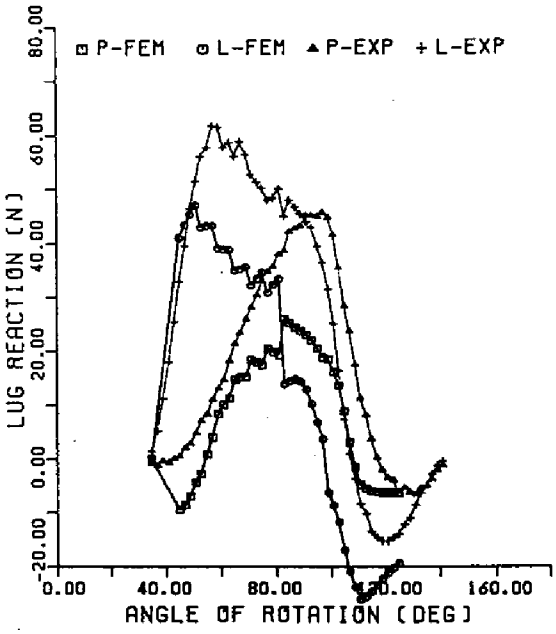

Fig.6-11. Soil reaction by RPFEM for CASE-III.

as in former two results. The negative pull at the first step becomes larger than other cases and maximum pull of 25.9 N is generated at θ= 82.8 deg. The value of L_{max} increases to 47.1 N at 50.8 deg rotational angle. Maximum pull shows no remarkable difference from other cases.

Discussion

Rotational angle difference between calculated P_{max} and L_{max} and experimental results is summarized in Table 6-2. As the rotational angle difference does not show large difference in each case and the soil reaction behavior as seen in this section clearly reflects the experimental result, current RPFEM simulation is done better than the first level simulation of RBSM. The main reason of this superior performance is regarded as the result of inclusion of the information on concurrent deforming soil boundaries.

Table 6-2. Angle difference between calculation and experiments.

Lug	Calculation				Experiments				Difference	
Angle (deg)	P_{max} (N)	θ_{pmax} (deg)	L_{max} (N)	θ_{lmax} (deg)	P_{max} (N)	θ_{pmax} (deg)	L_{max} (N)	θ_{lmax} (deg)	$\Delta\theta_{pmax}$ (deg)	$\Delta\theta_{lmax}$ (deg)
30	28.6	87.2	36.4	55.2	54.9	99.2	58.0	57.2	12.0	2.0
45	25.2	96.5	45.7	48.5	50.6	102.5	47.6	56.5	6.0	8.0
60	25.9	82.8	47.1	50.8	45.7	96.8	61.7	56.8	14.0	6.0

Note: θ_{pmax}=wheel rotational angle where pull of lug P becomes maximum
θ_{lmax}=wheel rotational angle where lift of lug L becomes maximum

The effect of lug angle in RPFEM is seen as the similarity in the behavior of pull and lift curves in the experimental result, which is already stated in former items. It should be noted that the increase in lug angle brings the increasing tendency in maximum lift but

slightly decreasing tendency which may be regarded as almost constant behavior in maximum pull as seen in Table 6-2. The reason of this point is considered as the result of strong stress variation near the lug outer tip which was caused by the currently used mesh size.

The average value of pull and lift cannot be derived here because of the lack of the final stage results. The extension of analyzing step numbers and more realistic calculation in all cases will depend on the fundamental knowledge of soil-lug interface adhesion effects which must be well studied for further development of present analysis.

For more quantitative evaluation, the predicted graph generally exhibits the lower variance in most cases. In the soil behavior results, the clear rotational displacement of soil which exists between the lug and the preceding lug trench is observed. And as stated in the former discussion, the current calculation overestimates the soil boundary motion at the left side of foregoing ditch of lug and the left of lug outer tip. The negative value of pull at the first step is considered as the strong effect of soil strength in front of the exterior lug tip. Furthermore, as the magnitude of reaction directly reflects the value of undrained shear strength of soil, the assumed value for C_u from vane shear test might be lower than the true value under the lug action. Those factors would associate one another and result in the reduced estimation of soil reaction especially for pull of lug.

The behavior of sudden change in soil reaction just after the rezoning of mesh is thought as the result of incomplete regeneration of free boundary surface of soil and the change in equivalent nodal forces which is brought as the difference in elemental stresses before

and after the rezoning.

Since the current RPFEM exhibits the better performance for both soil reaction and soil behavior analysis, it is expected that the effective simulation may be done by RPFEM with the assumption of existence of preceding lug trench and through penalty formulation with mesh rezoning function. It is the merit of RPFEM for wet and almost saturated cohesive soil that the necessary material constants are only C_u and γ. And *a priori* assumption of slip line fields which is inevitable for the upper bound analysis such as RBSM is not required in RPFEM and this point is also important for the applicability of current method as a versatile simulation tool.

6.5 Conclusion

Rigid Plastic Finite Element Method (RPFEM) was firstly applied to the problem of soil-lug interactions as the second level more precise numerical analysis and the following several points were obtained as the conclusion in this chapter;

(1) Both soil behavior under a lug and soil reaction on a lug were found to be qualitatively analyzed by RPFEM with penalty formulation and rezoning function under the mesh configuration with preceding lug trench.

(2) By the assumption of no sliding slip at the soil-lug interface, the non-deforming region below the lug plate was appeared in numerical result during the former part of lug action until the lug outer tip reached the lowest position.

(3) From the result of soil reaction calculation, the effect of lug angle which was similar with the experimental result was obtained.

That is, the smoothed graphs of pull and lift showed almost the same tendency as in the example in each lug angle case. And the calculated maximum lift was almost constant and the calculated maximum pull decreased slightly as lug angle increased, which was the same tendency as in the experiments. Furthermore, the negative pull at the first step of calculation became small for 30 deg lug angle case.

(4) Although the used material constants were only undrained shear strength and specific weight, the analysis turned out to be more effective and useful as a versatile numerical simulation tool than RBSM since the initial slip line construction as in RBSM was not required in RPFEM.

(5) The necessity of further studying the local mechanical interaction at soil-lug interface such as adhesion on the lug plate was again recognized.

Chapter 7 SIMULATION OF SOIL-LUG INTERACTIONS

7.1 Introduction

Based on the achievements in the last chapter, procedures of numerical simulation of soil-lug interaction problems by RPFEM are demonstrated with the example of fixed sinkage condition and the requirements and limitations of current RPFEM simulation are discussed.

7.2 Procedures of Computer Simulation

7.2.1 Data Preparation

List of necessary data for current simulation system which must be given in advance is summarized in Table 7-1. In the table, e_L is the length of lug which is defined as the distance of **A** and **B** in Fig.3-2. The width of lug is expressed by w_L. Undrained shear strength C_u is measured by vane shear test with various shearing velocity condition.

Table 7-1. Necessary data for current simulation.

a) Basic Data Generation

Velocity Condition of Apparatus	:	V_c V_w
Sinkage Variation Parameters	:	Z_0 Z_a Ω ϕ_0
Lug Parameters	:	α n_L R_0 e_L w_L

b) RPFEM

Material Constants	:	C_u γ

7.2.2 Procedures of Simulation

Fig.7-1 shows the flow of procedures of computer simulation of soil-lug interactions and the recommended system for each part.

Basic data generation is in principle based on the experimental result on sinkage variation. But by assuming the no sinkage variation condition such as Z_0=0 which will later be demonstrated as an example, the constant sinkage simulation for certain value of Z_a is possible without prior experiments on sinkage fluctuation of lugged wheel.

For main calculation of RPFEM, the used material constants are C_u and γ as shown in 6.3.2. It is commonly admitted that the shear velocity affects the shear strength of wet cohesive soil. Thus, the velocity effect of shear strength must be checked by the suitable test such as vane shear test. Calculation itself is not time consuming for the mainframe system as stated in Chapter 6.

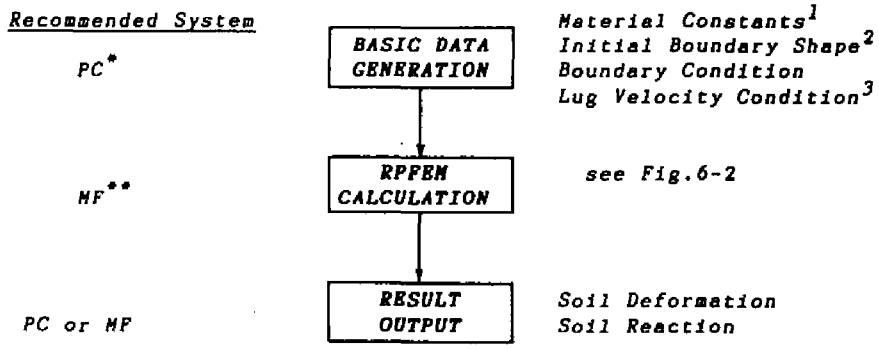

*) Personal Computer (NEC PC-9801 VM)
**) Mainframe System (FACOM M-780)
1) Prior test for C_u determination is necessary.
2) The shape of soil can be decided by either experiments or calculation.
3) Experiments are recommended for calculation of lug velocity.

Fig.7-1. Procedures of computer simulation.

Display of simulated result may be done either by personal computer system or by mainframe system. This process takes a lot of time to get the result at hand because of the large number of data on nodal and marker coordinates.

7.2.3 Example of Simulation and Result Interpretation

As an example of simulation, constant sinkage condition for CASE-I(α=30 deg) and CASE-II(α=45 deg) of n_L=6, i_w=43.1% is simulated to get the information on soil reaction difference from the variable sinkage condition.

Used Data

Table 7-2 shows the used data for the example of simulation. Same time increment Δt=0.2375 sec is used as in the last chapter.

Table 7-2. Used data for constant sinkage simulation example.

a) Basic Data Generation

Velocity Condition of Apparatus : V_c=1.26 cm/s, V_w=2.2 cm/s

Sinkage Variation Parameters : z_0=0, Ω=0, ϕ_0=0
z_a=6.3 cm for CASE-I
z_a=5.3 cm for CASE-II

Lug Parameters : α=30 deg for CASE-I, α=45 deg for CASE-II
n_L=6, R_0=15 cm, e_L=4.95 cm, w_L=15 cm

b) RPFEM

Material Constants : C_u=0.88 kN/m^2, γ=17.64 kN/m^3

Simulated Results

Figs.7-2 and 7-3 show the results of soil deformation simulation for CASE-I and -II respectively. In Fig.7-2, the change in prior lug trench shape from Fig.6-6 is evident because of constant sinkage condition. Especially, the trench becomes symmetrical in terms of its

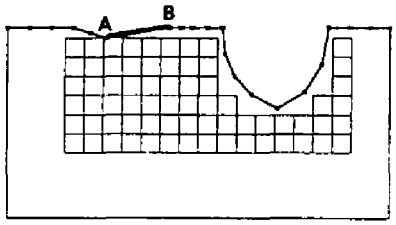

(a) Step 1 (θ=41.5 deg)

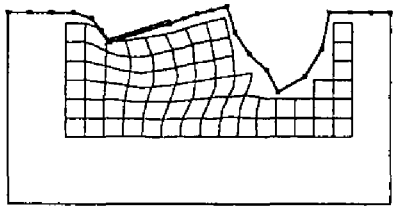

(b) Step 5 (θ=49.5 deg)

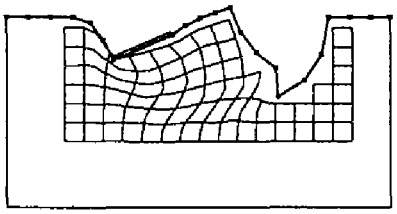

(c) Step 8 (θ=55.5 deg)

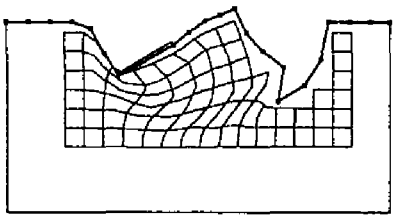

(d) Step 11 (θ=61.5 deg)

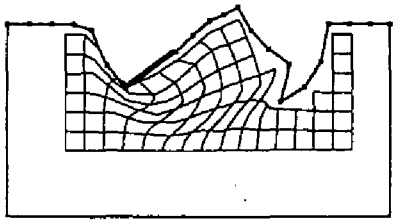

(e) Step 14 (θ=67.5 deg)

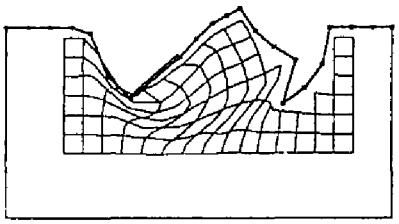

(f) Step 17 (θ=73.5 deg)

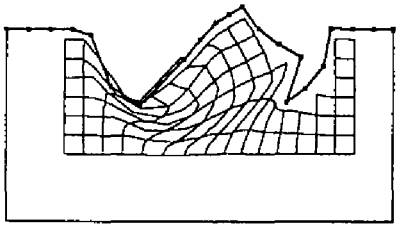

(g) Step 20 (θ=79.5 deg)

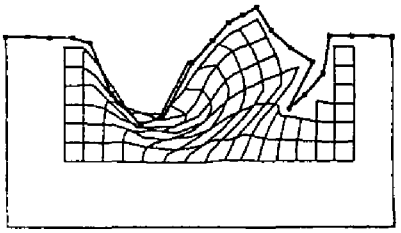

(h) Step 28 (θ=95.5 deg)

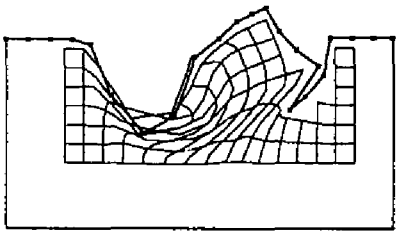

(i) Step 32 (θ=103.5 deg)

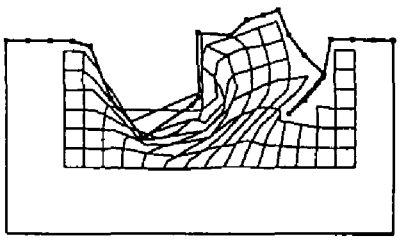

(j) Step 42 (θ=123.5 deg)

Fig.7-2. Soil deformation simulation for CASE-I.

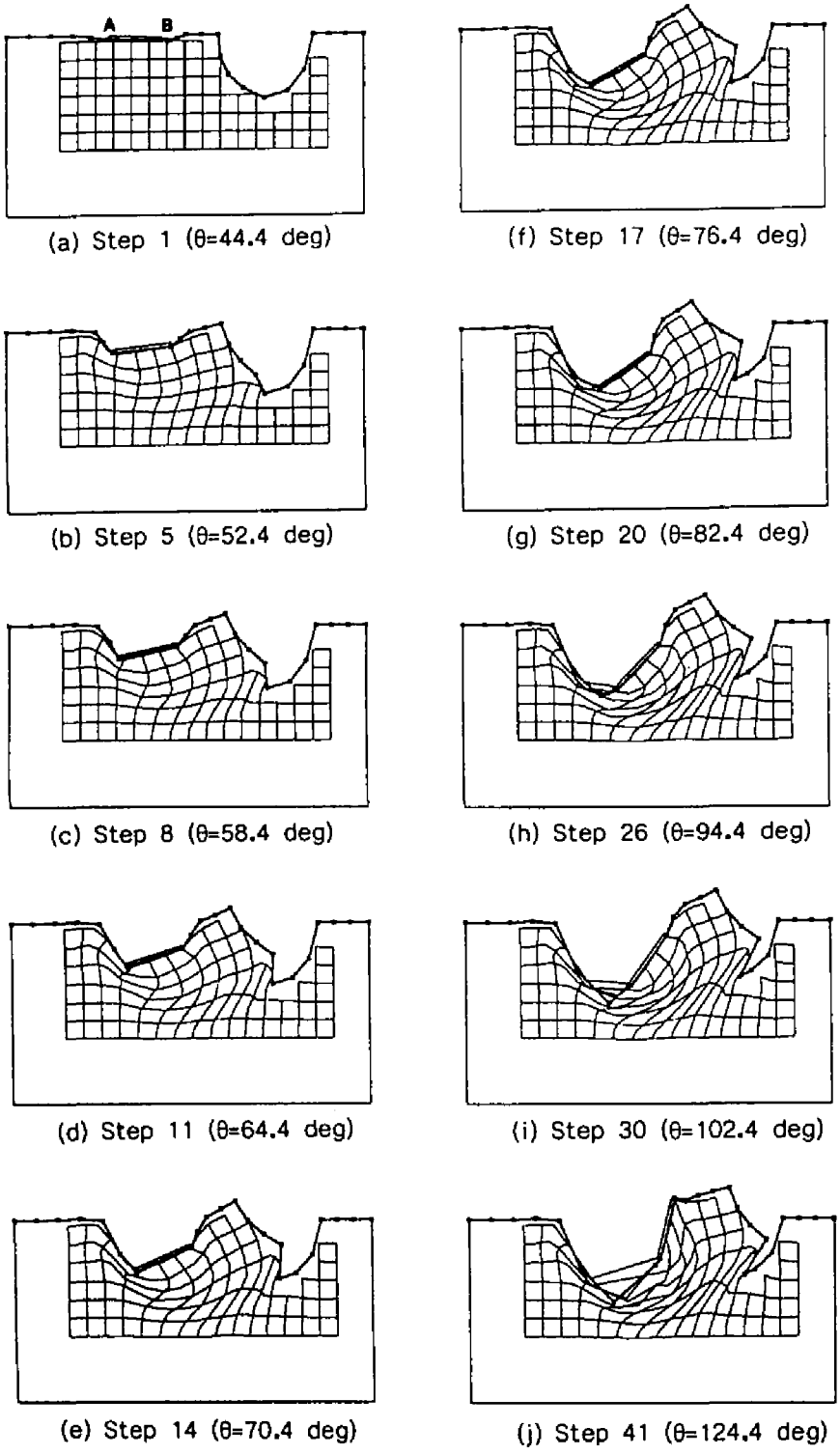

Fig.7-3. Soil deformation simulation for CASE-II.

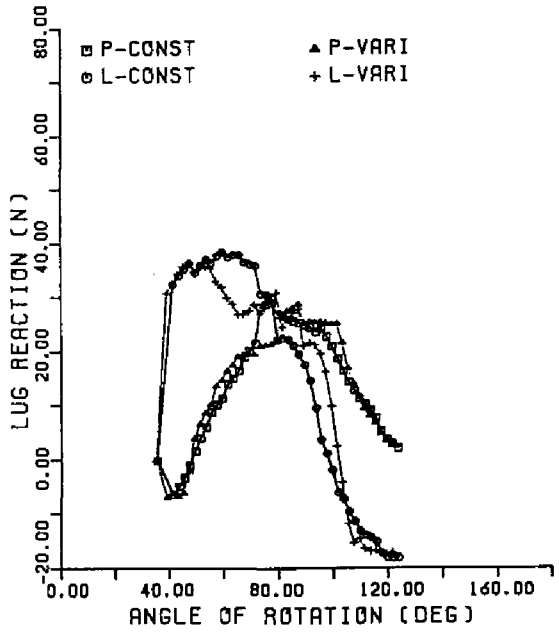

Fig.7-4. Soil reaction simulation for CASE-I.

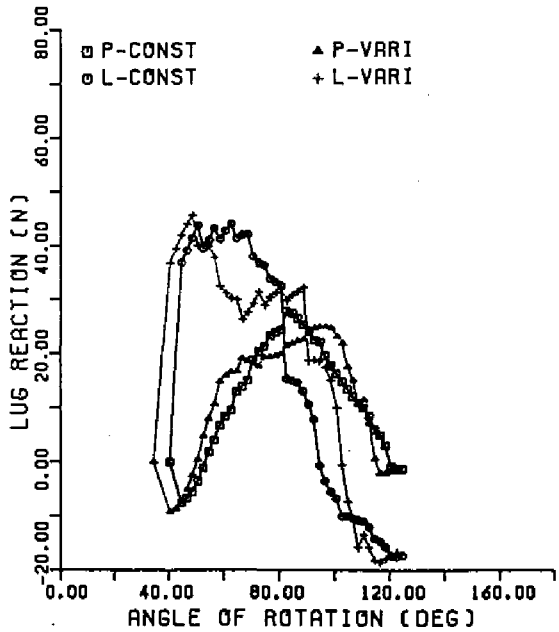

Fig.7-5. Soil reaction simulation for CASE-II.

lowest bottom point with the change in outer lug loci from complex behavior to simple cycloid with slippage. And the the left side of trench comes to contact with the opposite side later than the former result of Fig.6-6. Similar tendency is also observed for Fig.7-3.

Figs.7-4 and 7-5 show the simulated results of soil reaction for CASE-I and -II with corresponding sinkage variation results which are shown as VARI. It should be noted that the constant sinkage condition brings the later peak angle of L and the earlier peak of P compared with the results in Chapter 6. Among others, the behavior of pull graph exhibits the interesting tendency. After the first negative value of pull is taken, the pull value increases almost linearly until about 80 deg rotational angle where it takes the maximum value. For lift graph, the behavior suddenly becomes weak after the angular position of L_{max}.

Interpretation and Discussion

From the simulated results, the interesting behavior of each P and L reaction is seen. P_{max} and L_{max} in constant sinkage calculation become almost the same values as in the sinkage variation results. In this sense, current method of simulation which is based on the sinkage variation equation might be helpful for predicting the maximum values for P and L with an arbitrary constant sinkage condition, i.e. without sinkage variation consideration. In order to predict precisely the soil reaction characteristics which include the evaluation of average pull and average lift of lug, however, the condition of sinkage variation will become significant since the calculation of average values clearly depends on the rotational angles for P_{max} and L_{max}, on the angular length for lug contact and on the behavior of P and L graphs.

The difference in lug angle cannot be clearly exhibited except for the tendency of decreasing maximum pull of lug with the increase in lug angle. And it is also admitted that the pull graph for CASE-I decreases more slowly than that for CASE-II after P_{max}. This phenomenon is regarded as the persistence of effective pull generation in small lug angle case even after the maximum value of P.

7.3 Current Requirements and Limitations

7.3.1 Requirements

Required data and computer capacity for current simulation are summarized as follows.

Program Size

The program size of RPFEM including working area currently needs about 1.5 MB as mentioned in Chapter 6. In this sense, the mainframe computer simulation is inevitable for the time being in terms of the calculation cost.

Material Constants

The present simulation is based on Mises yield condition, which means that the yield stress is independent of indeterminate pressure (or average stress) thus the plastic deformation occurs without volume change. This is why the undrained shear strength of soil C_u must be prepared by proper tests. For current analysis, the quasi-static assumption is done so that the shear strength of cohesive soil would not depend on the shear velocity. For higher shear velocity case as in the real working velocity of lugged wheel, vane shear test with corresponding shear velocity would be required. Data on specific

weight of soil can be included but not always needed for quasi-static condition.

7.3.2 Limitations

In the formulation, some assumptions were made on items as summarized below which must be understood in the application of simulation program.

Soil Behavior

Rigid-perfect plastic constitutive relation with no volume change is adopted in the current formulation in order to express the behavior of very soft soil with more than Liquid Limit moisture content. In general, the effect of internal friction angle may not be disregarded for the soil with less moisture content. As the formulation of RPFEM with the effect of C and ϕ is already developed by Tamura *et al.* (1987), the inclusion of internal friction effect is possible for future application.

Soil-Lug Interface Condition

Since the action of lug to soil is very complicated, the simplest assumption that the soil sticks to lug without any sliding is used throughout the action of lug. At the first contact of lug to soil, rotational angle step is increased until all the surface of lug plate locates below or equal to the initial undeformed soil surface line. For the latter part of lug action to soil, the special treatment of detachment condition as in metal forming analysis is not included since the effect of adhesion at the interface cannot be considered in the current analysis because of the difficulty in measurement of adhesion for soils with moisture content of more than Liquid Limit.

Sinkage Variation

Sinkage variation must be known by the prior experiments. In this sense, current simulation is yet semi-empirical. But if constant sinkage condition is simulated, no experiments are necessary as shown in 7.2. For more complex simulation by RPFEM which includes the calculation of sinkage variation in the program, the behavior of soil must be precisely simulated with the mathematical model and the basic observations on load-sinkage relations for lugged wheel are necessary so that the proper implementation of sinkage variation condition to the numerical simulation can be realized.

Lug Velocity Condition

In order to simulate interactions more precisely, the lug velocity must contain the information of successive contact of the part of lug plate when the initial contact is occurred and that of detachment when lug is about to leave the soil. Ideally speaking, the all lug velocity condition which is prepared by pre-processor can be calculated in the simulation. But as shown in Chapter 6, the yet remaining irregular shape of element prevents the continuing of calculation at certain stage especially as in Fig.6-6. In this sense, adaptive mesh rezoning scheme with fast calculation capability should be included for further development of RPFEM simulation.

Structural Anisotropy

In the current analysis, the soil must be homogeneous in all direction within the soil. But as Tanaka(1984) stressed, the soil structure in the real paddy field shows the strong structural anisotropy which is generated by the hardpan. In terms of the realistic

simulation, this anisotropic characteristics should be included by proper assumption of the structural model of hardpan.

7.4 Conclusion

In this chapter, simulation procedures on soil-lug interaction by Rigid Plastic FEM are summarized with an example. If the constant sinkage was assumed for numerical simulation as was demonstrated in the example, it was predicted that the pull of lug interestingly took the smaller rotational angle where pull of lug became maximum and the lift moved to larger angular position when it reached the peak value in comparison with the sinkage variation results in Chapter 6 and that maximum pull and lift showed almost the same values in sinkage variation case and in constant sinkage condition. By understanding the current requirements and limitations, the further applicability of current simulation method will easily be extended not only to single lug tester simulation but also to the simulation of blocking phenomenon of cage wheel.

Chapter 8 CONCLUDING REMARKS

In this thesis, the following summarized four points can be stated as conclusions. Detailed description on each point is shown at corresponding conclusions from Chapter 3 to 6.

(1) The experiments for soil reaction on a lug of lugged wheel with no confined wheel sinkage condition were done and obtained results showed that the dependence of maximum soil reaction on the total number of lug and wheel slippage. And the effect of lug angle on average pull and lift of lug was verified and the sinkage variation can be approximated as a trigonometric function.

(2) The behavior of wet cohesive soil was observed to be almost incompressible with the dependence of lug loci which was decided by lug parameters of lug angle, total number of lug and wheel slippage.

(3) If proper slip mechanism could be constructed with the well assumed material constants, it was understood that Rigid Body Spring Model may be considered as the first level simple prediction method. The importance of rotational boundary condition of lug was also verified.

(4) Rigid Plastic Finite Element Method with appropriate mesh rezoning function was shown to be applicable as the useful and precise simulation tool for both soil reaction and soil behavior analysis with the consideration of prior lug trench existence and the sinkage variation.

Current achievements can be used as the fundamental engineering tool for lugged wheel design, once the necessary data as shown in Table 7-1 are given. Because the simulation by RPFEM will have the result of not only maximum pull and lift with wheel rotational angle for P_{max} and L_{max} but also minimum pull and lift with corresponding

wheel rotational angle. Therefore, the engineering calculation of average pull and lift may at any rate be possible by assuming the angle of detachment of lug from soil, although the detailed investigations on the detachment condition of lug must be done to obtain the more realistic result.

In future, numerical simulation which was partly demonstrated in this thesis will occupy the important position in the analysis of interaction problems and design processes in wet cohesive soil terramechanics with the fast development of high performance computers. In such an integrated system, the experiments for material constants determination will become indispensable and important for the calculation accuracy of prior reaction prediction and design of soil engaging machine prototypes. In order to realize effective CAD/CAE system with better wheel performance estimation capability, further continuous efforts should be concentrated on the fundamental investigations of soil-machine interface problems.

References

Asaoka, A. and Ohtsuka, S. (1986): The analysis of failure of a normally consolidated clay foundation under embankment loading, Soils and Foundations, Vol.26, No.2, pp.47-59.

Asaoka, A. (1988): Bearing capacity and effective stresses, Tsuchi-to-kiso, JSSMFE, Vol.36, No.6, pp.43-49 (in Japanese).

Cheng, J.H. and Kikuchi, N. (1986): A mesh re-zoning technique for finite element simulations of metal forming processes, Int. J. Numer. Methods Eng., Vol.23, pp.219-228.

Collins, I.F. (1968): The algebraic-geometry of slip line fields with applications to boundary value problems, Proc. Roy. Soc. London, Ser. A, No.303, pp.317-338.

Collins, R.J. (1973): Bandwidth reduction by automatic renumbering, Int. J. Numer. Methods Eng., Vol.6, pp.345-356.

Dickson, J.W., Gee-Clough, D. and Henshall, J.K. (1981): The tractive performance and compaction produced in agricultural soils by open, flat-lugged wheels mounted alone, Proc. 7th Int. Conf. ISTVS, Calgary, CANADA, pp.551-583.

Dickson, J.W., Campbell, D.J. and Henshall, J.K. (1983): An assessment of seedbed compaction by open, flat-lugged, steel tractor wheels, J. agric. Engng Res., Vol.28, pp.45-60.

Durocher, L.L. and Gasper, A. (1979): A versatile two-dimensional mesh generator with automatic bandwidth reduction, Computers & Structures, Vol.10, pp.561-575.

Ewing, D.J.F. (1967): A series-method for constructing plastic slipline fields, J. Mech. Phys. Solids, Vol.15, pp.105-114.

Gee-Clough, D. and Chancellor, W. (1976): Pull and lift characteristics of single lugs on rigid wheels in wet rice soils, Trans. ASAE, Vol.19, pp.433-441.

Gee-Clough, D. (1978): A method for calculating the forces produced by open, lugged wheels, Proc. 6th Int. Conf. ISTVS, Vienna, AUSTRIA, pp.707-733.

Gee-Clough, D., Aggarwal, S., Jayasundera, M.L., Singh, A., Tiangco, V.M. and Shah, N.G. (1981): Recent research into vehicle performance in wetland conditions, Proc. 7th Int. Conf. ISTVS, Calgary, CANADA, pp.205-237.

Gee-Clough, D. (1985): The special problem of wetland traction and floatation, J. agric Engng Res., Vol.32, pp.279-288.

Gelten, C.J.M. and Konter, A.W.A. (1982): Application of mesh-rezoning in the updated lagrangian method to metal forming analyses, Numerical Methods in Industrial Forming Processes (Pittman, J.F.T. et al., Eds.), Pineridge Press, Swansea, UK, pp.511-521.

Hashiguchi, K., Kamei, M., Hiroma, T., Sakai, J., Ide, Y. and Imamura, T.(1988): A traveling performance of rigid lugged wheels (Part 1)--A measurement of soil reaction on a lug and a rim--, J. JSAM, Vol.50, pp.27-36 (in Japanese).

Hettiaratchi, D.R.P., Witney, B.D. and Reece, A.R. (1966): The calculation of passive pressure in two-dimensional soil failure, J. agric. Engng Res., Vol.11, pp.89-107.

Hettiaratchi, D.R.P. and Reece, A.R. (1974): The calculation of passive soil resistance, Géotechnique, Vol.24, pp.289-310.

Hettiaratchi, D.R.P. and Reece, A.R. (1975): Boundary wedges in two-dimensional passive soil failure, Géotechnique, Vol.25, pp.197-220.

Hill, R. (1950): The mathematical theory of plasticity, Clarendon Press, Oxford.

James, R.G. and Bransby, P.L. (1971): A velocity field for some passive earth pressure problems, Géotechnique, Vol.21, pp.61-83.

Kawai, T. (Ed.)(1980): Analysis of problems in continuum mechanics by physical model (Part 3), Course 57, Seminar text, Institute of Industrial Sciences, The University of Tokyo (in Japanese).

Kikuchi, N. (1986): Adaptive grid-design methods for finite element analysis, Computer Methods in Applied Mechanics and Engineering, Vol.55, pp.129-160.

Kikusawa, M. and Hasegawa, T. (1987): Application of rigid plastic finite element method in soil mechanics, J. JSIDRE, Vol.55, pp.957-963 (in Japanese).

Kim, Y.S., Tomita, Y. and Shindo, A. (1987): Application of the rigid body-spring model to plane strain analysis of plastic collapsing and fracturing behaviours, Trans. JSME, Ser.A, Vol.53, pp.339-343 (in Japanese).

Kishine, T (1974): Statistics--theory and application--, Yokendo, Tokyo (in Japanese).

Kohnke, H. (1968): Soil physics, McGraw-Hill, New York.

Lee, C.H. and Kobayashi, S. (1973): New solutions to rigid-plastic deformation problems using a matrix method, J. Engng. Ind., ASME, Vol.95, pp.865-873.

Lu, H.Z. and Shao, Y.J. (1987): Experimental research on the soil flow and soil reaction beneath lugs of powered wheel, Proc. 9th Int. Conf. ISTVS, Barcelona, SPAIN, pp.373-380.

Mahrenholtz, O. and Dung, N.L. (1987): Mathematical modeling of metal forming processes by numerical methods, Proc. 2nd Int. Conf. on Technology of Plasticity, Stuttgart, FRG, pp.3-10.

Masuda, S. and Tanaka, T. (1964): Tractive performance of wheel-type tractor (Part 6)--Theoretical analysis of the stress distribution on the lug surface by the soil--, J. JSAM, Vol.26, pp.9-13 (in Japanese).

Masuda, S., Tanaka, T., Nishimura, I. and Yamazaki, M. (1966): Performance of the crawler tractors on muddy field, J. JSAM, Vol.28, pp.141-148 (in Japanese).

Mori, K., Osakada, K. and Fukuda, M. (1983): Simulation of severe plastic deformation by finite element method with spatially fixed elements, Int. J. Mech. Sci., Vol.25, pp.775-783.

Nakamura, Y., Murase, H., Nakashima, H. and Nakano, M. (1985): Basic studies on soil-lug system interactions (Part 1)--On the relation of total lug number and soil reaction--, Report of Kansai branch of JSAM, No.58, PP.35-36 (in Japanese).

Nakashima, H. and Tanaka, T. (1986a): Studies on soil-lug system interactions (Part 2) --Lug reaction characteristics when lug angle is varied--, Abstract of 45th annual meeting of JSAM, Matsue, p.33 (in Japanese).

Nakashima, H. and Tanaka, T. (1986b): Soil reaction on a lug of lugged wheel, Proc. 1st Asian-Pacific Conf. ISTVS, Beijing, PRC, pp.429-444.

Nakashima, H. and Tanaka, T. (1988a): Interactions in soil-lug system (Part 2)--Effect of lug angle on soil reaction--, J. JSAM, Vol.50, No.6, pp.3-10 (in Japanese).

Nakashima, H. and Tanaka, T. (1988b): Interactions in soil-lug system (Part 3)--Soil behavior under lug and sinkage variation of lugged wheel--, J. JSAM (to appear) (in Japanese).

Nakashima, H. and Tanaka, T. (1988c): Interactions in soil-lug system (Part 4)--Numerical simulation of interactions--, J. JSAM (submitted) (in Japanese).

Oh, S.I., Tang, J.P. and Badawy, A. (1984): Finite element mesh rezoning and its applications to metal forming analysis, Proc. 1st Int. Conf. on Technology of Plasticity, Tokyo, JAPAN, pp.1051-1058.

Okabe, M. (1972): Performance of transplanter wheels in terms of lug width, Report of Kyushu branch of JSAM, No.21, pp.23-30 (in Japanese).

Osakada, K. (1983): Finite element analysis of plastic deformation (6), Science of Machine, Vol.35, pp.761-765 (in Japanese).

Pragar, W. (1959): An introduction to plasticity, Addison-Wesley.

Sakai, J., Hashiguchi, K., Yamanaka, S., Hiroma, T., Kishimoto, T., Ide, Y. and Kamei, M. (1984): Dynamic characteristics of iron wheels for farm vehicles --Analysis of soil reaction acting on lugs by slip-line method--, Report of Kyushu branch of JSAM, No.33, pp.14-19 (in Japanese).

Salokhe, V.M. and Gee-Clough, D. (1987a): Behaviour of wet clay soil

under single cage wheel lugs, J. agric. Engng Res., Vol.37, pp.255-266.

Salokhe, V.M. and Gee-Clough, D. (1987b): Formation of a boundary wedge on a single lug in wet clay soil, J. agric. Engng Res., Vol.38, pp.113-125.

Salokhe, V.M. and Gee-Clough, D. (1987c): Studies on effect of lug surface coating on soil adhesion of cage wheel lugs, Proc. 9th Int. Conf. ISTVS, Barcelona, SPAIN, pp.389-396.

Salokhe, V.M. and Gee-Clough, D. (1988): Wet clay soil behaviour under multiple cage wheel lugs, J. agric. Engng Res., Vol.39, pp.57-70.

Shao, Y.J. and Wong, J.Y. (1986): Experimental study into soil flow beneath lugs of powered wheel, Proc. 1st Asian-Pacific Conf. ISTVS, Beijing, PRC, pp.514-526.

Sokolovski, V.V. (1960): Statics of soil media, Butterworths, London.

Tamura, T., Kobayashi, S. and Sumi, T. (1984): Limit analysis of soil structure by rigid plastic finite element method, Soils and Foundations, Vol.24, No.1, pp.34-42.

Tamura, T. (1986): Introduction and application of rigid plastic finite element method, Seminar text on numerical analysis in soil mechanics, Kansai Branch of JSSMFE, pp.50-79 (in Japanese).

Tamura, T., Kobayashi, S. and Sumi, T. (1987): Rigid-plastic finite element method for frictional materials, Soils and Foundations, Vol.27, No.3, pp.1-12.

Tanaka, T. (1958): Studies of the power tiller on the moist paddy land (Part 4)--On the soil deformation and stress by the surface and lug of the farm wheel(1)--, J. JSAM, Vol.20, pp.104-108 (in Japanese).

Tanaka, T. (1959a): Studies of the power tiller on the moist paddy land (Part 5)--On the soil deformation and stress by the surface and lug of the farm wheel(2)--, J. JSAM, Vol.20, pp.142-146 (in Japanese).

Tanaka, T. (1959b): Studies of the power tiller on the moist paddy land (Part 6)--On the soil deformation and stress by the surface and lug of the farm wheel(3)--, J. JSAM, Vol.20, pp.147-151 (in Japanese).

Tanaka, T., Nishimura, I. and Azuma, T. (1965): Prediction of the trafficability of the tractor on the soft paddy field (Part 4)--On the drawbar pull of the tractor and their running elements--, J. JSAM, Vol.27, pp.218-224 (in Japanese).

Tanaka, T. (1984): Operation in paddy fields : state-of-the-art report, J. Terramechanics, Vol.21, pp.153-179.

Tanaka, T. and Nakashima, H. (1986): Interactions in soil-lug system (Part1)--Characteristics of soil reaction on a lug with lug angle of 30 degree--, J. JSAM, Vol.48, No.2, pp.225-232 (in Japanese).

Tanaka, T., Nakashima, H. and Suzuki, H. (1986): Basic studies on soil-lug system interactions (Part 2)--On the relation of soil reaction and lug angle--, Report of Kansai branch of JSAM, No.60, pp.38-39 (in Japanese).

Tanaka, T. and Nakashima, H. (1987): Studies on soil-lug system interactions (Part 3)--Analysis of soil deformation under lug by rigid plastic finite element method--, Abstract of 46th annual meeting of JSAM, Tokyo, p.21 (in Japanese).

Tanaka, T., Nakashima, H. and Kishida, A. (1987): Basic studies on soil-lug system interactions (Part 3)--On the relation of wheel load and sinkage--, Report of Kansai branch of JSAM, No.62, pp.11-12 (in Japanese).

Tanaka, T., Nakashima, H. and Nagi, T. (1987): An analysis of soil deformation under lug by finite element method, Report of Kansai branch of JSAM, No.62, pp.13-14 (in Japanese).

Tanaka, T., Nakashima, H. and Kawashima, S. (1988): Data generation method for finite element analysis in terramechanics (Part 1)--On performance of band minimizer--, Report of Kansai branch of JSAM, No.64, pp.13-14 (in Japanese).

Tanaka, T., Nakashima, H. and Riichi, H. (1988): Vane shear strength of cohesive soil with various shearing velocity, Report of Kansai branch of JSAM, No.64, pp.11-12 (in Japanese).

Tomita, Y. (1987): Numerical analysis of industrial forming processes (9), Science of Machine, Vol.39, pp.1255-1259 (in Japanese).

Tsuchiya, M. and Honami, N. (1962): Studies on the lugs of garden tractor wheels (Part 1)--The characteristics of lugs on sand of sand hill--, J. JSAM, Vol.23, pp.149-155 (in Japanese).

Tsuchiya, M. and Honami, N. (1965): Studies on the lugs of garden tractor wheels (Part 2)--The reaction forces to lugs and the rolling resistance of garden tractor wheel with spade lugs--, J. JSAM, Vol.26, pp.236-240 (in Japanese).

Tsunematsu, S. and Matsui, K. (1954): Study on the wheel of garden tractors (Part 1)--Relation between shapes of lugs and slip of wheel--, J. JSAM, Vol.16, pp.19-23 (in Japanese).

Tsunematsu, S. and Matsui, K. (1956): Study on the wheel of garden tractors (Part 2)--Relation between shapes of lugs and rolling resistance--, J. JSAM, Vol.18, pp.19-22 (in Japanese).

Wang, X.L., Tanaka, T. and Yamazaki, M. (1988): Study on reaction forces and lug motion of paddy wheel lug, Terramechanics, No.8, pp.29-35 (in Japanese).

Wu, S.X., Hu, J.H. and Wong, J.Y. (1984): Behaviour of soil under a lugged wheel, Proc. 8th Int. Conf. ISTVS, Cambridge, UK, pp.545-559.

Wu, S.X., Hu, J.H. and Wong, J.Y. (1986): The failure pattern of soil

beneath wheel lugs, Proc. 1st Asian-Pacific Conf. ISTVS, Beijing, PRC, pp.594-602.

Yamada, Y., Yoshimura, N. and Sakurai, T. (1968): Plastic stress-strain matrix and its application for the solution of elastic-plastic problems by the finite element method, Int. J. Mech. Sci., Vol.10, pp.343-354.

Yamanaka, I. (1962): Fundamental researches on lug of iron wheel for small type tractor, Memoirs of the Faculty of Agriculture, Tokyo University of Education, No.8, pp.117-177 (in Japanese).

Zhang, T.L. and Shao, Y.J. (1984): The analysis on the dynamic performance of a single lug, Proc. 8th Int. Conf. ISTVS, Cambridge, UK, pp.575-591.

Zienkiewicz, O.C. and Godbole, P.N. (1975): A penalty function approach to problems of plastic flow of metals with large surface deformations, J. Strain Analysis, Vol.10, pp.180-183.

Zienkiewicz, O.C. (1977): The finite element method, 3rd Edition, McGraw-Hill, London.

[List of Abbreviations]

ASAE : The American Society of Agricultural Engineers
ASME : The American Society of Mechanical Engineers
ISTVS : The International Society for Terrain-Vehicle Systems
JSAM : The Japanese Society of Agricultural Machinery
JSIDRE : The Japanese Society of Irrigation, Drainage and Reclamation Engineering
JSME : The Japan Society of Mechanical Engineers
JSSMFE : The Japanese Society of Soil Mechanics and Foundation Engineering